



University of Pennsylvania  
**ScholarlyCommons**

---

Publicly Accessible Penn Dissertations


---

2021

## Elucidating The Role Of The African-Centric P47s Variant Of Tp53 In Metabolism And Ferroptosis

Keerthana Gnanapradeepan  
*University of Pennsylvania*

Follow this and additional works at: <https://repository.upenn.edu/edissertations>

 Part of the [Biochemistry Commons](#), [Cell Biology Commons](#), and the [Oncology Commons](#)

---

### Recommended Citation

Gnanapradeepan, Keerthana, "Elucidating The Role Of The African-Centric P47s Variant Of Tp53 In Metabolism And Ferroptosis" (2021). *Publicly Accessible Penn Dissertations*. 3953.  
<https://repository.upenn.edu/edissertations/3953>

This paper is posted at ScholarlyCommons. <https://repository.upenn.edu/edissertations/3953>  
For more information, please contact [repository@pobox.upenn.edu](mailto:repository@pobox.upenn.edu).

---

# Elucidating The Role Of The African-Centric P47s Variant Of Tp53 In Metabolism And Ferroptosis

## Abstract

The tumor suppressor gene TP53 is the most frequently mutated gene in cancer and plays a key role in mediating several processes that are critical for preventing tumor formation and progression. Known as the guardian of the genome, p53 regulates hundreds of genes involved in various pathways such as apoptosis, cell cycle arrest and senescence. In recent years, the role of p53 in metabolism, redox state and ferroptosis has begun to emerge. Our lab has identified an African-specific polymorphic variant of p53 that encodes a serine residue instead of a proline at amino acid 47 (hereafter S47) and predisposes carriers to cancer. The S47 variant is impaired for tumor suppression and ferroptosis, and S47 cells have an altered redox state. We sought to use the tumor prone S47 model as a tool to better understand the role of p53 in tumor suppression. Our results demonstrate that mice carrying the S47 variant have greater metabolic efficiency compared to those with WT p53, along with increased mTOR activity. This difference in mTOR stems from an impaired protein-protein interaction that occurs in S47, ultimately due to a difference in cellular redox state. We next identified PLTP as a p53 target gene that shows decreased transactivation in the S47 variant and mediates ferroptosis resistance by enhancing lipid storage in HepG2 cells. Taken together, this work sheds light on the emerging roles p53 plays in tumor suppression, metabolism and ferroptosis. It also provides a better understanding of an ethnic genetic variant of p53. We expect this work will enable better personalized medicine approaches and therapeutic options for people who carry this variant.

## Degree Type

Dissertation

## Degree Name

Doctor of Philosophy (PhD)

## Graduate Group

Biochemistry & Molecular Biophysics

## First Advisor

Maureen E. Murphy

## Keywords

cancer, ferroptosis, metabolism, mTOR, p53, variant

## Subject Categories

Biochemistry | Cell Biology | Oncology

ELUCIDATING THE ROLE OF THE AFRICAN-CENTRIC P47S VARIANT OF *TP53* IN  
METABOLISM AND FERROPTOSIS

Keerthana Gnanapradeepan

A DISSERTATION

in

Biochemistry and Molecular Biophysics

Presented to the Faculties of the University of Pennsylvania

in

Partial Fulfillment of the Requirements for the

Degree of Doctor of Philosophy

2021

Supervisor of Dissertation

---

Maureen E. Murphy, Ph.D.

Ira Brind Professor and Program Leader, Wistar Institute

Graduate Group Chairperson

---

Kim A. Sharp, Ph.D., Associate Professor of Biochemistry and Molecular Biophysics

Dissertation Committee

Kathryn E. Wellen, Ph.D., Associate Professor of Cancer Biology

Xiaolu Yang, Ph.D., Professor of Cancer Biology

Zachary T. Schug, Ph.D., Assistant Professor, Wistar Institute

Donna L. George, Ph.D., Associate Professor of Genetics

*To my parents - for their sacrifice, strength, and unwavering faith in me.*

## ACKNOWLEDGMENT

My heartfelt gratitude goes out to every person who has helped me reach this point of culmination today. I feel truly blessed to have had the privilege of training and pursuing a doctorate degree at Penn Medicine, and hope to take what I have learned during my time here to make a positive impact on society.

To the best mentor, Dr. Maureen Murphy – Maureen, you have molded me into a strong scientist and even better person. I am grateful for all the time you have invested in me – weekly meetings, practice prelims, going through all my talks and written works with such attentiveness to detail – it is something very few PI's do, and I feel extremely fortunate to have had your guidance. I appreciate all the opportunities you have given me, from the chance to be on so many high impact papers, to allowing me to travel to amazing conferences across the world. Most importantly, you have shown me the importance of kindness. Your munificence and willingness to help others is something that has truly inspired me. Thank you for everything, I can only hope to pay it forward as I progress through my career.

To my thesis committee – Dr. Katy Wellen, Dr. Xiaolu Yang and Dr. Zach Schug– thank you for your invaluable advice and guidance over the years. You are all luminaries in your respective fields, and it has been a true privilege to train with you all. To Dr. Donna George, you have been a second mentor to me, and I am extremely grateful for all your insight and support over the years.

To the BMB Graduate Group – It has been an honor to receive training through this program. BMB has fostered such a stimulating yet fun learning environment. Special

thanks to Dr. Kristen Lynch and Dr. Kim Sharp for being our fearless leaders and for ensuring each student feels supported throughout our graduate school experience.

To my lab mates – You all lifted me up when my experiments failed and cheered me on when they succeeded. It has been such a joy to work with each of you and you have made my PhD journey such a positive experience. Special thanks to Joshua Parris and Dr. Tim Barnoud for being by my side throughout, Dr. Subhasree Basu for training me, and Dr. Julie Leu for all the technical help and expertise.

To my BMB cohort – From our wacky Halloween costumes to our “whine & wine” nights to all our annual traditions, I could not have asked for a better set of friends to share this ride with. You are all some of the most intelligent yet most humble people I have met, and I look forward to seeing all of you reach great heights in your careers.

To my roommates – Raju and Apexa– thank you for being my family here and making Philadelphia feel like home. The two of you have been with me through the best of times and worst of times, and I am so thankful for our friendship.

To all my friends – Thank you for distracting me from the purgatory of failed experiments and for being my cheerleaders with every milestone achieved. The FaceTimes and phone calls, weddings and weekend trips, dance breaks and foodie adventures, spiritual discussions and philosophical book clubs, all helped give me the strength and motivation I needed to push through the ups and downs of graduate school. I am so very grateful for each and every one of you.

To all my teachers and gurus – from the musty hallways of Medford High School to the dank floors of the dance studio to the incense filled sanctum of the temple – each of you have helped instill a sense of discipline and diligence within me, while fueling my sense of wonder. I look to each of you with humility and reverence and will always be grateful for the lessons you have taught me.

Most importantly, to my dear parents – You left a war-torn country with very little in hand and worked tirelessly to achieve the American Dream. You have taught me the value of hard work, to strive for excellence, and to always work towards helping others. Thank you for believing in me when I didn't believe in myself, for standing by my side no matter what, and for the love you have showered upon me. This degree is the fruition of your sacrifice and perseverance; my success in life stems from the seeds you have planted and nurtured.

Thank you all.

## ABSTRACT

### ELUCIDATING THE ROLE OF THE AFRICAN-CENTRIC P47S VARIANT OF *TP53* IN METABOLISM AND FERROPTOSIS

Keerthana Gnanapradeepan

Maureen E. Murphy

The tumor suppressor gene *TP53* is the most frequently mutated gene in cancer and plays a key role in mediating several processes that are critical for preventing tumor formation and progression. Known as the guardian of the genome, p53 regulates hundreds of genes involved in various pathways such as apoptosis, cell cycle arrest and senescence. In recent years, the role of p53 in metabolism, redox state and ferroptosis has begun to emerge. Our lab has identified an African-specific polymorphic variant of p53 that encodes a serine residue instead of a proline at amino acid 47 (hereafter S47) and predisposes carriers to cancer. The S47 variant is impaired for tumor suppression and ferroptosis, and S47 cells have an altered redox state. We sought to use the tumor prone S47 model as a tool to better understand the role of p53 in tumor suppression. Our results demonstrate that mice carrying the S47 variant have greater metabolic efficiency compared to those with WT p53, along with increased mTOR activity. This difference in mTOR stems from an impaired protein-protein interaction that occurs in S47, ultimately due to a difference in cellular redox state. We next identified *PLTP* as a p53 target gene that shows decreased transactivation in the S47 variant and mediates ferroptosis resistance by enhancing lipid storage in HepG2 cells. Taken together, this work sheds light on the emerging roles p53 plays in tumor suppression, metabolism and ferroptosis. It also provides a better understanding of an ethnic genetic variant of p53. We expect this work will enable better personalized medicine approaches and therapeutic options for people who carry this variant.



## TABLE OF CONTENTS

<b>ACKNOWLEDGMENT .....</b>	<b>III</b>
<b>ABSTRACT .....</b>	<b>VI</b>
<b>LIST OF TABLES .....</b>	<b>X</b>
<b>LIST OF ILLUSTRATIONS .....</b>	<b>XI</b>
<b>CHAPTER 1: INTRODUCTION .....</b>	<b>1</b>
<b>1.1 p53: Guardian of the Genome .....</b>	<b>1</b>
1.1.1 The role of p53 in cancer .....	1
1.1.2 The story of p53: A brief history.....	2
<b>1.2 The structure and function of p53 .....</b>	<b>5</b>
1.2.1 The Structure of p53 .....	5
1.2.2 Transactivation Domains of p53.....	6
1.2.3 p53 Activation .....	8
1.2.4 Canonical functions of p53.....	9
<b>1.3 Emerging roles of p53 .....</b>	<b>12</b>
1.3.1 p53 and metabolism.....	12
1.3.2 p53 and mTOR.....	14
1.3.3 p53 regulates lipid metabolism .....	15
1.3.4 Ferroptosis .....	18
1.3.5 The role of p53 in the regulation of ferroptosis has been controversial.....	19
1.3.6 The African-specific P47S variant .....	23
<b>1.4 Thesis objectives .....</b>	<b>27</b>
<b>CHAPTER 2: INCREASED MTOR ACTIVITY AND METABOLIC EFFICIENCY FOUND IN THE P47S VARIANT OF <i>TP53</i>.....</b>	<b>28</b>
<b>2.1 Abstract .....</b>	<b>28</b>
<b>2.2 Introduction.....</b>	<b>29</b>
<b>2.3 Results .....</b>	<b>31</b>
2.3.1 Higher basal mTOR activity in cells containing the S47 variant.....	31
2.3.2 Enhanced mitochondrial function and glycolysis in S47 cells.....	35
2.3.3 Increased mTOR activity in S47 is due to increased mTOR-Rheb interaction .....	40
2.3.4 Enhanced metabolic efficiency of S47 mice .....	47
<b>2.4 Discussion .....</b>	<b>50</b>

<b>2.5 Materials and Methods</b> .....	<b>55</b>
2.5.1 Mammalian cell culture.....	55
2.5.2 Western blot .....	56
2.5.3 Immunohistochemistry .....	57
2.5.4 Co-Immunoprecipitation .....	57
2.5.5 Mitochondrial metabolism and mTOR inhibition assays.....	58
2.5.6 Metabolite measurements.....	59
2.5.7 GSH/GSSG abundance and BMH crosslinking .....	60
2.5.8 Proximity Ligation Assay.....	61
2.5.9 Immunofluorescence staining .....	62
2.5.10 Body composition and metabolic cage studies .....	62
2.5.11 Treadmill and serum metabolite studies.....	63
2.5.12 Statistical Analysis .....	64
<b>2.6 Supplemental Figures</b> .....	<b>65</b>
<b>CHAPTER 3: <i>PLTP</i> IDENTIFIED AS A P53-TARGET GENE THAT MEDIATES FERROPTOSIS RESISTANCE IN HEPG2 CELLS</b> .....	<b>74</b>
<b>3.1 Abstract</b> .....	<b>74</b>
<b>3.2 Introduction</b> .....	<b>75</b>
<b>3.3 Results</b> .....	<b>77</b>
3.3.1 <i>PLTP</i> identified as gene that is downregulated by the S47 variant of p53.....	77
3.3.2 The role of p53 in regulating <i>PLTP</i> and ferroptosis in HepG2 cells .....	80
3.3.3 <i>PLTP</i> promotes ferroptosis resistance.....	82
3.3.4 <i>PLTP</i> silencing does not impact other cell death processes .....	85
3.3.5 <i>PLTP</i> protects cells from ferroptotic cell death by promoting lipid storage.....	87
<b>3.4 Discussion</b> .....	<b>90</b>
<b>3.5 Materials and Methods</b> .....	<b>93</b>
3.5.1 RNA Sequencing .....	93
3.5.2 qRT-PCR.....	94
3.5.3 Silencing and overexpression studies.....	94
3.5.4 Flow cytometry.....	95
3.5.5 Immunofluorescence staining .....	96
3.5.6 Immunohistochemistry .....	96
3.5.7 Viability assays .....	96
3.5.8 Mammalian Cell Culture.....	97
3.5.9 Western blot .....	98
3.5.10 Statistical Analysis .....	98
<b>CHAPTER 4: FUTURE DIRECTION AND CONCLUDING REMARKS</b> .....	<b>99</b>
<b>4.1 Summary of findings</b> .....	<b>99</b>
<b>4.2 Outstanding questions regarding p53, S47, mTOR, ferroptosis and tumor suppression</b> .....	<b>102</b>

**BIBLIOGRAPHY ..... 108**

## LIST OF TABLES

<b>Table 3.1:</b> Genes identified as being at least 3-fold downregulated in S47 LCLs.....	78
--	----

## LIST OF ILLUSTRATIONS

<b>Figure 1.1:</b> Domains of p53 .....	8
<b>Figure 1.2:</b> p53 activation and response .....	11
<b>Figure 1.3:</b> Role of p53 in metabolism .....	17
<b>Figure 1.4:</b> Various roles of p53 in ferroptosis.....	22
<b>Figure 1.5:</b> The S47 mouse .....	26
<b>Figure 2.1:</b> Increased markers of mTOR activity in S47 cells and tissues .....	34
<b>Figure 2.2:</b> Increased metabolism in S47 cells compared to WT cells .....	37
<b>Figure 2.3:</b> S47 mitochondria show decreased sensitivity to mTOR inhibition .....	39
<b>Figure 2.4:</b> Increased mTOR-Rheb binding in S47 cells is due to decreased GAPDH-Rheb binding .....	42
<b>Figure 2.5:</b> Increased glutathione drives decreased GAPDH-Rheb binding in S47 cells.....	46
<b>Figure 2.6:</b> Increased size and improved metabolic efficiency in S47 mice.....	49
<b>Figure 2.7:</b> Proposed model of how S47 contributes to increased metabolism .....	53
<b>Supplemental Figure 2.1:</b> Altered metabolic markers in S47 cells and tissues .....	65
<b>Supplemental Figure 2.2:</b> Increased metabolism in S47 MEFs but no differences in mitochondrial content in WT and S47 cells.....	67
<b>Supplemental Figure 2.3:</b> Attenuated response to mTOR inhibition in S47 cells.....	68
<b>Supplemental Figure 2.4:</b> No differences in the level of mTOR regulators in WT and S47 cells.....	69
<b>Supplemental Figure 2.5:</b> Glutathione depletion by BSO alters GAPDH cross-linking and the GAPDH-Rheb interaction.....	71
<b>Supplemental Figure 2.6:</b> Serum metabolites and protein markers pre- and post- exercise....	72
<b>Figure 3.1:</b> PLTP is differentially regulated by WT p53 and the S47 variant.....	79
<b>Figure 3.2:</b> p53 positively regulates PLTP but negatively regulates ferroptosis in HepG2 cells...81	81
<b>Figure 3.3:</b> Knockdown of PLTP increases RSL3-induced ferroptosis sensitivity.....	83
<b>Figure 3.4:</b> Overexpression of PLTP confers ferroptosis resistance .....	84
<b>Figure 3.5:</b> PLTP silencing does not affect sensitivity to other forms of cell death.....	86
<b>Figure 3.6:</b> A model for PLTP in ferroptosis resistance by promoting lipid storage .....	89

## Chapter 1: Introduction

This chapter contains excerpts from the following manuscript:

Gnanapradeepan K, Basu S, Barnoud T, Budina-Kolomets A, Kung CP, Murphy ME. The p53 tumor suppressor in the control of metabolism and ferroptosis. *Frontiers in Endocrinology* (2018); 9:124.

### 1.1 p53: Guardian of the Genome

#### 1.1.1 *The role of p53 in cancer*

Cancer is most simply described as a disease of uncontrolled cell growth, resulting from genetic mutations. Hundreds of genes have been identified as playing a role in tumorigenesis, but among the most notable genes in cancer is *TP53*, mutated in more than 50% of human tumors (Leroy et al., 2014). Since first being discovered in 1979, there have been more than 80,000 somatic and germline mutations that have been observed in this single gene (<http://p53.fr>). Many factors determine the prevalence of p53 mutations, such as cancer type and the stage of the tumor. For example, *TP53* mutations are found in 80% of small-cell lung cancer and 90% of ovarian cancer, while there are less than 5% observed in cervical cancer and 10% in leukemia. Exogenous influences such as viral infection and geographic distribution, in other words how environmental conditions affect carriers from different areas of the world, are also factors that can affect the frequency of *TP53* mutations (Leroy et al., 2014).

In many tumor suppressor genes, such as the Retinoblastoma susceptibility gene *RB1*, it has been observed that mutations inactivating the tumor suppressive function are due to loss of the wild-type form of the protein. Interestingly, most cancer-causing *TP53* mutations still express a version of the p53 protein. Mutants of p53 generally possess a single amino acid change that has a profound impact on the function of the protein (Vousden and Lane, 2007). The most well studied mutations in *TP53* occur in the DNA binding domain of the protein. Mutations in this region impair the ability of p53 to bind to its target genes and result in the accumulation of mutant p53 (Soussi and Lozano, 2005). Mouse models expressing mutant p53 develop more aggressive cancers and increased metastasis compared to mice lacking p53 all together (Lang et al., 2004; Olive et al., 2004).

Most patients carry somatic mutations of p53, in which mutations spontaneously arise in a certain subset of cells. Germline transmission of p53 mutations has been characterized as Li-Fraumeni syndrome. Individuals with this disease are born with a wild-type and mutant form of p53 in all tissues, and exhibit an extremely high incidence of cancer (Vousden and Lane, 2007). Li-Fraumeni patients have an estimated cancer risk of 90% by the age of 60, highlighting the devastating impacts of *TP53* mutations (Malkin et al., 1990).

### *1.1.2 The story of p53: A brief history*

In 1979, several research groups independently discovered p53 while studying the small DNA tumor virus, SV40. These groups reported that when SV40 large tumor antigen was immunoprecipitated from either SV40 induced tumors or SV40 transformed

cells, a non-viral protein with a molecular mass of roughly 53 kilodaltons was also pulled down with it (Lane and Crawford, 1979; Linzer and Levine, 1979). Shortly after, it was revealed that this same protein was produced at high levels in tumors whereas very low levels were found in normal tissue (Rotter, 1983). This corroborated earlier findings that this protein is abundant in transformed cells and cancer cells, but not in non-transformed cells (DeLeo et al., 1979). By the mid 1980s, it was widely believed that p53 functioned as an oncogene, as p53 expression appeared to correlate with enhanced tumorigenesis (Levine and Oren, 2009).

As more groups began publishing on this protein, each group derived their own name resulting in confusion in this rapidly growing field. In 1983 at the first International p53 Workshop in Oxted, UK, several researchers in the field came together and collectively agreed upon the name 'p53', as this protein appears at a molecular weight of 53 kDa when run on an SDS-polyacrylamide gel. Interestingly, it was later found that the predicted molecular mass is around 43.7 kDa and the overestimation in size is due to the fact that the proline-rich region hinders the migration of the protein. By then, p53 had become the standard nomenclature in the field thus this name for the protein remains today (Levine and Oren, 2009).

As research and technology progressed, many groups began to recognize the discrepancies with the theory that p53 functioned as an oncogene. Varda Rotter's group discovered that the coding sequences for *TP53* were essentially deleted in the cell line HL60, derived from human leukemia (Wolf and Rotter, 1985). Meanwhile the Vogelstein group found that human colorectal tumors did not contain WT p53, and that the *TP53* allele was subject to mutations and/or deletions (Vogelstein et al., 1989). Finlay and Hinds began studying a clone of p53 that could not recapitulate the transforming



phenotype observed with other clones. They began investigating the DNA sequences of p53 clones they had used in the past, as well as clones obtained from other groups. It was discovered that each clone carried a unique sequence, suggesting it was very likely that almost all the clones studied until then carried p53 mutations (Finlay et al., 1988). This was further validated by comparing the sequence of wild type (WT) *Trp53* taken from normal mouse tissue to the *Trp53* sequence taken from mouse tumor tissue. It was found that the mouse tumor tissue did, in fact, contain mutations of p53 and that these mutants were capable of inducing cell transformation whereas the WT p53 did not (Halevy et al., 1991). When WT p53 was overexpressed in the presence of oncogenes such as MYC and HRAS, transformation was suppressed thus validating the tumor suppressive function of p53 (Eliyahu et al., 1989; Finlay et al., 1989).

In order for a gene to be considered a tumor suppressor gene, it typically should meet at least two criteria: 1) humans who harbor germline mutations of this gene should show increased risk of cancer and 2) animal models who lose this gene should display a cancer-prone phenotype (Levine and Oren, 2009). *TP53* meets both these criteria, as germline *TP53* mutations in humans cause Li-Fraumeni syndrome which results in early-onset cancer, and p53 null mice were found to be extremely cancer prone (Donehower et al., 1992; Malkin et al., 1990; Srivastava et al., 1990). All these data, in addition to many other studies, indicated that *TP53* is a tumor suppressor gene and not an oncogene as originally thought.

## 1.2 The structure and function of p53

### 1.2.1 The Structure of p53

The structure of p53 is composed of two transactivation domains located on the intrinsically disordered N-terminal region, adjacent to a conserved proline-rich domain, then followed by the central DNA binding domain (Figure 1.1). The C-terminal region of the protein encodes its nuclear localization signals, and contains the oligomerization domain required for p53 transcriptional activity (Kasthuber and Lowe, 2017). p53 typically exists as a homotetramer (a dimer of dimers), composed of four subunits each containing 393 amino acids. Under normal conditions, p53 is expressed at low levels. Each subunit alone has low thermodynamic stability and will rapidly unfold at body temperature. However, upon stress such as DNA damage, p53 is stabilized by post translational modifications. The primary dimers are stabilized by antiparallel intermolecular  $\beta$ -sheet and helix packing interactions. The two dimers come together via a hydrophobic helix and interact to form a tightly packed tetramer that now has high thermodynamic stability (Canadillas et al., 2006; Cho et al., 1994). The modular structure of p53 along with the regions of intrinsic disorder enable p53 to adopt various conformations, allowing it to interact with a number of other proteins.

In order to bind to DNA, a specific response element is required that is generally composed of two 10 basepair motifs separated by a spacer. The spacer can range from 0-13 basepairs but is typically 0-1 basepairs in most p53 response elements. Different spacer lengths can pose various conformational restraints and generally, increasing spacer length decreases the binding affinity of p53. For example, a 5 basepair spacer would result in two p53 dimers on opposite faces of DNA, whereas a 10 basepair spacer would result in two dimers on the same face of DNA, requiring significant bending of

DNA to enable this interaction (Joerger and Fersht, 2016). *TP53* mutations are generally categorized as contact mutants or conformation mutants, and the majority of tumor causing *TP53* mutations occur in the DNA binding domain. Contact mutants impede p53 from binding to DNA, such as the R273H and R245W mutants, resulting in loss of transactivation of target genes. Conformation mutants disrupt the physical structure of p53, such as V143A and R175H mutants (Raj and Attardi, 2017).

### *1.2.2 Transactivation Domains of p53*

Two transactivation domains (TADs) are located on the N-terminus of p53 and are essential for protein-protein interactions that regulate p53 stability. For example, the histone acetyltransferase p300, or its paralog CBP, binds in this region and promotes stabilization of p53 through the acetylation of lysine residues on the C-terminal region of the protein. This also results in acetylation of nearby histones, enabling chromatin unwinding and transcription of target genes (Miller Jenkins et al., 2015). Various proteins bind to this region, such as TFIID, which is a key component in transcriptional machinery, or RPA, a protein that plays an important role in DNA replication. Proteins involved in p53 regulation also bind to this region, such as MDM2 and MDMX, which both work to inhibit p53 function (Raj and Attardi, 2017).

Under basal conditions, the TAD1/2 domains are intrinsically disordered regions that adopt a helical conformation when bound to another protein. This disordered structure in the unbound state allows p53 to adapt easily, bind to a broad range of proteins and allows for post translational modifications (Miller Jenkins et al., 2015). The transactivation domains are composed of several acidic amino acids that are interspersed with bulky hydrophobic residues, which are key to promote binding to other

proteins. There are also several serines and threonines in the TAD region, which serve as targets of phosphorylation and further affect interactions with binding partners (Raj and Attardi, 2017). For example, phosphorylation of threonine 18 prevents MDM2 from binding to TAD1 of p53, while enhancing the affinity for many domains of CBP/p300 (Lee et al., 2010; Teufel et al., 2009). Phosphorylation at serine 46 and threonine 55 enables subunits of TFIIH to bind (Di Lello et al., 2006). These examples highlight how modification of the transactivation domains via phosphorylation can modulate p53 function in response to stress (Joerger and Fersht, 2016).

The two transactivation domains (TAD) are both necessary for full p53-mediated tumor suppression and target gene transactivation, however there are differences with regards to how certain mutations in each TAD affects gene expression (Hafner et al., 2019). Brady et al. demonstrated that creating a knock-in mouse with a mutation in the TAD1 domain (L25Q, W26S) severely impairs transactivation of the majority of p53 dependent genes (Brady et al., 2011). Interestingly, the TAD1 mutant is still capable of tumor suppression despite being unable to induce apoptosis or cell cycle arrest. When the TAD2 domain is mutated (F53Q, F54S), no major changes in the transcriptional activity of p53 were found and at a glance this synthetic mutant appears to retain the functions of WT p53. However, when both TAD1 and TAD2 are mutated, p53 loses all transcriptional function and can no longer inhibit tumorigenesis, resembling a p53-null phenotype (Brady et al., 2011). It is believed that these two domains act in a synergistic fashion, rather than an additive fashion, and are both required for p53 to prevent oncogenesis (Raj and Attardi, 2017).

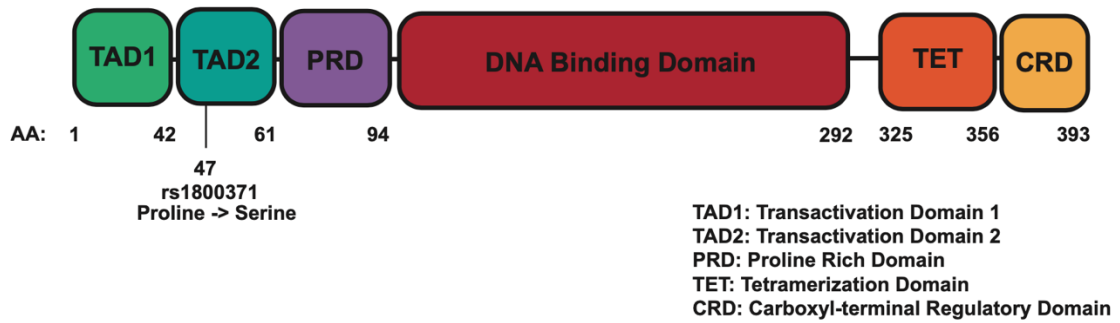


**Figure 1.1: Domains of p53.**

Structural organization of p53, with amino acid residue numbers labeled from amino-terminus to carboxyl-terminus. The P47S variant occurs in TAD2.

### 1.2.3 p53 Activation

The p53 tumor suppressor protein has been dubbed the “Guardian of the Genome”. It acts as a transcription factor and serves as a master regulator of hundreds of target genes. Several transcription independent functions of p53 have also been identified, for example p53 can promote apoptosis by interacting with Bcl-2 and Bcl-XL in the mitochondria (Chipuk et al., 2004; Tomita et al., 2006). Additionally, p53 can directly or indirectly repress transcription of certain genes such as *SLC7A11*, *GLUT1* and *Nanog* (Kaiser and Attardi, 2018).

There are several cellular stresses that can activate p53, such as DNA damage, replication stress, oncogene activation, hypoxia, telomere erosion and nutrient deprivation. Depending on the stress encountered, p53 will induce the appropriate response that will halt the accumulation of oncogenic mutations and ultimately prevent

the initiation and spread of cancer (Figure 1.2). If damage to the cell is beyond repair, p53 can eliminate the cell completely through a form of cell death, such as apoptosis or ferroptosis. If the cell can be rescued, p53 can arrest the growth of a cell, presumably to give the cell enough time to correct the damage that has been done and resume normal proliferation after the mutation has been repaired (Kasthuber and Lowe, 2017).

p53 controls a diverse range of responses, thus it is important to keep in mind that the activation and function of p53 can be context dependent. For example, the response of p53 depends on cell type, differentiation state, the activating stress, epigenetic state, and tissue microenvironment. Post-translational modifications are also important to consider when assessing p53 activity, as specific post-translational modifications can alter the affinity of p53 for different target genes and trigger various responses. For example, phosphorylation of the Ser46 site of p53 is key event necessary for stimulating apoptosis (Smeenk et al., 2011). There are several other modifications such as SUMOylation, glycosylation, acetylation, and prolyl isomerization that occur throughout the p53 protein, and result in modifying protein stability and target gene binding (Kasthuber and Lowe, 2017). These multiple levels of control enable p53 to selectively regulate different sets of target genes to ensure the cell will have the optimal response to the specific stress that is encountered.

#### *1.2.4 Canonical functions of p53*

The most well-studied functions of p53 include controlling cell cycle arrest, senescence and apoptosis. Upon DNA damage in the cell, DNA damage response kinases phosphorylate and stabilize p53, enabling p53 to turn on the appropriate downstream target genes (Williams and Schumacher, 2016). Initially p53 was found to

halt proliferation in response to DNA damage by inducing a brief G1 cell cycle arrest, giving the cell time to correct any mutations that could lead to tumorigenesis (Kastan et al., 1991). It was found that *CDKN1A* is key p53 target gene that drives this induced cell cycle arrest, as this gene encodes the cyclin dependent kinase inhibitor p21 (Brugarolas et al., 1995; Deng et al., 1995). When damage is irreparable and the cell must permanently shut down, p53 can induce senescence through target genes such as *CDKN1A/p21*, *PAI-1* or *PML*. Alternatively, p53 can halt proliferation by inducing apoptosis through target genes such as *PUMA* and *NOXA* (Kaiser and Attardi, 2018).

Though apoptosis, cell cycle arrest and senescence are widely regarded as the predominant functions of p53, many studies have recently emerged demonstrating that p53 can suppress cancer through other pathways. These other pathways regulated by p53 include autophagy, metabolism, ferroptosis, cellular plasticity and pluripotency, ROS control, inflammation, the epithelial-to-mesenchymal (EMT) transition, and angiogenesis (Kastenhuber and Lowe, 2017).

Many studies have shown p53 promotes differentiation of stem cells and suppresses the programming of somatic cells into pluripotent stem cells (Hong et al., 2009; Marion et al., 2009). If cells exhibit less plasticity and are instead more differentiated, it will result in a less plastic phenotype in young cancer cells and prevent proliferation of cancer stem cells. There is also evidence that p53 opposes EMT and restricts cancer cell invasion and metastasis to other sites. It has been shown that p53 downregulates transcription factors such as Snail1, Slug and Zeb, that are all crucial for EMT (Kim et al., 2011; Wang et al., 2009). Several *in vitro* studies have demonstrated that p53 plays a role in impeding motility and invasiveness of various cancer cell types (Kaiser and Attardi, 2018). p53 has also been indicated in playing a role in immune

response, by activating a subset of genes involved in immune cell recruitment and surveillance. For example, in liver carcinoma it has been shown that p53 activation leads to the transcription of cytokines such as *Csf1* and *Il15*. The activation of these cytokines will promote the recruitment of neutrophils, natural killer cells and macrophages, which in turn will halt tumorigenesis (Xue et al., 2007).

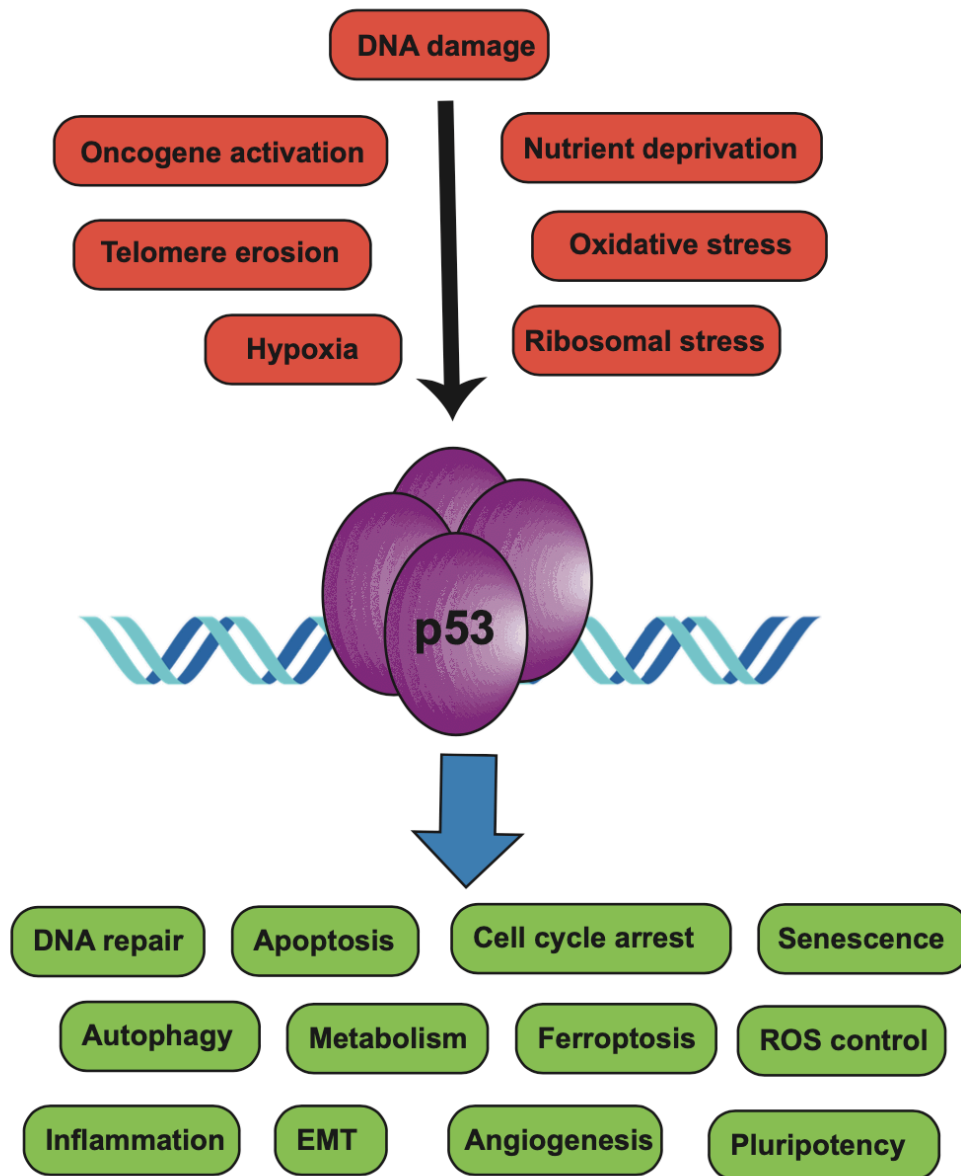




## **Figure 1.2: p53 activation and response.**

p53 is activated by various stresses, indicated by the red words, and responds by turning on the appropriate downstream response, as depicted by the green words.

### **1.3 Emerging roles of p53**

#### *1.3.1 p53 and metabolism*

A major function of p53 that has been gaining momentum in recent years is the ability of p53 to respond to metabolic stress and limit cell proliferation and growth. Metabolic stresses that activate p53 tend to be more transient, such as hypoxia or low nutrient availability. These stresses require a more adaptive response from the cell, rather than complete shutdown of the cell that tends to occur when a genotoxic stress is encountered (Berkers et al., 2013). A common feature of cancer cells is the ability to reprogram metabolic pathways. Doing so enables a cancer cell to survive under adverse conditions such as low nutrients or low oxygen, promotes the activation of anabolic pathways, and can limit oxidative damage to the cell (Vousden and Prives, 2009).

Generally, p53 will oppose tumorigenesis by increasing catabolism and decreasing proliferation. Glucose is one of the primary sources of energy for the cell and cancer cells exhibit increased glucose consumption and increased glycolysis. p53 has been shown to transcriptionally repress two of the major glucose transporters in the cell, *GLUT1* and *GLUT4* (Schwartzberg-Bar-Yoseph et al., 2004). It has been shown to decrease glycolysis by inducing the transcription of *RRAD* and *TIGAR*, which are both known inhibitors of glycolysis (Bensaad et al., 2006; Zhang et al., 2014). While p53 generally acts to suppress glycolysis, it is believed to increase oxidative phosphorylation.

p53 transactivates the *SCO2* gene, which encodes a protein that facilitates the transfer of electrons during mitochondrial respiration (Matoba et al., 2006). p53 also transactivates *GLS2*, which encodes an enzyme that catalyzes the conversion of glutamine to glutamate, enabling glutamate to be used as an alternate energy source in the mitochondria (Hu et al., 2010).

There are also transcription-independent functions of p53 that regulate metabolism, as p53 can bind to and inhibit glucose-6-phosphate dehydrogenase (G6PDH). G6PDH is an enzyme that catalyzes the rate limiting step of the pentose phosphate pathway, using a product of glycolysis as a substrate. The pentose phosphate pathway serves as a major source of NADPH generation. NADPH serves as a key reducing agent for many reactions such as glutathione generation and de novo lipid synthesis. The pentose phosphate pathway is found to be upregulated in cancer cells, thus by inhibiting G6PDH, p53 is able to suppress cancer cell proliferation (Jiang et al., 2011).

It is important to note that p53 can perform opposing functions on the same metabolic process depending on the cell type (Kasthuber and Lowe, 2017). Studies have clearly demonstrated that p53 inhibits glycolysis in breast and lung cells by repressing the expression of glycolytic enzymes (Kim et al., 2013) or by impeding glucose uptake (Zhang et al., 2013). However, in muscle cells p53 induces glycolytic enzymes resulting in increased glycolysis (Kruiswijk et al., 2015). Thus, when assessing the role of p53 in metabolism, it is necessary to consider the context such as the stress encountered, tissue location and other biochemical pathways that have been activated (Figure 1.3).

### 1.3.2 p53 and mTOR

mTOR (mechanistic target of rapamycin), is a serine/threonine kinase that serves as a master regulator of metabolism and cell growth, and functions by phosphorylating its downstream targets. This pathway is activated by environmental signals such as nutrients and growth factors, thus levels of glucose and amino acids play an important role in regulating mTOR activity. In addition to proliferation, mTOR is known to regulate translation, ribosome biogenesis, autophagy, and cytoskeletal reorganization (Liu and Sabatini, 2020b). However, heightened mTOR activity can also contribute to oncogenesis thus a delicate balance must be maintained between the mTOR and p53 pathways in order to balance the requirement for normal cell growth and stress response (Hasty et al., 2013).

p53 target genes such as *PTEN*, *LKB1* and *TSC2* that are also tumor suppressors have been found to be negative regulators of mTOR (Shaw et al., 2004). The TSC2 subunit of the TSC1:TSC2 complex serves as a GTPase-activating protein for the protein Rheb, which is a GTPase known to activate mTOR. Through this interaction, TSC2 binds to and inhibits Rheb, thereby decreasing mTOR activity (Corradetti and Guan, 2006; Hay and Sonenberg, 2004). AMPK-activated protein kinase (AMPK) is an enzyme that monitors the ATP/AMP ratios in the cell and is activated under low nutrient levels or energy stress (Feng et al., 2007; Feng et al., 2005). When nutrient levels fall below a certain threshold, AMPK will phosphorylate and thereby activate TSC2 which then shuts down mTOR activity. AMPK $\beta$ 1 is a subunit of the AMPK complex which plays an important role in regulating AMPK activity and localization within the cell (Warden et al., 2001). It has been shown that AMPK $\beta$ 1 is a direct p53 target gene, further highlighting how p53 negatively regulates the mTOR pathway (Feng et al., 2007). AMPK

can also activate p53 by inducing phosphorylation of p53 at the serine 15 site (Jones et al., 2005). Sestrin1 (*SESN1*) and Sestrin 2 (*SESN2*) are two p53 target genes that are generally induced upon DNA damage and oxidative stress; however, both have also been shown to inhibit mTOR signaling. These genes activate AMPK, which in turn will phosphorylate TSC2 and stimulate its GAP activity, ultimately resulting in the inhibition of mTOR. *In vivo* studies confirmed that Sestrin2-deficient mice are unable to inhibit mTOR signaling upon genotoxic stress (Budanov and Karin, 2008). Taken together, these studies demonstrate that there are multiple nodes connecting the p53 pathway to the mTOR pathway and how a homeostasis must be maintained for optimal cell function.

### 1.3.3 p53 regulates lipid metabolism

Though p53 is well known for regulating metabolic pathways commonly studied in cancer, such as glycolysis and the TCA cycle, p53 has also been shown to play a major role in mediating lipid metabolism (Berkers et al., 2013). Wild-type and mutant p53 regulate lipid metabolism on both the transcriptional level and on the protein-protein interaction level (Parrales and Iwakuma, 2016). It is believed that p53 enhances fatty acid oxidation while inhibiting fatty acid synthesis, thus acting as a negative regulator of lipid synthesis. Fatty acid oxidation involves the breakdown of fatty acids in the mitochondria; this is one mechanism cells use to produce substrates such as NADH, acetyl-CoA and FADH<sub>2</sub>, which are subsequently used in the TCA cycle and electron transport chain (Berkers et al., 2013). Sanchez-Macedo and colleagues demonstrated that carnitine palmitoyltransferase 1C (CPT1C), an enzyme that aids in the transport of activated fatty acids to the mitochondria, is expressed in a p53-dependent manner both *in vitro* and *in vivo* and that Cpt1c deficient mice displayed delayed tumor development and higher survival rates (Sanchez-Macedo et al., 2013). Lipin 1 (*LPIN1*) is a p53 target

gene necessary for proper adipocyte development and was found to be induced under low nutrient conditions (Assaily et al., 2011). Using a series of gain-of-function and loss-of-function experiments, Finck and colleagues showed that LPIN1 interacts with PGC1-alpha, another known p53 metabolic target, and that this interaction activates the expression of other genes involved in promoting fatty acid oxidation (Finck et al., 2006).

The sterol regulatory element-binding proteins (SREBP) family are a family of transcription factors that modulate the expression of genes involved in cholesterol, fatty acid, triacylglycerol and phospholipid synthesis, and is often upregulated in many types of cancer (Ettinger et al., 2004; Guo et al., 2009; Parrales and Iwakuma, 2016). Deleting p53 in ob/ob mice led to increased levels of SREBP-1 and downstream targets, meanwhile ob/ob mice expressing p53 displayed low levels of SREBP-1 and downstream targets, indicating that p53 represses SREBP-1 (Yahagi et al., 2003).

A microarray analysis of human liver-derived cells identified phospholipid transfer protein (*PLTP*), ATP binding cassette A12 (*ABCA12*) and carboxyl ester lipase (*CEL*) as three p53 target genes that all play a role in lipid transport (Goldstein et al., 2012). *PLTP* is a secreted molecule bound to high-density lipoprotein (HDL) that transfers phospholipids from very low-density lipoproteins (VLDL) and low-density lipoproteins (LDL) to HDL particles in the liver, where reverse cholesterol transport occurs (Masson et al., 2009). Both *ABCA12* and *ABCA5*, another p53 target gene, have been shown to mediate cholesterol efflux and both genes have been implicated in atherosclerosis (Fu et al., 2013; Ye et al., 2010). *CEL* is an enzyme that hydrolyzes dietary lipids into fatty acids and cholesterol and also plays a role in HDL uptake in the liver (Goldstein et al., 2012). It is evident that p53 plays an important role in lipid shuttling as it regulates a variety of genes that mediate lipid transport (Goldstein and Rotter, 2012). Though there

is a clear role of p53 in mediating several genes that are essential for lipid metabolism, many of these genes have not been directly shown to be involved in suppressing tumor formation. The exact mechanism for how and when p53 induces many of these genes remains to be uncovered, for example it is not known if p53 activates these genes in response to metabolic stress or if basal levels of p53 are required to maintain lipid homeostasis (Goldstein and Rotter, 2012). Some may argue that this implies the role of p53 extends beyond a tumor suppressor, however one could also postulate that there are other tumor suppressor functions of p53 involving lipids that have not been fully explored.

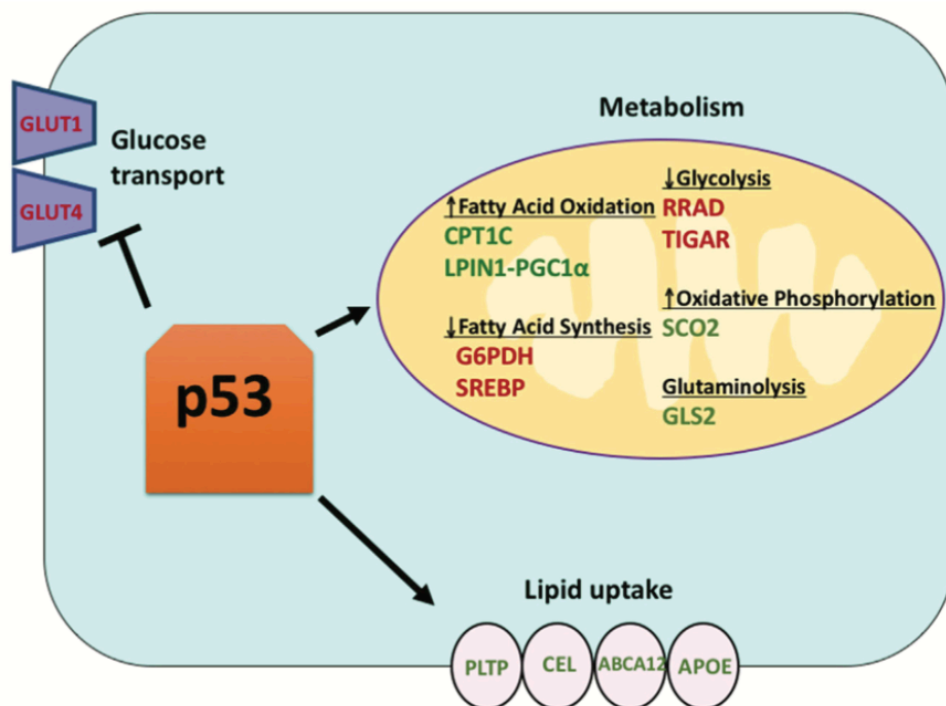


**Figure 1.3: Role of p53 in metabolism.**

The role of WT p53 in metabolism. Genes positively regulated by p53 are shown in green, genes negatively regulated by p53 are shown in red. p53 inhibits glucose transport, glycolysis and fatty

acid synthesis while it promotes lipid uptake, fatty acid oxidation, oxidative phosphorylation and glutaminolysis.

#### *1.3.4 Ferroptosis*

In 2012, Dixon and colleagues discovered a novel form of regulated cell death called ferroptosis, which is best described as an iron-dependent, caspase-independent form of cell death resulting from the accumulation of lipid reactive oxygen species (Dixon et al., 2012; Yang et al., 2014). This process is driven by the inactivation of glutathione peroxidase 4 (GPX4), an enzyme that is responsible for converting lethal lipid hydroperoxides to non-toxic lipid alcohols and requires glutathione to function (Yang et al., 2014). Ferroptosis is commonly induced using either erastin or 1S,3R-RSL3 (hereafter referred to as RSL3). Erastin inhibits the cystine/glutamate antiporter SLC7A11, which results in depleted glutathione and subsequent inactivation of GPX4. RSL3 directly binds to and inhibits GPX4, resulting in the induction of ferroptosis (Dixon et al., 2012; Jiang et al., 2015; Yang et al., 2016).

It is believed that peroxidation of polyunsaturated fatty acids (PUFAs) is the stimulus that drives ferroptosis. PUFAs contain bis-allylic protons that can easily be abstracted and produce radicals that will react with oxygen, creating more radicals and resulting in a chain reaction of lipid ROS (Yang et al., 2016). The exact mechanism of cell death remains unknown, however one hypothesis is that the lipid damage leads to the destruction of the cell membrane (Magtanong et al., 2016). It has been postulated that ferroptosis could be another mechanism of tumor suppression by eliminating cells that are nutrient deprived or have been exposed to an environmental stress or infection. Death by ferroptosis can be prevented by suppressing lipid peroxidation, which can be

accomplished by using lipophilic antioxidants such as ferrostatin-1 or Vitamin E, as well as by using iron chelators or depleting PUFAs (Stockwell et al., 2017).

### *1.3.5 The role of p53 in the regulation of ferroptosis has been controversial*

Wei Gu's research group developed a mouse model in which three normally acetylated lysine residues in the DNA binding domain of p53 were mutated to arginine, hereafter referred to as the 3KR model. The 3KR mouse lost the ability to undergo apoptosis, cell cycle arrest and senescence, and failed to transactivate the majority of p53 target genes. Interestingly, this mouse model did not develop cancer implying p53 has an alternate mechanism of tumor suppression (Li et al., 2012). It was found that the mutant p53 3KR fully retains the ability to undergo ferroptosis and regulate cystine metabolism by repressing *SLC7A11* expression, thus explaining the observed phenotype. When wild-type and 3KR MEFs were treated with the ferroptosis inducer, erastin, almost 50% cell death was observed whereas p53 null MEFs exhibited only 20% cell death, indicating that p53 sensitizes cells to ferroptosis. Perhaps the most compelling piece of data that ferroptosis is key to p53 function was the phenotype of *p53<sup>3KR/3KR</sup>Mdm2<sup>-/-</sup>* embryos treated with ferrostatin-1. Prior studies have demonstrated that apoptosis, cell cycle arrest and senescence cause lethality in *p53<sup>+/+</sup>Mdm2<sup>-/-</sup>* yet interestingly, the *p53<sup>3KR/3KR</sup>Mdm2<sup>-/-</sup>*, which retains the ability to undergo these processes, were still unable to bear offspring. After treating the *p53<sup>3KR/3KR</sup>Mdm2<sup>-/-</sup>* embryos with ferrostatin-1, it was found that the embryos were significantly larger with more well-developed physiology compared to the untreated embryos, thus demonstrating p53 mediated ferroptosis is what drives embryonic lethality in the 3KR model (Jiang et al., 2015).



An additional acetylation site was identified at K98, and a 4KR mouse model was developed. Mutating this single residue from a lysine to arginine had very little effect on p53 mediated transactivation of downstream targets, however mutating this residue in addition to the three lysine residues in the 3KR model completely ablated the ability of p53 to regulate its metabolic targets, including SLC7A11. Unlike the 3KR model, the 4KR model is unable to suppress tumor growth in mouse xenograft models and lost the ability to induce ferroptosis (Wang et al., 2016). Taken together, these results indicate that p53 plays an important role in mediating ferroptosis and that p53 acetylation can dictate ferroptotic responses and tumor suppression.

Other p53 target genes associated with ferroptosis include *PTGS2*, *SAT1* and *GLS2* (Gao et al., 2015; Ou et al., 2016; Yang et al., 2014). *PTGS2* is significantly upregulated upon ferroptotic induction and is often used as a marker of ferroptosis, however the exact role and function remain unclear (Yang et al., 2014). Activation of *SAT1* was found to sensitize cells to ferroptosis and induce lipid peroxidation through regulating the lipoxygenase ALOX15 (Ou et al., 2016). *GLS2* converts glutamine to glutamate and knockdown of *GLS2* was found to completely inhibit ferroptosis in MEFs (Gao et al., 2015; Jennis et al., 2016).

Though many studies suggest that p53 plays a role in enhancing ferroptosis sensitivity, several groups have shown that under certain contexts, p53 can actually suppress ferroptosis. In work by Xie et al., the authors demonstrate that p53 functions in a transcription-independent manner by binding to and sequestering dipeptidyl-peptidase-4 (DPP4). This results in nuclear accumulation of DPP4 and renders it inactive. Upon loss of p53, DPP4 is able to localize to the plasma membrane and facilitate lipid peroxidation, ultimately contributing to ferroptotic cell death (Xie et al., 2017).

Tarangelo and colleagues also published evidence that p53 may negatively regulate ferroptosis (Tarangelo et al., 2018). It was found that pre-treating cells with Nutlin-3, a compound used to stabilize p53, for 48 hours prior to treating cells with a ferroptosis inducer delayed the onset of ferroptosis in several cell types. The delayed onset of ferroptosis was found to depend on *CDKN1A* (encoding p21), a critical p53 transcriptional target. The mechanism through which p21 delays ferroptosis has yet to be elucidated, however cell cycle arrest due to CDK 4/6 inhibition and enhanced NRF2 activity were excluded as a part of this mechanism. It was found that there is an increase in glutathione production during the pre-treatment phase, and it is believed that the conservation of intracellular glutathione is another contributing factor for reduced ferroptosis sensitivity. The authors concluded that the p53-p21 axis enables cancer cells to survive under conditions of metabolic stress, such as cystine deprivation, by suppressing the onset of ferroptosis (Tarangelo et al., 2018).

Work by the Prives group has shown that MDM2 and MDMX, known negative regulators of p53 activity, promote ferroptosis in a p53-independent manner. The MDM2-MDMX complex was found to alter the lipid profile of cells through regulating PPAR $\alpha$  activity and suppressing the antioxidant response of cells. This work supports the premise that ferroptotic regulation extends beyond the p53 axis (Venkatesh et al., 2020).

A role for p53 in the regulation of metabolism is quite clear: WT p53 limits glucose metabolism and lipid synthesis, while mutant p53 appears to do the opposite. The contribution of this activity to tumor suppression by p53, and to the ability of mutant p53 to drive tumor progression, remains to be unequivocally proven. However, the role of p53 in the regulation of ferroptosis, and the contribution of this function to tumor suppression is even less clear. While compelling data from mouse models support the

premise that p53 regulates the sensitivity of cells to ferroptosis, this may be restricted to the ability of basal p53 to suppress spontaneous tumor development, and in oncogene-stressed mouse models it is clear that senescence and apoptosis play the predominant role. Similarly, p53 may regulate ferroptosis sensitivity in a cell type-specific manner. More studies in animal models, with attention to ferroptosis in different tissues, need to be done to more fully understand the role of p53 in ferroptosis, and ferroptosis in tumor suppression. Additionally, a clearer idea of what p53-target genes play a role in sensitivity to ferroptosis needs to be attained (Figure 1.4).

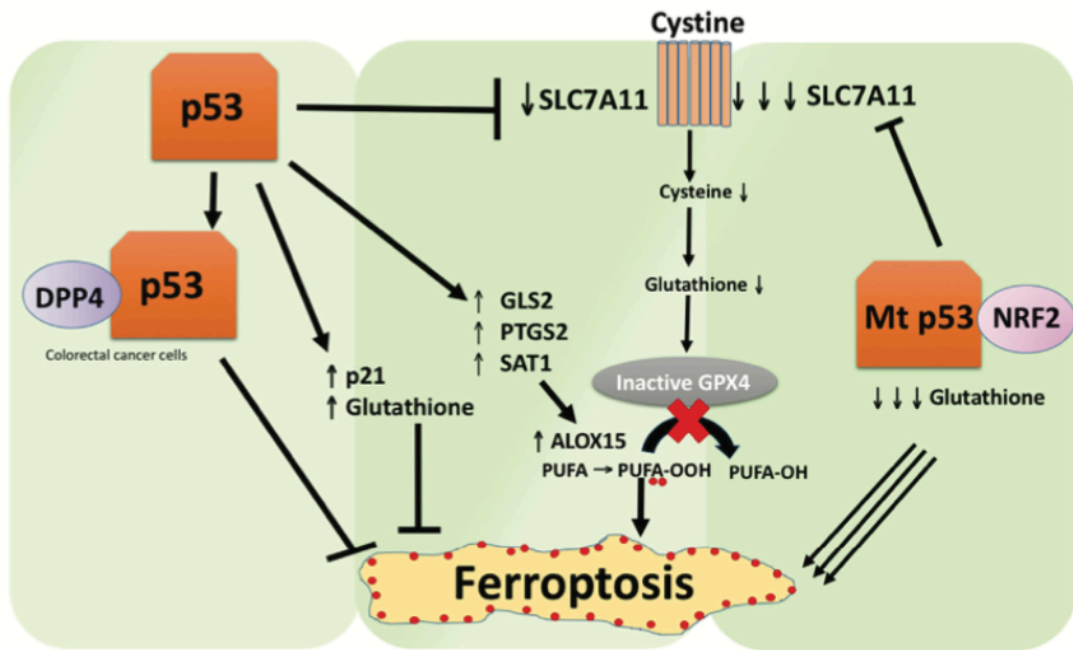


**Figure 1.4: Various roles of p53 in ferroptosis.**

Ferroptosis is driven by inhibition of GPX4, the enzyme that catalyzes the conversion of polyunsaturated fatty acids containing peroxides (depicted by red dots) to alcohols. Depending on the context, p53 can suppress ferroptosis or promote ferroptosis. Mutant p53 sensitizes cells to ferroptosis even more than WT p53.

### 1.3.6 The African-specific P47S variant

A naturally occurring polymorphism in *TP53* was reported in TAD2 at codon 47, in which a proline is replaced by a serine (P47S, rs1800371) (Felley-Bosco et al., 1993). This SNP, hereafter referred to as S47, was reported over two decades ago and is found predominantly in people of African and African American descent, with a frequency of about 6-8% in Africans and 1.5% in African Americans (Jennis et al., 2016). This SNP is also present in Hispanic populations and has not been reported in Caucasian Americans. Our group showed that women of African ancestry who carried the S47 allele had a higher risk of developing pre-menopausal breast cancer, with a per allele odds ratio of 1.72 (Murphy et al., 2017). It is believed that there may be a correlation between this SNP and other types of cancer in African descent populations; however due to the dearth of large sample or data sets from African descent populations, such associations await determination.

Interestingly, this polymorphism is adjacent to a key phosphorylation site in p53 located at the Serine 46 residue. The Serine 46 site is phosphorylated by proline directed kinases including p38 MAPK, HIPK2 and DYRK, and this phosphorylation event has been shown to be very important for p53's ability to induce apoptosis (Bulavin et al., 1999; Felley-Bosco et al., 1993; Hofmann et al., 2002). *In-vitro* kinase assays revealed that cells containing the S47 variant are impaired for phosphorylation at the Ser46 site by proline directed kinases, such as purified p38MAPK. It was also found that cells containing this variant have a 5-fold decreased ability to undergo cell death when compared to cells containing WT P47 form of p53 (Li et al., 2005).

To further study the biological consequences of this variant, our lab generated a knock-in mouse model using a humanized p53 knock-in (Hupki) containing the S47

allele. This humanized version of p53 replaces mouse exons four through nine with the corresponding human p53 exons (codon 32-332). Mice with the homozygous S47 allele spontaneously developed cancer between 12 to 18 months of age, and heterozygous mice were also found to be susceptible to cancer. The most common cancer type observed was hepatocellular carcinoma, however B-cell lymphoma, histiocytic sarcoma, colorectal carcinoma and pancreatic ductal adenocarcinoma were also observed. The S47 mouse phenotype is distinct from Li-Fraumeni mouse models generated by Lozano and Jacks, which develop more epithelial cancers (Lang et al., 2004; Olive et al., 2004). It is also very distinct from the p53 knockout mouse, which develops T cell lymphoma and sarcoma (Basu and Murphy, 2016).

Both WT and S47 cells exhibit similar transcriptional function, however gene expression studies revealed that S47 is impaired in its ability to transactivate *Gls2* and *Sco2*, two genes that play a key role in cellular metabolism. Cells containing the S47 variant are also found to have impaired apoptosis when confronted with various genotoxic stresses, particularly cisplatin. In addition to a defect in apoptosis, it was found that S47 cells are markedly resistant to ferroptosis (Jennis et al., 2016). The cystine/glutamate antiporter *SLC7A11* plays a key role in regulating ferroptosis, as cystine is a precursor to cysteine and glutathione. Excess glutamate or treatment with erastin prevents cystine uptake, leading to decreased accumulation of intracellular cysteine and glutathione, resulting in ferroptotic cell death. WT p53 has been shown to repress *SLC7A11*, thereby preventing the import of cystine and inducing ferroptosis (Jiang et al., 2015). We have observed that the S47 variant is impaired for repression of *SLC7A11*, and ChIP studies have indicated decreased binding of the S47 protein at the p53 binding site on the *SLC7A11* promoter region. S47 MEFs were found to be 27-fold

resistant to erastin-induced ferroptosis, and S47 LCLs were found to be 19-fold resistant to RSL3-induced ferroptosis. *Ptgs2* transactivation and GPX4 degradation, both key markers of ferroptotic induction, were shown to be impaired in S47 cells. This significant ferroptotic defect is believed to be the primary reason for impaired tumor suppression in S47 mice and highlights the role of p53 in regulating ferroptosis sensitivity as a mechanism of tumor suppression (Jennis et al., 2016) (Figure 1.5).

The ferroptotic defect in S47 cells can be attributed to elevated levels of intracellular antioxidants in S47 (Leu et al., 2019). Metabolomic analyses revealed S47 cells have increased levels of low molecular weight thiols including Coenzyme A (CoA) and glutathione (GSH). Increased levels of GSH were also observed in S47 livers, confirming that this phenotype has *in vivo* relevance. Antioxidants such as CoA and GSH affect the redox environment of the cell, particularly affecting cysteine residues in proteins. There are several proteins that are sensitive to redox regulation and can adopt an altered conformation when this redox state is altered. p53 contains conserved cysteine residues at or near the DNA binding domain, and under normal conditions, the reduced cysteine residues enable tetramerization and subsequent activation of the p53 protein. However, upon oxidation, the cysteine residues will form bonds with other thiol groups and prevent proper oligomerization of the protein. It was found that the higher levels of CoA and GSH feedback on p53, directly impacting structure and function of the protein. By modulating the redox state using reagents such as diethyl maleate or exogenous CoA, it is possible to manipulate p53 conformation and ferroptosis sensitivity (Leu et al., 2019; Leu et al., 2020). These findings are broadly consistent with data by Tarangelo, showing that conservation of glutathione is correlated with ferroptosis inhibition (Tarangelo et al., 2018).

Singh et al. demonstrated that the defect in ferroptosis results in iron accumulation in S47 macrophages, which ultimately results in more severe bacterial pathogenesis and greater susceptibility to *Listeria* infection. However, it was found that mice bearing the S47 variant show an improved response to malarial toxin hemozoin, suggesting that S47 might have provided an advantage in sub-Saharan Africa where there is a high risk of malaria. The ferroptotic defect has also been found to contribute to a higher risk of hereditary hemochromatosis in African Americans who carry this SNP (Singh et al., 2020).

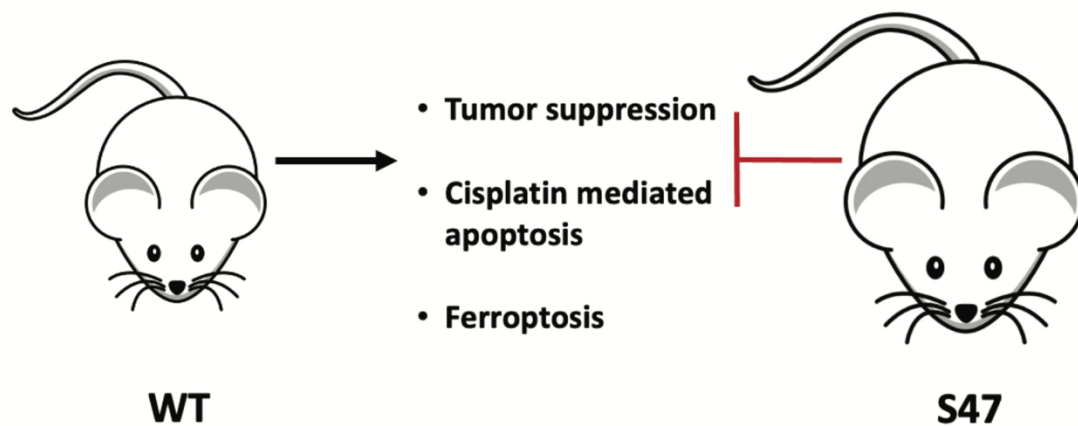


**Figure 1.5: The S47 mouse.**

Unlike mice bearing WT p53, the S47 mouse is impaired for tumor suppression, cisplatin mediated apoptosis and ferroptosis.

## 1.4 Thesis objectives

The aim of this dissertation is to explore the function of the S47 variant of *TP53* and to use this variant as a tool to better understand tumor suppression and ferroptosis. In Chapter 2, I describe the unique metabolic phenotype that was observed in S47 mice. I found that S47 cells and mice exhibit increased mTOR activity, ultimately stemming from an impaired protein-protein interaction due to the altered redox state. Our data support the premise that this increase in mTOR activity contributes to the increased size and superior metabolic efficiency observed in S47 mice. We hypothesize that the superior metabolic efficiency might have once provided an evolutionary fitness advantage, which could explain why the S47 variant remains in the population despite predisposing carriers to cancer. In Chapter 3, I describe how I used the S47 variant to identify a p53 target gene, *PLTP*, as a negative regulator of ferroptosis in liver cancer cells. An RNA-Seq experiment comparing WT and S47 cells led us to identify *PLTP* as significantly repressed in S47. I performed a series of assays to show that this gene contributes to ferroptosis resistance and demonstrate that the mechanism is due to increasing lipid storage, which sequesters lipids and prevents them from undergoing peroxidation at the cell membrane. To conclude, Chapter 4 provides a summary of both studies and discusses avenues for further studies on this work.



## CHAPTER 2: Increased mTOR Activity and Metabolic Efficiency Found in the P47S Variant of *TP53*

This chapter has been adapted from the following manuscript:

Gnanapradeepan K, Basu S, Barnoud T, Leu JIJ, Good M, Lee J, Quinn WJ, Kung CP, Ahima R, Baur J, Wellen K, Schug Z, George DL and Murphy ME.

Increased mTOR activity in mice with the tumor prone S47 variant of p53 confers enhanced size, metabolism and fitness. *eLife* (2020);9:e55994

### 2.1 Abstract

The Pro47Ser variant of p53 (hereafter S47) exists in African-descent populations and is associated with increased cancer risk in humans and mice. This variant shows impaired repression of the cystine importer *Slc7a11*. Consequently, S47 cells possess increased cysteine and glutathione (GSH) accumulation compared to cells with wild type p53. In this study we show that mice containing the S47 variant have increased mTOR activity, increased oxidative metabolism, larger size, and improved metabolic efficiency. Mechanistically, we show that there is increased association between mTOR and its positive regulator Rheb in S47 cells, due to altered redox state of GAPDH, which normally binds and sequesters Rheb. Compounds that decrease glutathione in S47 cells normalize GAPDH-Rheb complex formation and mTOR activity. The enhanced metabolic efficiency may have been selected for in early Africa, making the S47 variant one of a growing number of cancer-predisposing genetic variants that possesses other positive, potentially selectable attributes.

## 2.2 Introduction

The p53 tumor suppressor protein serves as a master regulator of the cellular response to intrinsic and extrinsic stress. Mutations in the *TP53* gene occur in more than 50% of human cancers, and this gene is well-known as the most frequently mutated gene in cancer (Hollstein et al., 1991). p53 works to suppress uncontrolled cellular growth and proliferation through various pathways including apoptosis, senescence, cell cycle arrest and ferroptosis (Stockwell et al., 2017; Vousden and Prives, 2009). More recently a role for p53 in the control of metabolism has emerged. The metabolic functions of p53 include the regulation of mitochondrial function, autophagy, cellular redox state, and the control of lipid and carbohydrate metabolism; for review see (Berkers et al., 2013; Gnanapradeepan et al., 2018).

As an integral part of its control of metabolism, p53 negatively regulates the activity of mTOR (mammalian target of rapamycin), which is a master regulator of metabolism in the cell. mTOR is a serine-threonine protein kinase that is stimulated by mitogenic signals, and phosphorylates downstream targets that in turn regulate protein synthesis and cell growth (Ben-Sahra and Manning, 2017). mTOR exists in two distinct signaling complexes: mTORC1 is primarily responsible for cell growth and protein synthesis, while mTORC2 plays roles in growth factor signaling, cytoskeletal control and cell spreading (Liu and Sabatini, 2020a). Not surprisingly, mTOR activity is frequently upregulated in a diverse range of cancers. p53 negatively regulates the mTOR pathway in part through transactivation of the target genes *PTEN*, *TSC2*, *PRKAB1* and *SESN1/SESN2* (Budanov and Karin, 2008; Feng et al., 2005). The regulation of mTOR

by p53 is believed to couple the control of genome integrity with the decision to proliferate (Hasty et al., 2013).

*TP53* harbors several functionally impactful genetic variants or single nucleotide polymorphisms (SNPs) (Basu et al., 2018; Jennis et al., 2016; Kung et al., 2016). A naturally occurring variant in *TP53* exists at codon 47, encoding serine instead of a proline (Pro47Ser, rs1800371, G/A). This variant exists predominantly in African-descent populations and occurs in roughly 1% of African Americans and 6% of Africans from sub-Saharan Africa (Murphy et al., 2017). The S47 variant is associated with increased risk for pre-menopausal breast cancer in African American women (Murphy et al., 2017). In a mouse model, the S47 mouse develops markedly increased incidence of spontaneous cancer, particularly hepatocellular carcinoma (Jennis et al., 2016). This variant is likewise defective in the regulation of the small subset of p53 target genes that play roles in ferroptosis sensitivity, including the cystine importer *SLC7A11*. As a result, increased levels of cysteine and glutathione (GSH) accumulate in cells from S47 humans and mice (Jennis et al., 2016; Leu et al., 2019). More recently, we showed that the ferroptotic defect in S47 mice leads to iron accumulation in their livers, spleens and macrophages. We also showed that the S47 variant is positively associated with markers of iron overload in African Americans, such as increased levels of saturated transferrin (Singh et al., 2020).

An emerging paradigm in the cancer literature is that tumor-predisposing genetic variants may paradoxically provide selection benefit to individuals, thus potentially explaining the frequency of these damaging alleles in the population. As an example, women carrying tumor-predisposing mutations in the *BRCA1* gene tend to be physically larger and show increased fertility (Smith et al., 2012). Here-in we show that mice

carrying a knock-in S47 allele in a pure C57Bl/6 background show increased size, lean content (muscle), and metabolic efficiency, relative to littermate mice with WT p53. We report that mouse and human S47 cells show a significant increase in mTOR activity, due in part to increased mTOR-Rheb binding in S47 cells. We propose that these attributes may have led to a positive selection for this variant in sub-Saharan Africa. Our studies shed further light on the intricate regulation that exists between p53, mTOR activity and metabolic output, in this case mediated by GSH and the control of cellular redox state.

## 2.3 Results

### 2.3.1 Higher basal mTOR activity in cells containing the S47 variant

We previously showed that human lymphoblastoid cells (LCLs) that are homozygous for the S47 variant of p53 are impaired for the transactivation of less than a dozen p53 target genes, compared to cells from family members with WT p53 (Jennis et al., 2016). We noted that several of these genes encode proteins that play roles in the negative regulation of mTOR (Budanov and Karin, 2008; Feng et al., 2007). We confirmed via qRT-PCR that S47 LCLs show modestly decreased expression of the p53 target genes *SESN1* and *PTEN*, and decreased transactivation of *PRKAB1*, relative to WT cells following cisplatin treatment (Supplemental Figure 2.1A and 2.1B). These findings prompted us to assess basal mTOR activity in WT and S47 LCLs, and in MEFs from WT and S47 mice. To corroborate our findings, we also analyzed tissues from humanized p53 knock-in (Hupki) mice carrying WT and S47 alleles on a pure C57Bl/6 background, which we previously generated and characterized (Jennis et al., 2016). Western blot analysis of WT and S47 LCLs, along with multiple clones of WT and S47

MEFs, revealed increased p-S6K1 (Thr389) in S47 cells; following normalization to total S6K1, this increase ranged between 2-3 fold (Figure 2.1A-B). We next compared age- and sex-matched pairs of lung and muscle tissue from WT and S47 mice, because mTOR activity is influenced by age and gender, with increased mTOR activity in female and older mice (Baar et al., 2016). We found increased levels of p-S6K1 (T389) and p-mTOR (Ser2448) in S47 lung and skeletal muscle, relative to WT tissues (Figure 2.1C and D). Immunohistochemical analysis of tissues from multiple age- and sex-matched WT and S47 mice confirmed these findings (Figure 2.1E). Interestingly, increased mTOR activity was not seen in all tissues of the S47 mouse (Supplemental Figure 2.1C), and lung and skeletal muscle were the most consistently different between WT and S47. We also did not detect significant differences in p-AKT (Ser473) in WT and S47 cells, suggesting that mTORC1 and not mTORC2 is likely responsible for the observed differences in mTOR activity (Supplemental Figure 2.1D).

We next sought to test the kinetics of mTOR activation in WT and S47 cells by subjecting early passage WT and S47 MEFs to nutrient deprivation, followed by monitoring of mTOR activation markers after nutrient restoration using antisera to p-S6K1 and p-mTOR. Glucose deprivation experiments revealed consistent but modestly increased p-S6K1 following glucose refeed in S47 MEFs, compared to WT (Figure 2.1F), while serum deprivation experiments revealed more pronounced results. For serum deprivation, we subjected three independent cultures each of WT and S47 MEFs to 0.1% serum for 16 hours, followed by 10% serum, after which total and phospho -S6K1 and -mTOR were monitored in a time course. S47 cells consistently showed increased induction of markers of mTOR activation after serum re-feed compared to WT cells (Figure 2.1G). We next performed amino acid deprivation experiments; these likewise

showed increased response in S47 cells (Supplemental Figure 2.1E). Combined densitometry results from all forms of nutrient deprivation revealed an approximately 2 to 3-fold increase in p-S6K1 in S47 cells following nutrient restoration at 30 or 60 minutes (Supplemental Figure 2.1F).

Given that mTOR plays a role in autophagy inhibition (Jung et al., 2010; White et al., 2011), we wondered whether basal autophagy or autophagic flux might be decreased in S47 cells. We were unable to see any differences in the steady state levels of LC3B or the autophagy adaptor protein p62<sup>SQSTM1</sup> in WT and S47 MEFs or tissues, either at steady state (Supplemental Figure 2.1G) or following HBSS treatment to induce autophagy (Supplemental Figure 2.1H). Likewise, we failed to see differences in autophagic flux (conversion of LC3-I to LC3-II when the lysosome is inhibited; Supplemental Figure 2.1I) between WT and S47 cells, or in cell viability after HBSS treatment (Supplemental Figure 2.1J). Therefore, while markers of mTOR activity are clearly increased in S47 cells and tissues, this does not appear to be accompanied by alterations of basal or induced autophagy.

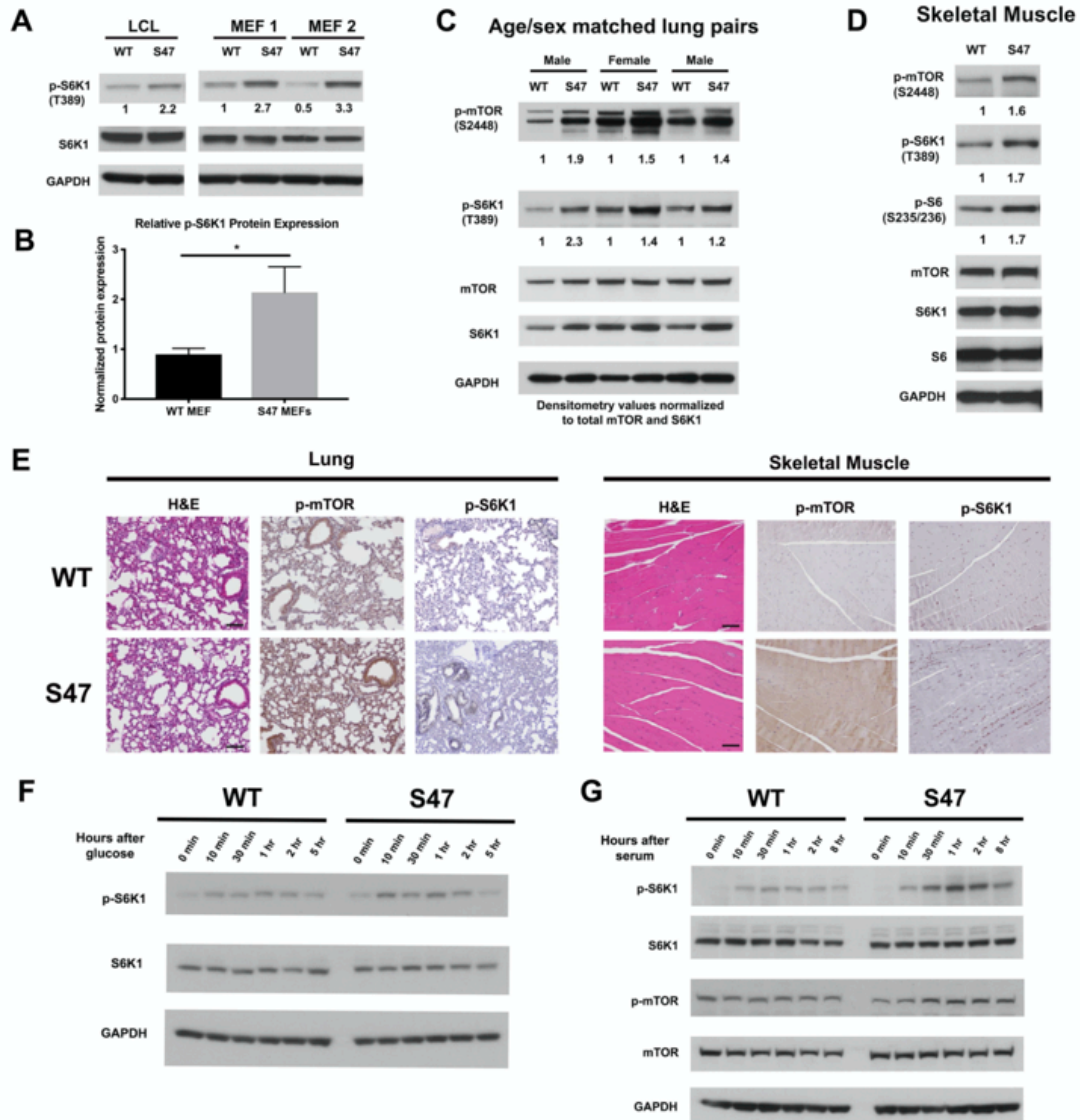


**Figure 2.1: Increased markers of mTOR activity in S47 cells and tissues.**

(A) Western blot analyses reveal higher phospho-S6K1 expression in S47 LCLs and S47 MEFs, obtained from two separate embryos per genotype. (B) Densitometry quantification of phospho-S6K1 protein expression in WT and S47 MEFs from 4 independent experiments; all values normalized to total S6K1. Error bars represent standard error, (\*) p value < 0.05. (C) Whole cell lysates were extracted from 3 WT and 3 S47 mouse lungs and analyzed by Western blot for the proteins indicated. Pair 1 and 3 are lungs isolated from male mice, pair 2 are lungs isolated from

female mice. Densitometry quantification of phospho-S6K1 and phospho-mTOR was performed and normalized to total S6K1 and total mTOR protein expression, respectively. (D) Whole cell lysates were extracted from WT and S47 mouse skeletal muscle and analyzed as described above. Densitometry quantification of phospho-S6, phospho-S6K1, phospho-mTOR was performed and normalized to total S6, total S6K1 and total mTOR protein expression, respectively. (E) Immunohistochemical analysis of hematoxylin and eosin (H&E), phospho-mTOR and phospho-S6K1 in WT and S47 mouse lung and skeletal tissue. Data are representative of n = 4 fields per genotype. Scale bar represents 100  $\mu$ M. (F) WT and S47 MEFs were starved in media containing no glucose for 16 hours, then media containing 4.5 g/L glucose was re-introduced. Samples were collected at indicated time points and analyzed by Western blot for p-S6K1, total S6K1 and GAPDH. (G) WT and S47 MEFs were starved in media containing 0.1% FBS for 16 hours, then media containing 10% serum was re-introduced and samples were collected at indicated time points. Cell lysates were extracted from samples and subjected to Western blot analysis for the proteins indicated.

### *2.3.2 Enhanced mitochondrial function and glycolysis in S47 cells*

To determine the functional consequences of the increased markers of mTOR activity in S47 cells, we used a Seahorse BioAnalyzer to assess the oxygen consumption rate (OCR), as well as basal and compensatory glycolytic rate in WT and S47 MEFs and LCLs. Seahorse analyses revealed that S47 LCLs show increased OCR under stressed conditions compared to WT (Figure 2.2A). Seahorse analyses also revealed that human S47 LCLs and mouse S47 MEFs both show increased basal and compensatory glycolysis, compared to WT cells (Figure 2.2B and C). We next assessed glucose and glutamine consumption using a Yellow Springs Instrument (YSI) Analyzer. These analyses revealed that S47 cells show significantly increased consumption of glucose and glutamine, along with increased production of lactate and glutamate,



compared to WT cells (Figure 2.2D and E). S47 cells do not proliferate more quickly than WT cells (Jennis et al., 2016), suggesting that this increased nutrient consumption may be used for biomass instead of proliferation. Interestingly, LCLs from individuals heterozygous for the S47 variant (S47/WT), and MEFs from S47/WT mice, showed values typically intermediate between homozygous WT and S47 cells (Figure 2.2D and E). We next performed metabolic flux analyses in WT and S47 cells using  $^{13}\text{C}$ -labeled glucose. Analysis of  $^{13}\text{C}_6$ -glucose tracing in WT and S47 MEFs provided evidence for a higher contribution of glucose carbon into the TCA cycle in S47 cells compared to WT cells, as evidenced by increased labeling of citrate, malate, aspartate and glutamate in S47 MEFs (Supplemental Figure 2.2A-D). We reasoned that one possibility for the increased metabolism in S47 cells might be due to increased mitochondrial content, which is regulated by mTOR (Morita et al., 2013). However, MitoTracker analyses and Western blotting for mitochondrial proteins revealed no obvious increase in mitochondrial content in S47 cells (Supplemental Figure 2.2E and F).

Because mTOR is known to regulate mitochondrial function (Morita et al., 2013; Schieke et al., 2006; Ye et al., 2012), we next assessed the impact of mTOR inhibitors on mitochondrial function in WT and S47 cells. Seahorse analysis of WT and S47 LCLs revealed that S47 cells are less susceptible to inhibition of oxygen consumption rate and maximal respiration by mTOR inhibitors rapamycin (Figure 2.3A and B) and Torin1 (Figure 2.3C and D). This finding was not due to altered efficacy of each inhibitor, as evidenced by similar decreases in p-mTOR and p-S6 in WT and S47 cells following treatment with rapamycin (Supplemental Figure 2.3A) and Torin1 (Figure 2.3E), and by the finding that very high concentrations of Torin1 were able to inhibit oxygen consumption equally well in both WT and S47 cells (Supplemental Figure 2.3B). The

combined data support the premise that S47 cells possess enhanced metabolism compared to WT cells.

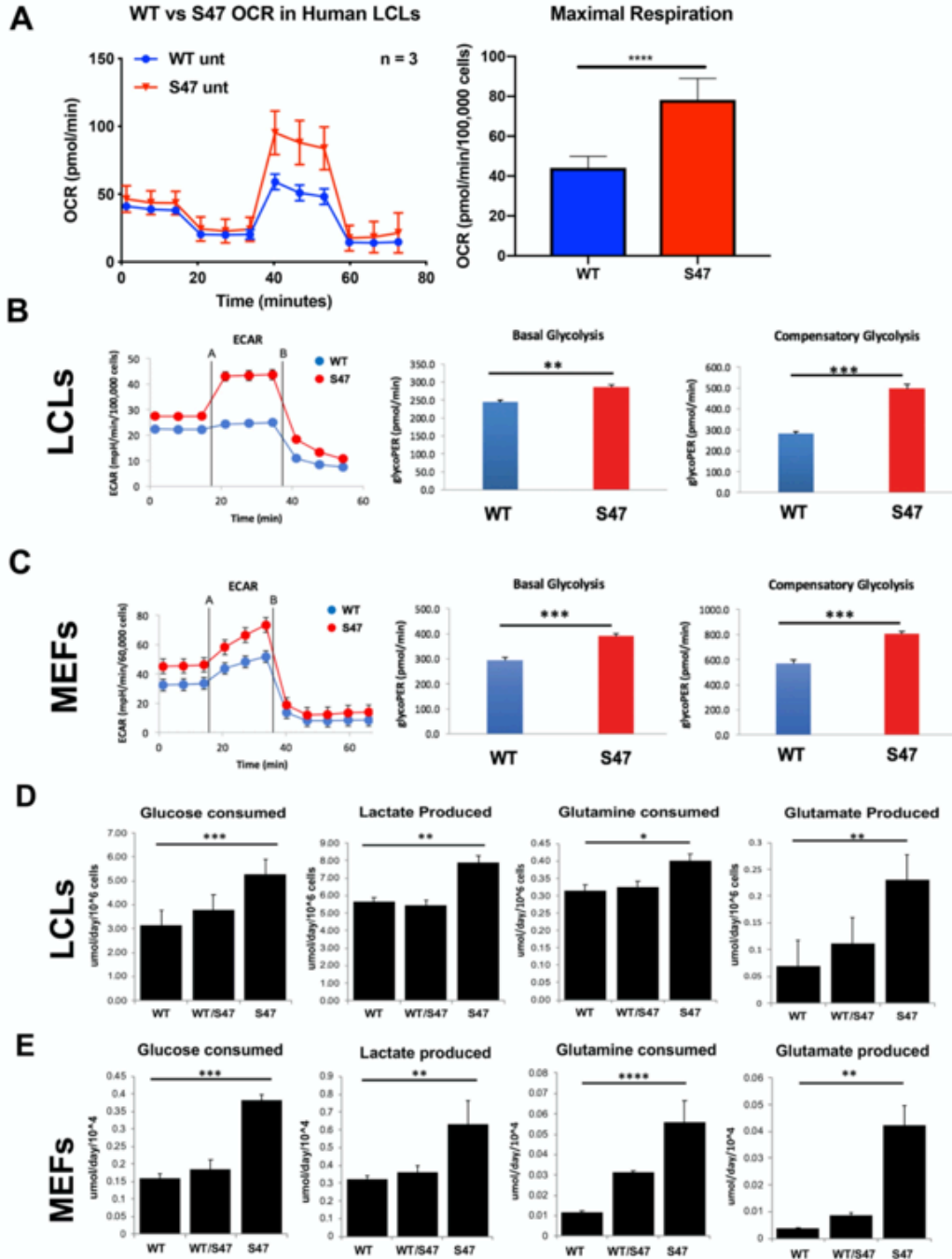


**Figure 2.2: Increased metabolism in S47 cells compared to WT cells.**

(A) Oxygen consumption rates (OCR) in WT and S47 LCLs were assessed using the Seahorse XF Mito Stress Test. OCR was measured first in basal conditions, and following oligomycin, FCCP and finally rotenone/antimycin. The bar graph depicts maximal OCR after FCCP injection at ~ 40 minute timepoint; data are representative of three independent experiments performed with at least six technical replicates, presented as mean  $\pm$  SD. (B-C) Basal and compensatory glycolysis in WT and S47 LCLs (B) and MEFs (C) were assessed using the Seahorse Glycolytic Rate Assay. Basal glycolysis is first measured, followed by treatment of cells with rotenone/antimycin and 2-deoxy-D-glucose (2-DG). The bar graph depicts basal glycolysis at ~1 minute timepoint and compensatory glycolysis after antimycin/rotenone injection at ~ 22 minute timepoint; data are representative of 3 independent experiments performed with at least ten technical replicates. Bar graphs are presented as mean  $\pm$  SD for all Seahorse analyses. (D-E) Consumption of glucose and glutamine from media and production of lactate and glutamate were analyzed from homozygous WT, heterozygous WT/S47 and homozygous S47 human LCLs (D) and primary MEFs (E) using a YSI-7100 Bioanalyzer. Means and SEM are shown (n= 5).

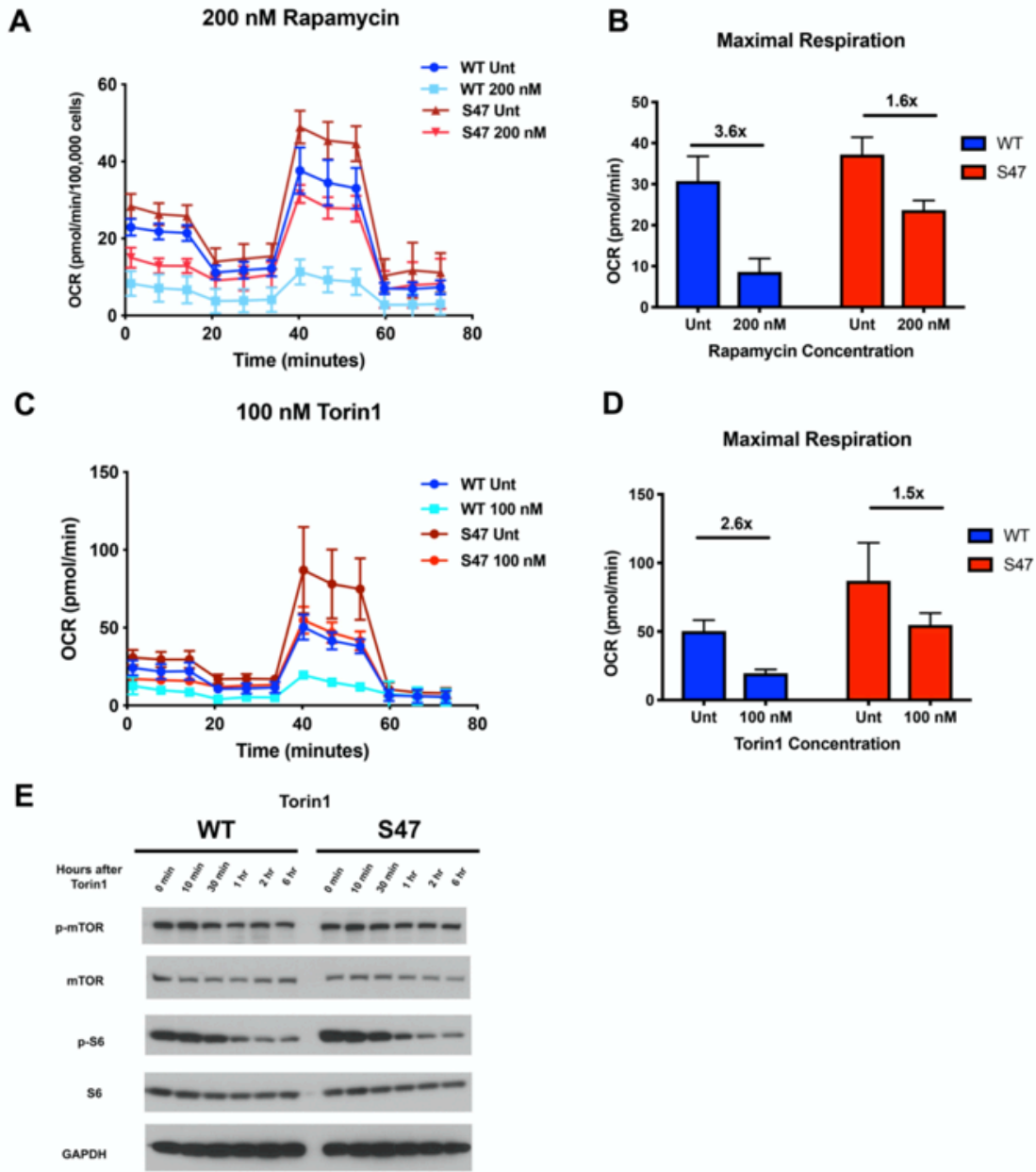


**Figure 2.3: S47 mitochondria show decreased sensitivity to mTOR inhibition.**

(A) Oxygen consumption rate (OCR) as measured by the Seahorse XF Mito Stress Test in WT and S47 LCLs treated with 200 nM of rapamycin for 24 hours. (B) Bar graph depicts maximal OCR after FCCP injection at ~ 40 minute timepoint; fold changes between rapamycin treated and untreated samples are shown. Data are representative of 2 independent experiments performed

with at least ten technical replicates. (C) OCR as measured by the Seahorse XF Mito Stress Test in WT and S47 LCLs treated with 100 nM of Torin1 for 24 hours. (D) Bar graph depicts maximal OCR after FCCP injection at ~ 40 minute timepoint; fold changes between Torin1 treated and untreated samples are shown. Data are representative of 2 independent experiments performed with at least eight technical replicates. (E) WT and S47 LCLs were treated with 100 nM of Torin1, harvested at indicated time points after treatment and analyzed for the shown mTOR markers via Western blot.

Because mTOR can regulate both cell size and protein translation, we were careful to normalize to both cell number and protein content. For example, when comparing metabolic changes using the Seahorse assay, the results were standardized to total cell number. When quantifying differences in mTOR activity, the results were normalized to total protein content. In addition, phospho-S6K1 was normalized to total S6K1 in each sample

### *2.3.3 Increased mTOR activity in S47 is due to increased mTOR-Rheb interaction*

We next sought to identify the mechanism underlying increased mTOR activity in S47 cells. Although we identified decreased mRNA levels of some mTOR regulators in S47 cells, we found no evidence for differences at the protein level of any p53-induced mTOR regulators in steady state MEFs (Supplemental Figure 2.4A) or following treatment with Nutlin to induce p53 (Supplemental Figure 2.4B). Therefore, we analyzed a key regulator of mTOR activity, the small GTPase Rheb, which binds and activates mTOR (Long et al., 2005). We monitored the mTOR-Rheb association in WT and S47 MEFs using the technique of proximity ligation assay (PLA), which quantitatively detects

protein-protein interactions. PLA experiments revealed that there were consistently increased mTOR-Rheb complexes in S47 cells, compared to WT; this was true in multiple replicates, in multiple MEF clones, and using single antibody controls that showed no signal (Figure 2.4A). Quantification of multiple experiments revealed an approximately two-fold increase in mTOR-Rheb complexes in S47 cells compared to WT (Figure 2.4B).

A recently-identified regulator of the mTOR-Rheb interaction is the cytosolic enzyme GAPDH. This enzyme binds to Rheb and sequesters it from mTOR in cultured cells, in a manner that is regulated by glucose levels (Lee et al., 2009). First, we confirmed that the interaction between Rheb and GAPDH is detectable in the skeletal muscle of mice using IP-western, and that this interaction is regulated by glucose (Supplemental Figure 2.4C). Next, we performed immunoprecipitation (IP)-western of skeletal muscle extracts from WT and S47 mice; we found that there was increased mTOR, and significantly decreased GAPDH, in Rheb IPs from S47 skeletal muscle compared to WT (Figure 2.4C). The combined data from three independent IPs of Rheb in WT and S47 skeletal muscle revealed an approximately 2-fold decrease in the amount of GAPDH co-precipitating with Rheb in S47 skeletal muscle compared to WT ( $p < 0.05$ , Figure 2.4D). In contrast there were no differences in the levels of mTOR, Rheb and GAPDH in these extracts (Figure 2.4C – WCL, Supplemental Figure 2.4D). Consistent with these IP-western findings, PLA analyses corroborated that the GAPDH-Rheb association is markedly decreased in S47 MEFs relative to WT MEFs (Figure 2.4A). Confocal microscopy analyses revealed no significant differences in the cellular localization of Rheb at the lysosome, as assessed by LAMP1 localization, nor were there any differences in TSC2 localization at the lysosome in WT and S47 MEFs

(Supplemental Figure 2.4E). The combined data support the premise that the increased mTOR activity in S47 cells is due to increased Rheb-mTOR association, along with a decreased Rheb-GAPDH association.

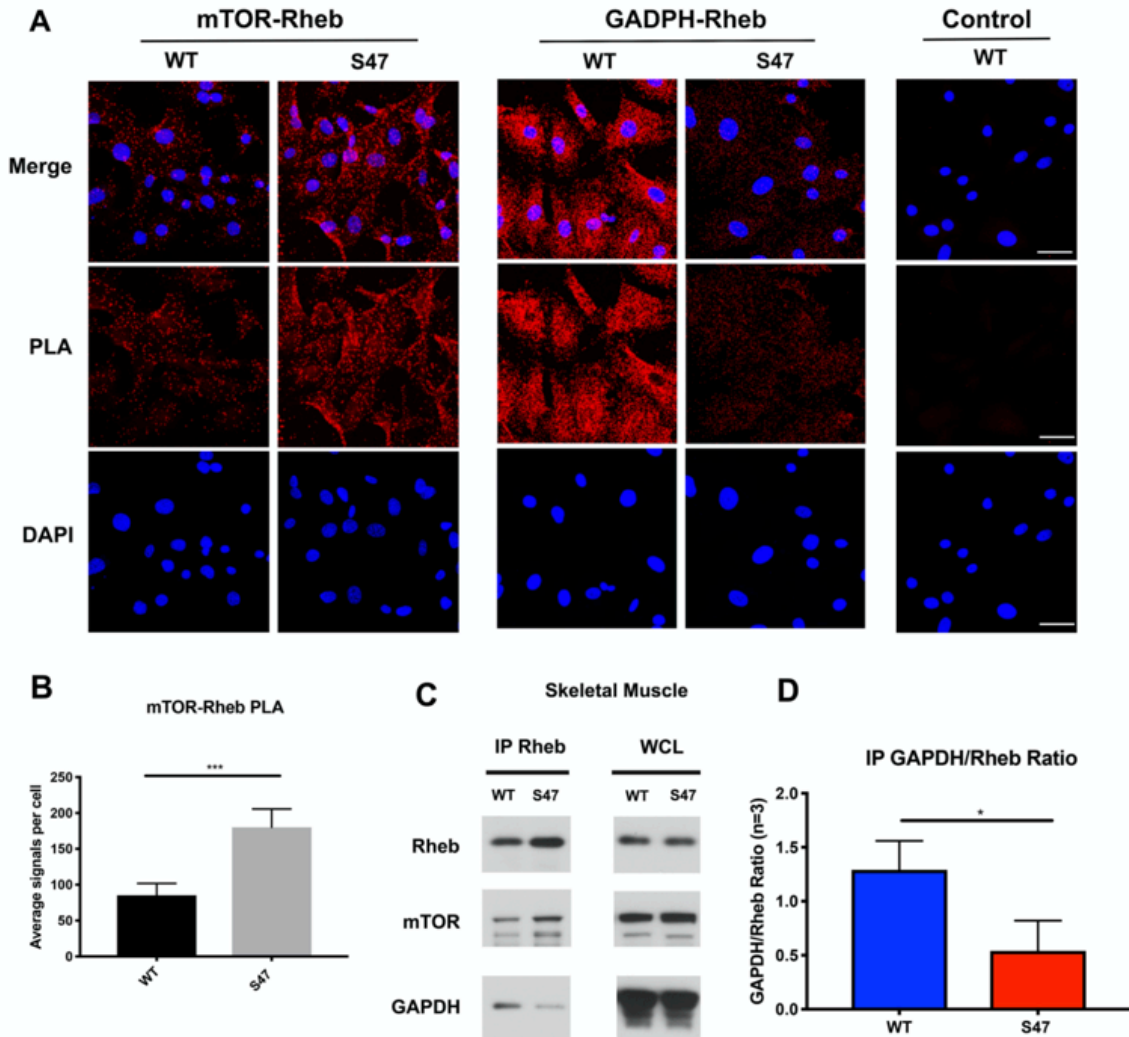


**Figure 2.4: Increased mTOR-Rheb binding in S47 cells is due to decreased GAPDH-Rheb binding**

(A-B) An *in situ* proximity ligation assay (PLA) was performed in WT and S47 MEFs. Each red dot represents an interaction between mTOR-Rheb or GAPDH-Rheb as indicated; scale bar represents 50  $\mu$ M. The samples were counterstained with DAPI to detect nuclei. Cells stained in the absence of one primary antibody were used as a negative control. (B) Quantification of the mTOR-Rheb interactions, measured as the average number of PLA signals per nuclei. Data were quantified by counting the number of cells in five random fields per experimental condition. (\*\*\*) p-value < 0.001, Student's t-test. (C) Lysates extracted from WT and S47 skeletal tissue were immunoprecipitated with anti-Rheb. The amount of co-precipitating mTOR and GAPDH, as well as immunoprecipitated Rheb, were assessed by Western blot. Whole cell lysate (WCL) is shown on the right. (D) Quantification of the amount of GAPDH bound to Rheb, divided by total Rheb pulled down, in WT and S47 skeletal tissue, n = 3 independent experiments, (\*) p-value < 0.05.

GAPDH is a multi-functional enzyme that is well-known to be sensitive to redox status (Brandes et al., 2009; Chernorizov et al., 2010). We hypothesized that the increased glutathione (GSH) levels in S47 cells (Leu et al., 2019) might alter the redox state of GAPDH and impact its ability to bind to Rheb. We first verified that lung tissue and skeletal muscle from S47 mice possess increased GSH compared to WT tissues, as assessed by an increased ratio of reduced versus oxidized glutathione (GSH:GSSG) (Figure 2.5A). We also validated that the GSH alkylating agent diethylmaleate (DEM) could successfully decrease the level of GSH, and the GSH/GSSG ratio, in cells (Figure 2.5A); these findings are consistent with previously published findings by our group (Leu et al., 2019). Notably, DEM treatment of immortalized S47 MEFs (iMEFs) caused a



dramatic decrease in markers of mTOR activity (p-mTOR and p-S6K1), showing for the first time that modulation of GSH, even for as little as five hours, can impact mTOR activity. We found that the impact of DEM on mTOR activity was further enhanced by the addition of glutamate (Figure 2.5B); glutamate decreases cystine import through System Xc(-), leading to decreased level of GSH.

We next sought to test the hypothesis that the redox state of GAPDH was altered in WT and S47 cells. Toward this end we employed cross-linking experiments using the cysteinyl cross-linking agent bismaleimido-hexane (BMH), which cross-links cysteine residues within 13Å by covalently conjugating free (reduced) sulfhydryl groups (Green et al., 2001). We treated freshly isolated lung and skeletal muscle lysates from WT and S47 mice, and from immortalized WT and S47 MEFs (iMEFs), with BMH. Cysteinyl-crosslinked proteins were resolved on SDS-PAGE gels and compared to untreated extracts. Notably, we found consistent differences in GAPDH cross-linking patterns in S47 samples compared to WT, as evidenced by altered mobility of GAPDH on SDS-PAGE of BMH-treated samples (Figure 2.5C). This altered mobility of GAPDH in S47 cells could be reversed by glutathione depletion by DEM treatment (Figure 2.5C) and by the compound BSO (buthionine sulfoximine; Supplemental Figure 2.5A), which inhibits GSH biosynthesis. Treatment with the compound erastin, which inhibits the system Xc(-) cystine transporter, also led to altered mobility of GAPDH in S47 and WT cells (Supplemental Figure 2.5B).

We next tested the impact of modulating GSH on the interaction between Rheb and GAPDH in WT and S47 cells using both IP-western and PLA. By IP-western we found that supplementation of culture media with exogenous GSH decreased the Rheb-GAPDH interaction in WT cells; conversely, depleting free GSH using either BSO or

DEM increased the Rheb-GAPDH interaction in S47 cells (Figure 2.5D). These findings were corroborated using PLA, which revealed that depleting GSH in WT and S47 cells using either DEM or BSO completely restores GAPDH-Rheb complex formation and mTOR-Rheb complex formation in S47 cells, to levels equivalent to WT cells (Figure 2.5E and F; Supplemental Figure 2.5C). Our crosslinking experiments with BMH reveal that there is an altered conformation of GAPDH in S47 cells in tissues, however the exact change in conformation remains to be determined. In the future, it would be worthwhile to perform glutaraldehyde crosslinking experiments to determine if dimerization of GAPDH differs between WT and S47. The combined data support the conclusion that the increased GSH pool in S47 cells affects the status of reactive cysteines in GAPDH, and the ability of this protein to bind and sequester Rheb, thereby leading to increased Rheb-mTOR interaction and increased mTOR activity in S47 cells.

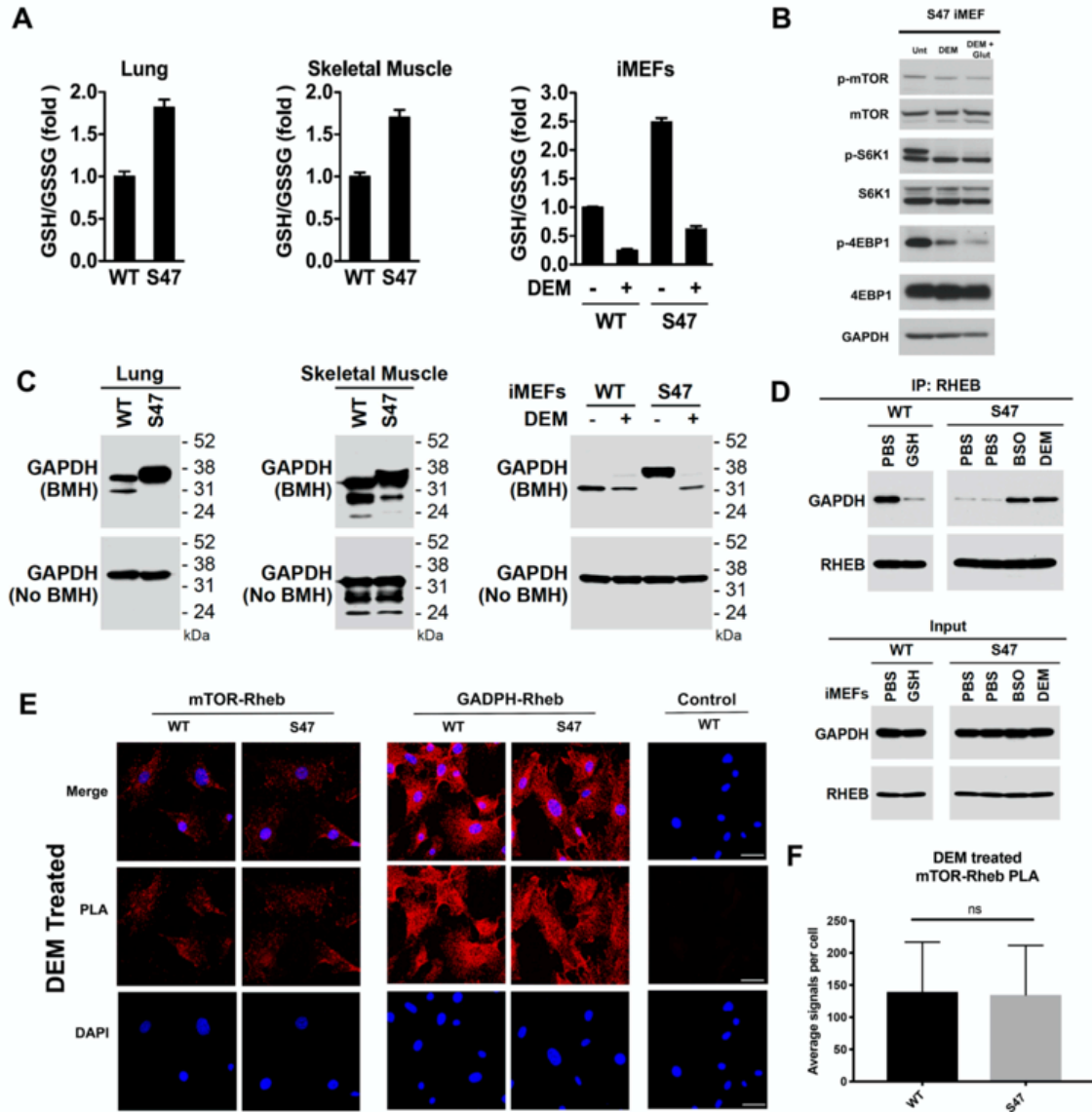


**Figure 2.5: Increased glutathione drives decreased GAPDH-Rheb binding in S47 cells**

(A) WT and S47 lung (left) and skeletal muscle (center) were assessed for GSH/GSSG ratio (mean  $\pm$  SD,  $n = 3$ ). WT and S47 immortalized MEFs (iMEFs), either untreated or treated with 50

$\mu\text{M}$  DEM for 5 h, were analyzed for GSH/GSSG ratio (mean  $\pm$  SD, n = 4). (B) WT and S47 iMEFs were either untreated, treated with 50  $\mu\text{M}$  of DEM or 50  $\mu\text{M}$  of DEM + 0.5 mM glutamate for 5 h and protein lysates were analyzed by Western blot for indicated mTOR markers. (C) Whole cell lysates were extracted from WT and S47 mouse lung (left) and skeletal (center) tissue. Proteins were cross-linked with BMH, resolved by SDS/PAGE, and detected by Western blotting with a GAPDH specific antibody (Top). Untreated protein lysates were analyzed by Western blot analysis for total GAPDH (Bottom). WT and S47 iMEFs were treated with 50  $\mu\text{M}$  of DEM for 5 h and protein lysates were analyzed as described (right). (D) WT cells were treated with PBS or 3 mM GSH for 24 hours. S47 cells were treated with PBS for 24 hours, PBS for 5 hours, 100  $\mu\text{M}$  BSO for 24 hours, or 50  $\mu\text{M}$  DEM for 5 hours. IP of the lysates with anti-Rheb followed by Western analysis for associated GAPDH and Rheb (top panel). The same lysates were analyzed by Western blotting for GAPDH and Rheb (bottom panel). (E-F) Proximity ligation analysis (PLA) was performed in WT and S47 MEFs treated with 50  $\mu\text{M}$  of DEM for 5 hours and analyzed as described in Figure 2.4A-B.

#### *2.3.4 Enhanced metabolic efficiency of S47 mice*

mTOR is known to regulate body mass and muscle regeneration (Laplante and Sabatini, 2012; Yoon, 2017). We therefore next assessed body weight and fat/lean content in age-matched male mice of WT and S47 genotypes. We also tracked body weight with age of multiple male and female sibling littermate mice of WT/WT, WT/S47 and S47/S47 genotypes in our colony. S47 mice showed significantly increased weight with time, compared to WT/WT and WT/S47 sibling littermates (Supplemental Figure 2.6A). Body composition analysis using nuclear magnetic resonance revealed that S47 mice had significantly increased fat and lean content, compared to WT mice (Figure 2.6A; Supplemental Figure 2.6B). We next analyzed the metabolic activities of WT and S47 mice using a comprehensive lab animal monitoring system (CLAMS) over the

course of 48 hours. In this analysis, S47 mice showed comparable locomotor activity to WT mice but reduced food intake, oxygen consumption and heat production (Figure 2.6B). These CLAMS data suggested that S47 mice might possess enhanced metabolic efficiency compared to WT mice and prompted us to assess the response of WT and S47 mice to exercise challenge.

We subjected WT and S47 mice to treadmill exercise with increasing intensity over time. For this analysis we studied eight age-matched male mice of each genotype during a 50-minute forced exercise at increasing speed and slope. During this time course, oxygen consumption and serum metabolites were quantified. Consistent with our CLAMS experiment, S47 mice started with lower basal  $VO_2$  and exhibited generally lower  $VO_2$  for the work being performed; however, as they approached the final, most strenuous point of the exercise, the  $VO_2$  values in WT and S47 converged, so the  $VO_2$  range for S47 mice was significantly greater than WT mice (Figure 2.6C-E). Analysis of serum metabolites and proteins before and after exercise revealed decreased lactate dehydrogenase (LDH) levels in the sera of S47 mice, suggesting decreased muscle damage in S47 mice compared to WT (Figure 2.6F). Moreover, prior to exercise, we noted that Ki-67 staining in S47 skeletal muscle was consistently increased relative to WT (Supplemental Figure 2.6C); the latter finding is suggestive of enhanced ability for S47 muscle to regenerate. There were no differences in p53 level or markers of mitochondrial content in the skeletal muscle of WT and S47 mice (Supplemental Figure 2.6D and E), nor were there other differences in other serum metabolites between WT and S47 mice (Supplemental Figure 2.6F). The combined data, like the CLAMS data, point to increased metabolic efficiency in S47 mice relative to WT mice. To address this further, we analyzed a small cohort of male WT and S47 mice on a continuous

strenuous treadmill run. Although the numbers are small, we found that three out of four WT mice failed to complete 60-minute strenuous run, while three out of four S47 mice successfully completed this run (Supplemental Figure 2.6G).

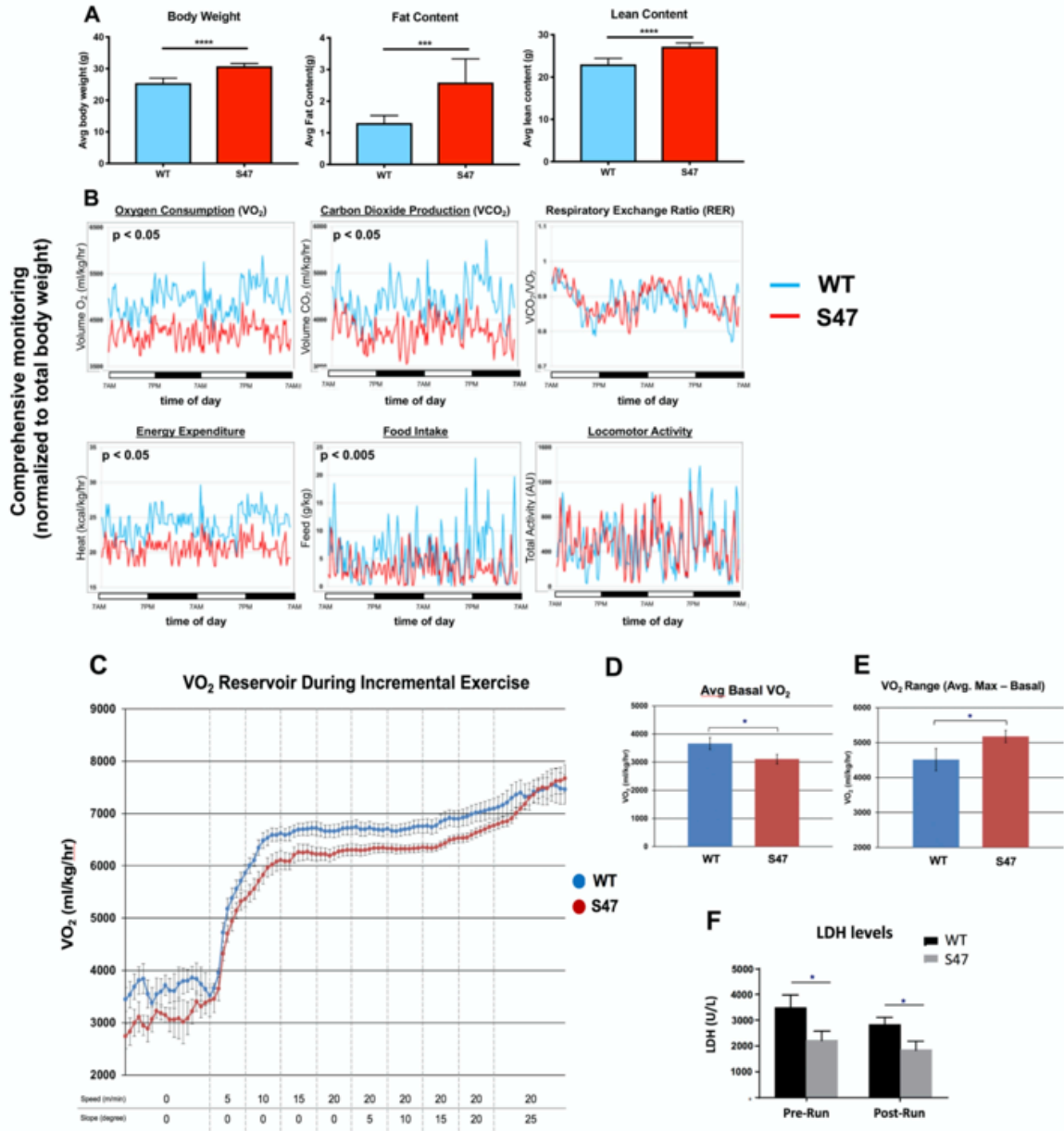


**Figure 2.6: Increased size and improved metabolic efficiency in S47 mice.**

(A) Nuclear magnetic resonance (NMR) studies revealed S47 mice have increased body weight, increased fat content and increased lean content, n=7 WT mice, n=8 S47 mice. (\*\*\*) p-value < 0.001, (\*\*\*\*) p-value < 0.0001. Bar graphs are presented as mean  $\pm$  SD. (B) Changes in metabolic parameters for WT mice (blue) and S47 mice (red) were determined by using the Comprehensive Lab Animal Monitoring System for 48 hours. Parameters assessed includes oxygen consumption, carbon dioxide production, respiratory exchange rate, energy expenditure, total food intake and locomotor activity. The data are representative of 5 six-week old male mice per genotype and are normalized to total body weight. (C) WT and S47 mice (n = 6-7) were subjected to a treadmill study of increasing intensity over time. Oxygen consumption (VO<sub>2</sub>) is normalized to body mass. (D) Mean basal VO<sub>2</sub> in WT and S47 mice. (E) VO<sub>2</sub> range in WT and S47 mice determined by subtracting the mean basal VO<sub>2</sub> from the VO<sub>2</sub> max, obtained during the most strenuous point of exercise at the tail end of the treadmill study. (F) Lactate dehydrogenase (LDH) levels measured in the serum of WT and S47 mice obtained before and after the treadmill study. (\*) p-value < 0.05, Student's t-test.

**2.4 Discussion**

In this study, we report that cells and mice with the S47 variant of p53 have increased mTOR activity and increased metabolic efficiency. The animals also display increased mass and signs of superior fitness. Our data support the premise that the enhanced mTOR activity is due, at least in part, to the higher levels of GSH in S47 cells and tissues. The increased GSH results in impaired ability of the redox sensitive protein GAPDH to bind to Rheb. This leads to greater mTOR-Rheb binding, resulting in increased mTOR activity in S47 cells and tissues. These data indicate that, along with

pH (Walton et al., 2018), cellular redox status can also regulate mTOR activity, in a manner controlled by p53. We show that oxidative metabolism in S47 cells is less sensitive to mTOR inhibitors, thus tying these two phenotypes together; this is not surprising, as a link between mTOR and a number of cellular metabolic processes is well known (Morita et al., 2013; Schieke et al., 2006).

We see evidence for increased mTOR activity only in certain tissues of the S47 mouse, so the metabolic impact of this genetic variant appears to be somewhat tissue restricted. At present we do not know if this tissue specificity is due to differences in GSH level, or to altered mTOR-Rheb or GAPDH-Rheb interactions in different tissues, or to other parameters. We also see evidence for some unexpected findings regarding the increase in mTOR activity in S47 cells: given that mTOR negatively regulates autophagy (Jung et al., 2010), we expected to see differences in steady state autophagy or autophagic flux in WT and S47 cells, but we found no evidence for this. This finding may be due to the rather complex relationship between mTOR and autophagy (Jung et al., 2010; White et al., 2011), and/or that other signaling pathways regulate autophagy aside from mTOR, including the PI3K pathway, GTPases, and calcium (Yang et al., 2005). It is also interesting to note that S47 cells exhibit increased use of the pentose phosphate pathway and generate more NADPH compared to WT cells. Our collaborators have observed decreased GAPDH activity, and an increase in G6PD activity, the rate limiting enzyme in the pentose phosphate pathway (Leu et al., 2020). Thus, changes in NADPH levels can also account for some of the redox differences observed in S47.

The increased lean content in S47 mice likely contributes to the increased fitness observed in these mice. Human studies have shown that mTOR activation is crucial for human muscle protein synthesis (Dickinson and Rasmussen, 2011). Treatment with the



well-studied mTOR inhibitor rapamycin blocks the effects of amino acid ingestion on mTOR activity and leads to decreased protein synthesis in human skeletal muscle (Dickinson and Rasmussen, 2011; Drummond et al., 2009). Additionally, mTOR signaling driven through IGF-1 plays a key role in promoting muscle hypertrophy (Coleman et al., 1995; Musaro et al., 2001; Vandeburgh et al., 1991). One caveat of this study, however, is that we do not directly demonstrate that the increased mTOR activity in S47 mice is causing their increased lean content or superior performance on treadmill assays. Transient treatment with mTOR inhibitors elicits highly complex and often contrasting effects on energy expenditure and treadmill performance, likely due to the existence of feedback loops and the effect of inhibitors on multiple organ systems in the mouse. As just two examples: rapamycin has shown contrasting effects on energy expenditure in animals, depending on how long mice are treated (Fang et al., 2013); similarly, treatment of mice with rapamycin has shown limited impact on treadmill endurance, despite causing decreased expression of genes involved in mitochondrial biogenesis and oxidative phosphorylation in the muscle (Ye et al., 2013). Possibly the most consistent findings in the literature reflect the general consensus that mTORC1 is involved in mechanisms that drive increased muscle mass (Goodman, 2019) and that heightened mTOR activity leads to enhanced muscle recovery after exercise (Song et al., 2017; Yoon, 2017). It remains to be tested if these are the pathways affected in S47 mice.

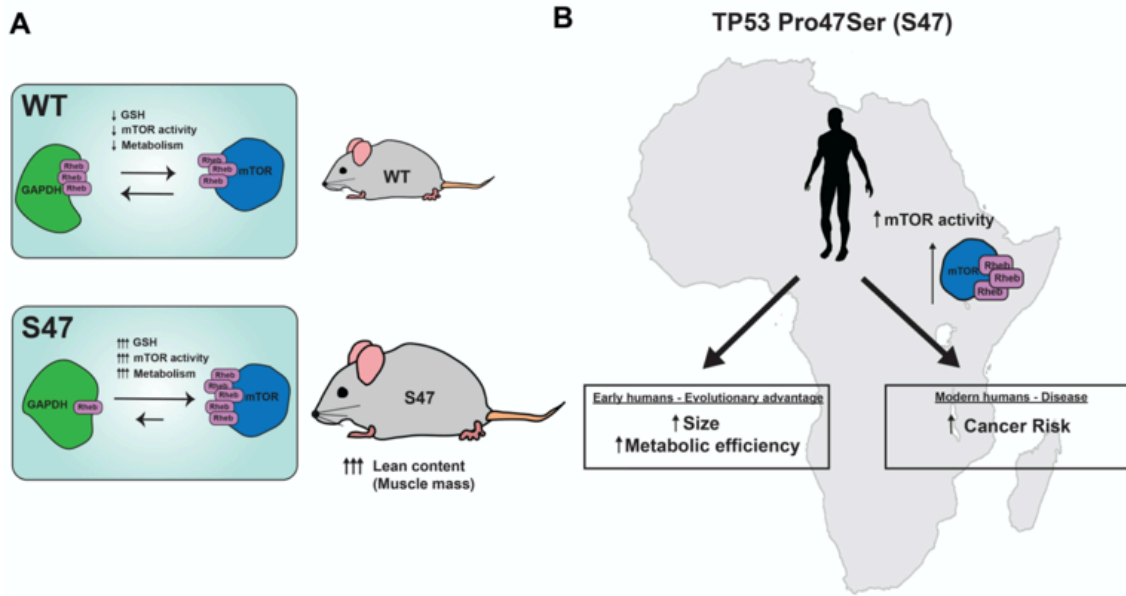


**Figure 2.7: Proposed model of how S47 contributes to increased metabolism**

(A) The elevated levels of GSH alter the redox state of the S47 cell, in turn affecting GAPDH conformation and impairing GAPDH-Rheb binding. This results in increased mTOR-Rheb binding, leading to increased mTOR activity and resulting an overall increase in metabolism in S47 mice, as seen by increased fat and lean content. (B) Broad impact of S47 variant: though providing an adaptive advantage to individuals residing in sub-Saharan Africa at one point in time, it now predisposes modern humans with this SNP to cancer.

We hypothesize that the more efficient metabolism and enhanced fitness provided by the S47 variant may have once provided carriers with a bio-energetic advantage in Sub-Saharan western Africa, where this variant is most common. For example, those carrying the S47 SNP may have possessed superior athletic prowess and/or ability to withstand famine (see model, Figure 2.7). This metabolic advantage may explain the high frequency of this genetic variant in sub-Saharan Africa, despite the

fact that it predisposes individuals to cancer later in life. A selection for this variant in Africa may also include an improved ability to withstand malaria infection: we recently reported that the S47 variant alters the immune micro-environment in mice and confers improved response to the malaria toxin hemozoin (Singh et al., 2020). Both of these activities may have conferred selection pressure for this variant in Africa.

Our findings provide further support for the growing premise that some tumor suppressor genetic variants may provide evolutionary selection benefit (Vicens and Posada, 2018). For example, women who carry the BRCA1/2 mutation exhibit increased size and enhanced fertility when compared to controls (Smith et al., 2012). Similarly, people with Li Fraumeni syndrome who inherit germline mutations in *TP53*, as well as mice with tumor-derived germline mutations in *Tp53*, demonstrate increased fitness endurance (Wang et al., 2013); however, this is due to increased mitochondrial content, which we do not see in S47 cells. A common genetic variant in *TP53* at codon 72, encoding proline at amino acid 72, confers increased longevity while conversely causing increased cancer risk (Zhao et al., 2018). In contrast, the arginine 72 variant of p53 induces increased expression of LIF, which improves fecundity (Kang et al., 2009). The take home message from all of these studies is that the diverse roles of tumor suppressor proteins like p53 in metabolism, fertility and fitness may allow for positive selection for certain variants, even at the expense of increased cancer risk. In mice, this increased cancer risk occurs quite late in life, well past reproductive selection (12-18 months). More needs to be done to analyze cancer risk in S47 humans. A more comprehensive understanding of the function of tumor suppressor genetic variants, including the S47 SNP, will enable improved understanding of cancer risk, along with

superior personalized medicine approaches, with the ultimate goal of improving clinical outcomes and survival of people who carry this variant.

## **2.5 Materials and Methods**

### *2.5.1 Mammalian cell culture*

WT and S47 MEFs were generated and maintained as previously described (Jennis et al., 2016). Human WT LCLs (Catalog ID GM18870) and S47 LCLs (Catalog ID GM18871) were obtained from the Coriell Institute (Camden, New Jersey) and maintained as previously described (Jennis et al., 2016). MEF cultured cells were grown in DMEM (Corning Cellgro) supplemented with 10% fetal bovine serum (HyClone, GE Healthcare Life Sciences) and 1% penicillin/streptomycin (Corning Cellgro). Human LCLs were grown in RPMI (Corning Cellgro) supplemented with 15% heat inactivated fetal bovine serum (HyClone, GE Healthcare Life Sciences) and 1% penicillin/streptomycin (Corning Cellgro). Cells were grown in a 5% CO<sub>2</sub> humidified incubator at 37°C. For serum starvation experiments, cells were starved in DMEM containing 0.1% FBS for 16 hours. Following starvation, DMEM containing 10% FBS was re-introduced and cells were harvested at 0 minutes, 10 minutes, 30 minutes, 1 hour, 2 hours and 8 hours after this point. For glucose starvation experiments, cells were starved in glucose-free DMEM (Thermo Fisher Scientific 11966025) for 16 hours. Following starvation, DMEM containing 4.5 g/L glucose was re-introduced and cells were harvested at 0 minutes, 10 minutes, 30 minutes, 1 hour, 2 hours and 5 hours after this point. For amino acid starvation experiments, cells were starved for 4 hours in EBSS (Thermo Fisher Scientific 24010043) containing 25 mM glucose, 0.5 mM Glutamine, 1X

MEM Vitamin (Thermo Fisher Scientific 11120052), 0.2% FBS, 25 mM HEPES, 1X Penicillin/Streptomycin. Following starvation, the same media recipe now containing 1X MEM Amino Acids (Thermo Fisher 1130051) was re-introduced and cells were harvested at 0 minutes, 10 minutes, 30 minutes, 1 hour, 2 hours and 5 hours after this point. For HBSS experiments, cells were washed once with PBS (Corning 21-031-CV) and then incubated with HBSS (Thermo Fisher Scientific 14025092) for 0, 2 or 6 hours. Viability was assessed using Trypan Blue (Thermo Fisher Scientific 15250061).

### *2.5.2 Western blot*

For Western blot analyses, 50-100 µg of protein was resolved over SDS-PAGE gels using 10% NuPAGE Bis-Tris precast gels (Life Technologies) and were then transferred onto polyvinylidene difluoride membranes (IPVH00010, pore size: 0.45 µm; Millipore Sigma). Membranes were blocked for 1 hour in 5% bovine albumin serum (Sigma Aldrich, A9647). The following antibodies were used for Western blot analyses: phospho-mTOR 1:1000 (Cell Signaling, 2971), mTOR 1:1000 (7C10, Cell Signaling, 2983), phospho-p70S6K1 1:1000 (Cell Signaling, 9205), p70S6K1 1:1000 (Cell Signaling, 9202), GAPDH 1:10,000 (14C10, Cell Signaling, 2118), TFAM 1:2000 (Abcam, ab131607), MTCO1 1:2000 (Abcam, ab14705), SDHA 1:1000 (Cell Signaling, 5839), Tom20 1:100 (F-10, Santa Cruz, sc17764), phospho-Akt (D9E, Cell Signaling, 4060), p62 1:1000 (Cell Signaling, 5114), LC3B 1:1000 (D11, Cell Signaling, 3868), HSP90 1:1000 (Cell Signaling, 4877S), Rheb 1:1000 (E1G1R, Cell Signaling, 13879), TSC2 1:1000 (D93F12, Cell Signaling, 4308), Akt 1:1000 (Cell Signaling, 9272), Deptor 1:1000 (Novus Bio, NBP1-49674SS), phospho-AMPK $\alpha$  (Cell Signaling, 2535). Rabbit or mouse secondary antibodies conjugated to horseradish peroxidase were used at a 1:10,000 dilution (Jackson Immunochemicals), followed by a 5-minute treatment with

ECL (Amersham, RPN2232). Protein levels were detected using autoradiography and densitometry analysis of protein content was conducted using ImageJ software (NIH, Rockville, MD).

### *2.5.3 Immunohistochemistry*

Tissues were harvested and fixed in formalin overnight at 4°C, followed by a wash with 1X PBS and were then placed in 70% ethanol prior to paraffin embedding. The Wistar Institute Histotechnology Facility performed the tissue embedding and sectioning. For the immunohistochemistry (IHC) studies, paraffin embedded tissue sections were deparaffinized in xylene (Fisher, X5-SK4) and re-hydrated in ethanol (100%-95%-85%-75%) followed by distilled water. Samples underwent antigen retrieval by steaming slides in 10 mM Citrate Buffer (pH 6). Endogenous peroxidase activity was quenched with 3% hydrogen peroxide and slides were incubated in blocking buffer (Vector Laboratories, S-2012) for 1 hr. The slides were incubated with phospho-p70S6K1 (1:100, ThermoFisher Scientific, PA5-37733) or phospho-mTOR (1:100, Cell Signaling, 2971) primary antibody overnight at 4°C. The following day, slides were washed with PBS and incubated with HRP-conjugated secondary antibody for 30 mins. Antibody complexes were detected using DAB chromogen (D5637). Light counterstaining was done with hematoxylin. Slides were imaged using the Nikon 80i upright microscope and at least four fields were taken per section.

### *2.5.4 Co-Immunoprecipitation*

Following overnight seeding of WT and S47 immortalized MEFs, the cells were washed with 1X DPBS and the cell culture medium was replaced with 1% FBS DMEM medium

[pyruvate-free DMEM (Thermo Fisher Scientific #21013024) supplemented with 1% FBS, 1% penicillin/streptomycin, 0.1 mM L-Methionine, 0.5 mM L-Glutamine, and 0.033 mM L-Cystine]. WT cells were treated with PBS or 3 mM GSH for 24 h; while the S47 cells were treated with PBS for 5 h or 24 h, 100  $\mu$ M BSO for 24 h, or 50  $\mu$ M DEM for 5 h. Cells were harvested and centrifuged at 500 x g for 10 min at 4°C. The cell pellets were resuspended in CHAPS Lysis Buffer (1X DPBS with 0.3% CHAPS and freshly added protease inhibitors) at 4°C. Cell disruption was performed by passing the cells through a 23-gauge needle attached to a 1 ml syringe. The skeletal muscles were homogenized using the Qiagen Tissue Lyser II. Total cellular homogenates were rotated/nutated at 4°C for 30 min, and spun at 11,000 x g for 20 min at 4°C. Protein extracts (3 mg per reaction) were incubated with the Rheb antibody (Santa Cruz, sc-271509) overnight at 4°C. The Rheb-immunocomplexes were captured using recombinant protein G agarose (Thermo Fisher Scientific, 15920010) at 4°C for 2 h. Resins were washed three times using the CHAPS Lysis Buffer. Equal volumes of 2x Laemmli Sample Buffer were added to each reaction, samples were heated for 10 min at 100°C. The Rheb-associated proteins were analyzed by Western blotting, using GAPDH (Cell Signaling, 2118), Rheb (Cell Signaling, 13879) and mTOR (7C10, Cell Signaling, 2983) antibodies.

#### *2.5.5 Mitochondrial metabolism and mTOR inhibition assays*

The oxygen consumption rate (OCR) and glycolytic rate were determined using the Seahorse XF MitoStress Assay and the Seahorse XF Glycolytic Rate Assay, respectively, according to the manufacturer's protocol. Cells were plated one day prior to the assay, LCLs at 100,000 cells/well and MEFs at 60,000 cells/well. LCLs were treated with 200 nM rapamycin, 100 nM Torin1 or 1  $\mu$ M Torin1 for 24 hours prior to running the MitoStress Assay. To assess differences in mTOR inhibition, WT and S47

LCLs were treated with 200 nM rapamycin or 100 nM Torin1 for 0 minutes, 10 minutes, 30 minutes, 1 hour, 2 hours, or 6 hours and subsequently cells were harvested for Western blot analysis. To determine mitochondrial content, WT and S47 MEFs were incubated with 500 nM of MitoTracker Green (ThermoFisher Scientific, M7514) for one hour at 37°C. Cells were then spun down, washed once with PBS, spun down and resuspended in PBS. The FACSCelesta (BD Biosciences) was used to detect fluorescence and at least 10,000 events were measured per sample.

#### *2.5.6 Metabolite measurements*

Media was collected after 24 hours after plating LCLs or MEFs, and the YSI-71000 Bioanalyzer was used to determine glucose, glutamine, lactate and glutamate levels as previously described (Londono Gentile et al., 2013). For the metabolic flux studies, cells were incubated in uniformly labeled  $^{13}\text{C}$ -glucose (25 mM) as indicated in the figure legends. For intracellular extracts, after incubation, the culture medium was aspirated, and cells were washed once in ice-cold PBS. Metabolites were extracted by adding a solution of methanol/acetonitrile/water (5:3:2) to the well. Plates were incubated at 4°C for 5 minutes on a rocker and then the extraction solution was collected. The metabolite extract was cleared by centrifuging at 15,000  $\times g$  for 10 minutes at 4°C. Supernatants were transferred to LC-MS silanized glass vials with PTFE caps and either run immediately on the LC-MS or stored at -80°C. LC-MS analysis was performed on a Q Exactive Hybrid Quadrupole-Orbitrap HF-X MS (ThermoFisher Scientific) equipped with a HESI II probe and coupled to a Vanquish Horizon UHPLC system (ThermoFisher Scientific). 0.002 ml of sample is injected and separated by HILIC chromatography on a ZIC-pHILIC 2.1-mm. Samples were separated by ammonium carbonate, 0.1% ammonium hydroxide, pH 9.2, and mobile phase B is acetonitrile. The LC was run at a



flow rate of 0.2 ml/min and the gradient used was as follows: 0 min, 85% B; 2 min, 85% B; 17 min, 20% B; 17.1 min, 85% B; and 26 min, 85% B. The column was maintained at 45°C and the mobile phase was also pre-heated at 45°C before flowing into the column. The relevant MS parameters were as listed: sheath gas, 40; auxiliary gas, 10; sweep gas, 1; auxiliary gas heater temperature, 350°C; spray voltage, 3.5 kV for the positive mode and 3.2 kV for the negative mode. Capillary temperature was set at 325°C, and funnel RF level at 40. Samples were analyzed in full MS scan with polarity switching at scan range 65 to 975 m/z; 120,000 resolution; automated gain control (AGC) target of 1E6; and maximum injection time (max IT) of 100 milliseconds. Identification and quantitation of metabolites was performed using an annotated compound library and TraceFinder 4.1 software. The “M+X” nomenclature refers to the isotopolog for that given metabolite. Isotopologs are chemically identical metabolites that differ only in their number of carbon-13 atoms. For instance, “M+2 citrate” means that two of the six carbons in citrate are carbon-13 while the other four are carbon-12. “M+4 citrate” means that four of the six carbons in citrate are carbon-13 while the other two are carbon-12.

#### *2.5.7 GSH/GSSG abundance and BMH crosslinking*

Relative GSH/GSSG abundance was measured using the GSH/GSSG-Glo Assay (Promega catalog #V6611, according to the manufacturer’s instruction. Immortalized WT and S47 MEFs were generated and maintained as previously described (Jennis et al., 2016; Leu et al., 2019). For BMH crosslinking studies, the WT and S47 cells were cultured in 1% FBS DMEM medium and treated with PBS or 50 µM diethyl maleate (DEM, ThermoFisher Scientific AC114440010) for 5 h; PBS or 100 µM BSO (Cayman Chemical item #14484) for 24 h; or DMSO or 2 µM Erastin (Cayman Chemical item #17754) for 24 h. Proteins were extracted from cultured cells or mouse tissue (skeletal

muscle, lungs) using 1X DPBS (Thermo Fisher Scientific 14190144) supplemented with 0.5% IGEPAL CA-630, 1 mM PMSF, 6 µg/ml aprotinin, and 6 µg/ml leupeptin at 4°C. The tissues were homogenized using the Wheaton Overhead Stirrer. Total cellular homogenates were pulse sonicated using the Branson digital sonifier set at 39% amplitude. Total protein extracts (100 µg per reaction) were incubated with or without 1 mM BMH (Thermo Fisher Scientific 22330) for 30 min at 30°C. The samples were quenched with an equal volume of 2x Laemmli Sample Buffer (BioRad 1610737) supplemented with 5% β-Mercaptoethanol (BioRad 1610710) and heated for 10 min at 100°C. The protein samples were size fractionated on Novex 4-20% Tris-Glycine Mini Gels (Thermo Fisher Scientific XP04200BOX) at room temperature and subsequently transferred overnight onto Immuno-Blot PVDF membranes (BioRad 1620177) at 4°C. The membranes were blocked with 3% nonfat dry milk (BioRad 1706404) in 1X PBST for 30 min at room temperature and incubated with the GAPDH antibody (Cell Signaling Technology 2118) overnight with rotation/nutation at 4°C. After washing the blots in 1X PBST, the membranes were incubated with Donkey anti-Rabbit (Jackson ImmunoResearch 711-036-152) for 2 h at room temperature. Membrane-immobilized protein detection used ECL Western blotting Detection Reagents (GE Healthcare RPN2106; Millipore Sigma GERPN2106).

#### *2.5.8 Proximity Ligation Assay*

Cells were grown on Lab-Tek II 8-well chamber slides, and were either untreated, treated with 50 µM diethyl maleate (DEM, ThermoFisher Scientific AC114440010) for 5 hours or treated with 10 µM of buthionine sulfoximine for 24 hours (BSO, Cayman Chemicals, 83730-53-4) and fixed with 4% paraformaldehyde (Electron Microscopy Sciences, 15710). Protein-protein interactions were assessed using the PLA Duolink in

situ starter kit (Sigma Aldrich, DUO92101) following the manufacturer's protocol. The following primary antibodies were used: Rheb 1:50 (B-12, Santa Cruz, sc271509), mTOR 1:500 (7C10, Cell Signaling, 2983), GAPDH 1:1000 (14C10, Cell Signaling, 2118). ImageJ software (NIH, Rockville, MD) was used to quantify PLA signals.

#### *2.5.9 Immunofluorescence staining*

Cells were fixed in 4% paraformaldehyde for 10 minutes, followed by 3 PBS washes and then permeabilization with 0.25% Triton X-100 for 10 minutes. Cells were washed 3x with PBS, blocked for 1 hour in a PBS solution containing 1% bovine serum albumin and 5% normal goat serum (Jackson ImmunoResearch 005-000-121). Cells were incubated overnight at 4°C with the following primary antibodies diluted in blocking buffer: Rheb 1:800 (Cell Signaling Technologies, #13879), TSC2 1:100 (Cell Signaling Technologies, #4308), LAMP1 1:50 (Santa Cruz, sc-20011). Cells were washed with PBS and incubated with the following secondary antibodies at 37 °C for 45 minutes: Alexa Fluor 594 AffiniPure Goat Anti-Rabbit IgG (Jackson ImmunoResearch 111-585-144) and Alexa Fluor 488 AffiniPure Goat Anti-Mouse IgG (Jackson ImmunoResearch 115-545-062). The cells were mounted with media containing DAPI and images were captured using the Leica TSC SP5 microscope.

#### *2.5.10 Body composition and metabolic cage studies*

WT and S47 mice in a pure C57Bl/6 background are previously described (Jennis et al., 2016). All mouse studies were performed in accordance with the guidelines in the Guide for the Care and Use of Laboratory Animals of the NIH and all protocols were approved by the Wistar Institute Institutional Animal Care and Use Committee (IACUC). Mice

were fed an *ad libitum* diet and were housed in plastic cages with a 12-hour/12-hour light cycle at 22°C unless otherwise stated. Fat and lean content were measured in live male mice at 6 weeks of age using nuclear magnetic resonance (NMR) with the Minispec LF90 (Bruker Biospin, Billerica, MA). Indirect calorimetry was conducted to assess metabolic capabilities in mice (Oxyman/Comprehensive Laboratory Animal Monitoring System (CLAMS); Columbus Instruments). Data for the WT mice was previously published in supplemental data of Kung et al., 2016. Six-week old mice were single caged, provided with water and food *ad libitum* and allowed to acclimate to the cages for 2 days. Oxygen consumption ( $VO_2$ ) and carbon dioxide production ( $VCO_2$ ) were recorded for 48 hours using an air flow of 600 ml/min and temperature of 22°C. Respiratory exchange ratio (RER) is calculated as  $VCO_2/VO_2$  and heat (kcal/h) is calculated by  $3.815 + 1.232*(RER)$ . Photodetectors were used to measure physical activity (Optovarimex System; Columbus Instruments).

#### *2.5.11 Treadmill and serum metabolite studies*

Mice were allowed to acclimate to the metabolic treadmill (Columbus Instruments) for 5 minutes before beginning their runs. The treadmill was then set to 5m/min and speed increased by 5m/min every 2 minutes until 20m/min was reached. Upon reaching 20 m/min, the incline was increased by 5 degrees every 2 minutes until reaching a maximum of 25 degrees. Mice were allowed to run at this maximum speed and incline until exhaustion, defined by the mice spending 10 continuous seconds on the shock grid. Lactate (Nova Biomedical) and glucose (One Touch) measurements were taken using test strips just prior to treadmill entry and immediately after exhaustion using handheld meters. Tail blood was also taken prior to treadmill entry and immediately after

exhaustion and metabolites measured using the Vetest serum analyzer (Idexx Laboratories).

#### 2.5.12 Statistical Analysis

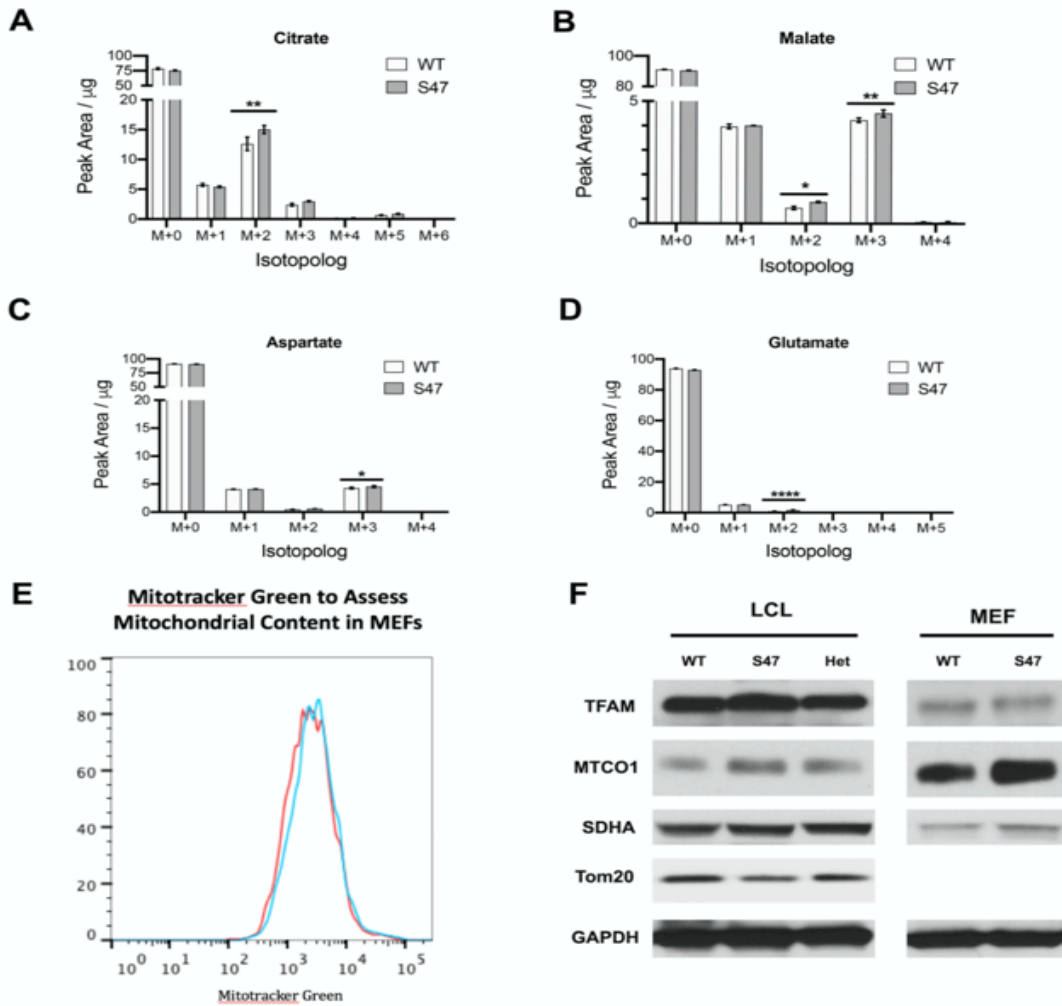
Unless otherwise stated, all experiments were performed in triplicate. The two-tailed unpaired Student t-test was performed. All *in vitro* data are reported as the mean  $\pm$  SD unless stated otherwise, and *in vivo* are reported as the mean  $\pm$  SE. Statistical analyses were performed using GraphPad Prism, p-values are as follows: (\*) p-value < 0.05, (\*\*) p-value < 0.01, (\*\*\*) p-value < 0.001, (\*\*\*\*) p-value < 0.0001. For the CLAMs and mouse exercise data, the Wilcoxon rank-sum test was used to compare the differences between S47 and WT mice.

#### Acknowledgments

This work was supported by R01 CA102184 (M.E.M), R01 CA139319 (D.L.G. and M.E.M), R01 CA238611 (M.E.M), P01 CA114046 (D.L.G. and M.E.M), F32 CA220972 and K99 CA241367 (T.B.), R01 CA174761 (K.E.W.), R01 AG043483 and DK098656 (J.A.B.), and the Rodent Metabolic Phenotyping Core (P30-DK19525). RSA is partly supported by a Bloomberg Distinguished Professorship. The authors would like to acknowledge the Histotechnology, Laboratory Animal and Imaging facilities at the Wistar Institute. The authors are grateful to Allie Lipshutz and Lindsey Schweitzer for expert technical help, and Matthew Jennis for the mouse weight data.



test. (C) Whole cell lysates were extracted from WT and S47 liver, lung, heart and kidney followed by Western blot analysis for the proteins indicated. (D) Whole cell lysates were extracted from 3 WT and 3 S47 mouse lungs and analyzed by Western blot for the phospho-Akt and GAPDH (loading control). Light and dark exposures are shown. (E) WT and S47 MEFs were starved in amino acid free media for 4 hours, then media containing amino acids was re-introduced and samples were collected at indicated time points. Cell lysates were extracted from samples and subjected to Western blot analysis for the proteins indicated. (F) Densitometry quantification of phospho-S6K1 protein expression in WT and S47 MEFs at one-hour time point for serum and glucose starvation, 30-minute time point for amino acid starvation; all values normalized to total S6K1. Densitometry values are averaged from a minimum of two independent experiments. (G) Whole cell lysates were extracted from WT and S47 mouse lung and skeletal tissue and were subjected to Western blot analysis, probing for p62, LC3B and HSP90 (loading control). (H) WT and S47 MEFs were treated with HBSS for 0, 2 and 6 hours and were subjected to Western blot analysis for the indicated proteins. (I) Autophagic flux was measured in WT and S47 MEFs pretreated with  $\text{NH}_4\text{Cl}$  for indicated time points, followed by HBSS treatment for 6 hours. Cell lysates were subjected to Western blot analysis and immunoblotted for LC3B and GAPDH (loading control). (J) WT and S47 MEFs were treated with HBSS for indicated time points and were subjected to viability analysis using Trypan Blue;  $n = 3$ , error bars indicate standard deviation.

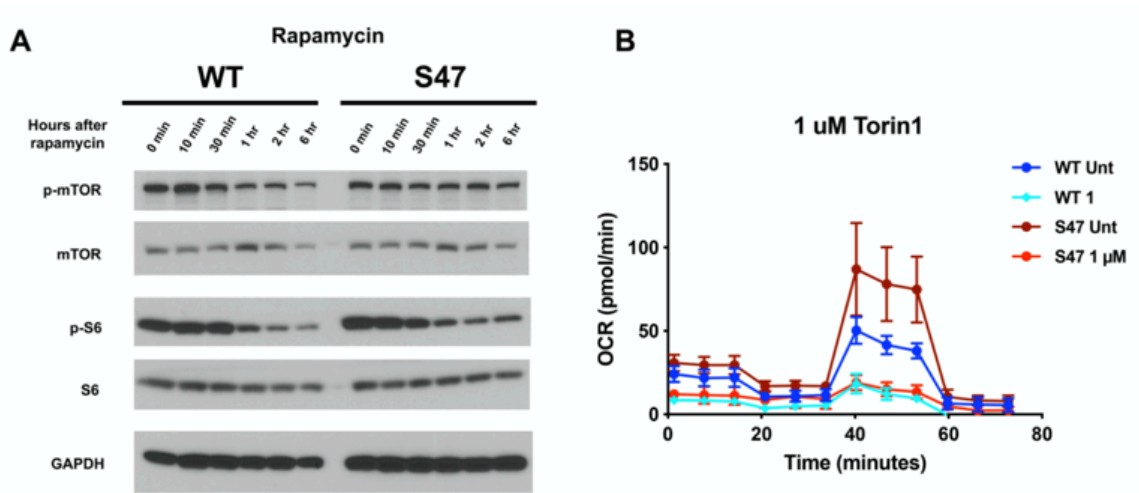


**Supplemental Figure 2.2: Increased metabolism in S47 MEFs but no differences in mitochondrial content in WT and S47 cells.**

(A-D) WT and S47 MEFs were incubated with 25 mM  $^{13}\text{C}$ -glucose for 15 minutes and the abundance of citrate (A), malate (B), aspartate (C) and glutamate (D) isotopologs was quantified by LC-MS/MS. Data are presented as mean  $\pm$  SD,  $n = 3$ ; 2-way ANOVA. (\*)  $p$ -value  $< 0.05$ , (\*\*)  $p$ -value  $< 0.01$ , (\*\*\*)  $p$ -value  $< 0.001$ , (\*\*\*\*)  $p$ -value  $< 0.0001$ . (E) Mitochondrial mass in WT and S47 MEFs measured by Mitotracker Green fluorescence. Data depicted are representative of three independent experiments performed in triplicate. (F) Cell lysates extracted from WT,

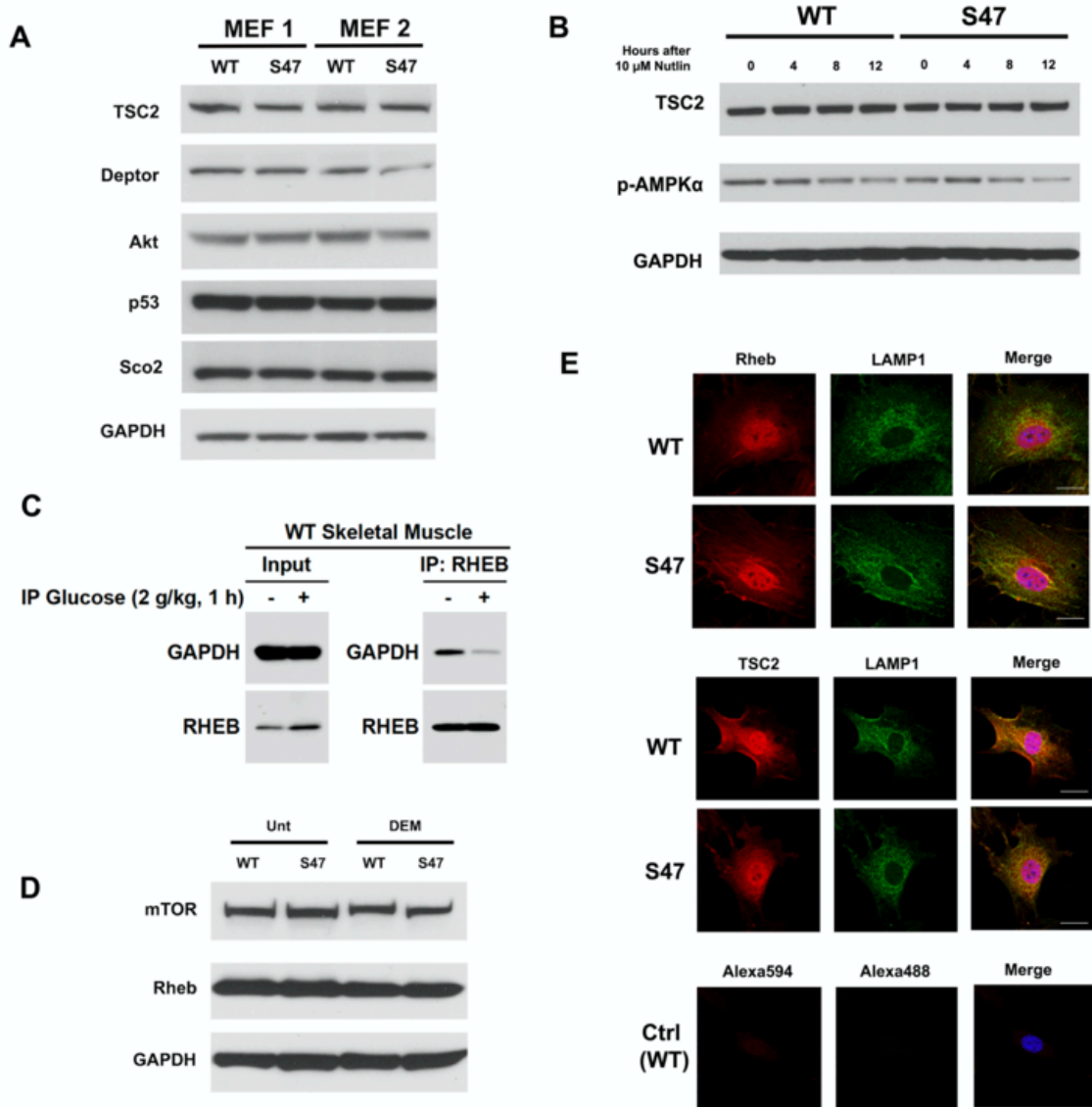


WT/S47 (het) and S47 LCLs and WT and S47 homozygous MEFs were subjected to Western blot analysis and immunoblotted for TFAM, MTCO1, SDHA, TOMM20 and GAPDH (loading control).



**Supplemental Figure 2.3: Attenuated response to mTOR inhibition in S47 cells**

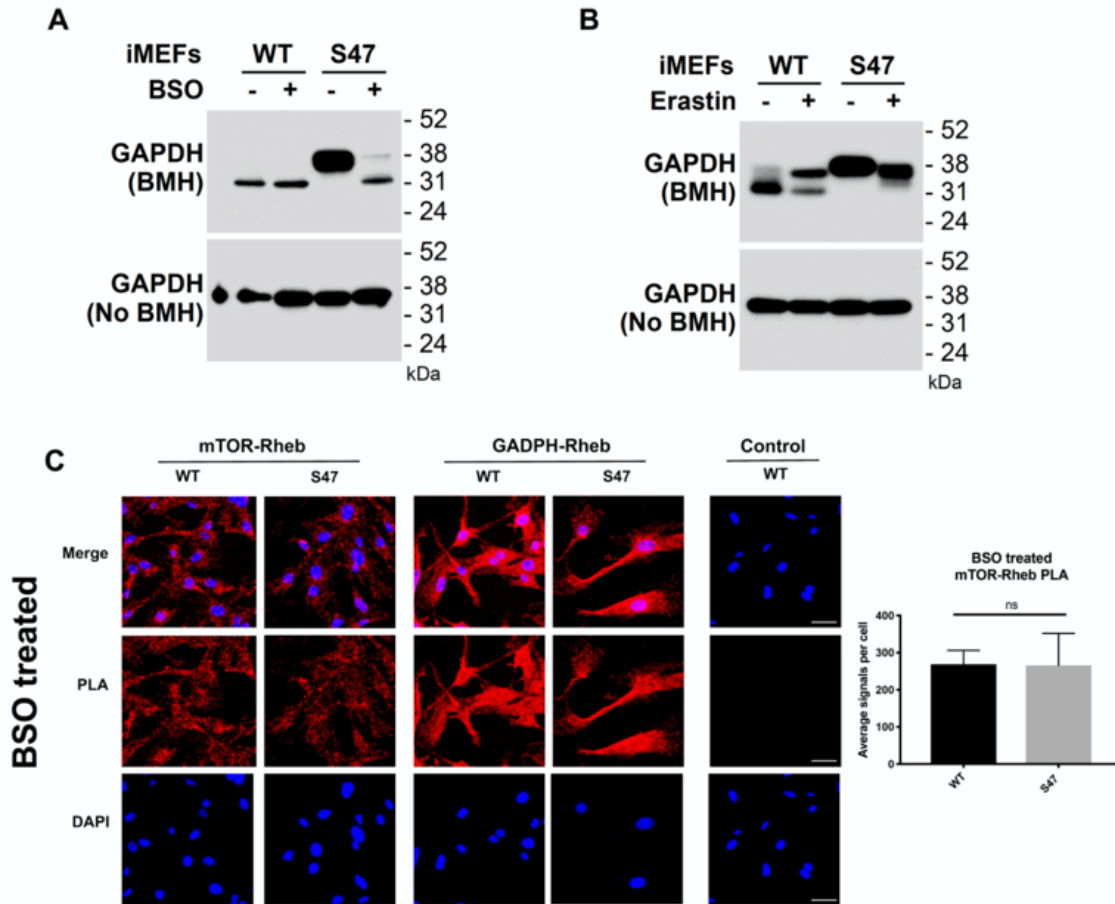
(A) WT and S47 LCLs were treated with 200 nM of rapamycin, harvested at indicated time points after treatment and analyzed for shown mTOR markers via Western blot. (B) OCR as measured by the Seahorse XF Mito Stress Test in WT and S47 LCLs treated with 1  $\mu$ M of Torin1 for 24 hours. Note that samples were run on the same plate as the data depicted in Figure 2.3C; therefore, the untreated samples are identical to Figure 2.3C but are presented here for comparison sake and clarity.



**Supplemental Figure 2.4: No differences in the level of mTOR regulators in WT and S47 cells**

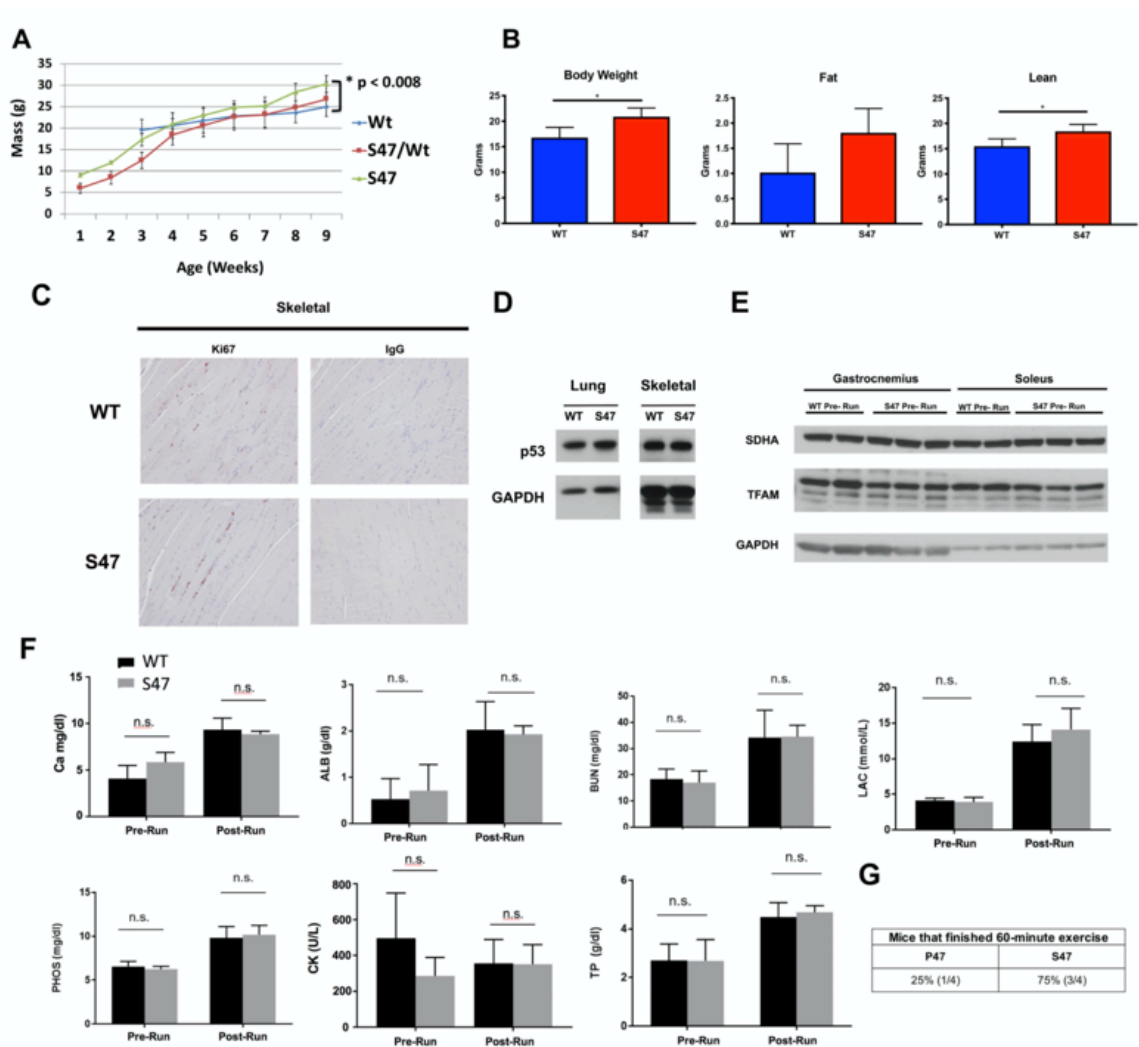
(A) Cell lysates were extracted from two sets of WT and S47 MEFs and were analyzed by Western blot for TSC2, DEPTOR, AKT, p53, Sco2 and GAPDH. (B) Cell lysates were extracted from WT and S47 MEFs treated with 10  $\mu$ M Nutlin for indicated time points. TSC2, phospho-AMPK $\alpha$  and GAPDH were assessed by Western blot. (C) Mice were fasted for 24 hours and

intraperitoneally injected with saline or glucose (2g/kg body weight). Whole cell lysates were extracted from skeletal muscles at 1 hour post-injection and subjected to Western blot analysis for GAPDH and Rheb (left). The same lysates were immunoprecipitated (IP) with Rheb antibody followed by Western analysis for the level of associated GAPDH and Rheb (right). (D) WT and S47 MEFs were untreated or treated with 50  $\mu$ M of DEM for 5 h. Cell lysates were subjected to Western blot analysis and immunoblotted for total mTOR, Rheb and GAPDH. (E) WT and S47 MEFs were immunostained with LAMP1 (Alexa488-green) and either TSC2 or Rheb (Alexa594-red) to determine co-localization. Nuclei are visualized with DAPI staining. Scale bars represent 30  $\mu$ M.



**Supplemental Figure 2.5: Glutathione depletion by BSO alters GAPDH cross-linking and the GAPDH-Rheb interaction**

(A) WT and S47 cells were treated with PBS or 100  $\mu$ M BSO for 24 hours. Lysates were prepared, treated with or without BMH, run on SDS-PAGE and detected by Western blotting with a GAPDH antibody. (B) WT and S47 cells were treated with DMSO or 2  $\mu$ M Erastin for 24 hours. Lysates were prepared, treated with or without BMH, resolved by SDS-PAGE, and probed by Western blotting for GAPDH. (C) An *in situ* proximity ligation assay was performed in WT and S47 MEFs that are treated with 10  $\mu$ M of BSO for 24 h. Shown on the right is the quantification of the mTOR-Rheb interactions, measured as the average number of PLA signals per nuclei.



**Supplemental Figure 2.6: Serum metabolites and protein markers pre- and post- exercise.**

(A) Record of mouse weights in WT, S47 and heterozygous WT/S47 mice over the course of 18 weeks; a minimum of 10 mice of each genotype were tracked, and error bars mark standard error. (B) Body weight, fat content and lean content as measured by proton magnetic resonance spectroscopy (H-MRS); n=5 mice per genotype, error bars mark standard error, (\*) p-value < 0.05. (C) Ki67 immunohistochemical staining of skeletal muscle from WT and S47 mice. IgG control shown on right. (D) Total p53 protein levels in WT and S47 lung and skeletal tissue. (E) Whole cell lysates were extracted from gastrocnemius or soleus muscle from untreated WT and

S47 mice and subjected to Western blot analysis for the proteins indicated. (F) Blood serum metabolite levels measured in WT and S47 mice before and after treadmill run: Ca (calcium), ALB (albumin), PHOS (phosphate), CK (creatinine kinase), BUN (blood urea nitrogen), LAC (lupus anticoagulant), TP (total protein). n.s. not significant, Student's t-test. (G) WT and S47 mice were subjected to a 60-minute treadmill run. Table indicates proportion of mice that completed run; n = 4.

## Chapter 3: *PLTP* Identified as a p53-Target Gene that Mediates Ferroptosis Resistance in HepG2 Cells

This chapter has been adapted from the following manuscript in preparation:

Gnanapradeepan K, Murphy ME. *PLTP* Identified as a p53-Target Gene that Mediates Ferroptosis Resistance in Liver Cancer Cells. (*in prep*)

### 3.1 Abstract

The tumor suppressor protein p53 prevents oncogenesis through processes such as apoptosis and cell cycle arrest, however recently its role in regulating ferroptotic cell death has begun to emerge. Ferroptosis is driven by the inactivation of glutathione peroxidase 4 (GPX4), a phospholipid peroxidase, leading to accumulation of lethal levels of lipid peroxidation and ultimately resulting in cell death. How exactly p53 mediates ferroptosis remains poorly understood, as it has been shown to play a role in both inducing and suppressing ferroptosis based on the context. Here, we identified *PLTP* (phospholipid transfer protein) as a direct p53 target gene that plays a role in mediating ferroptosis resistance in HepG2 cells. We found that silencing *PLTP* expression sensitized cells to RSL3-induced cell death and lipid peroxidation, while activation of *PLTP* expression protected cells from RSL3-induced cell death and decreased lipid peroxidation. Our data suggest that PLTP promotes lipid storage, sequestering lipids into lipid droplets and away from the cell membrane, thus protecting lipids from peroxidation at the membrane. Taken together, our findings reveal a novel role for p53 in driving ferroptosis resistance and indicate lipid transport as another key pathway involved in the regulation of ferroptosis.

### 3.2 Introduction

The *TP53* gene is the most frequently mutated gene in cancer and has a well-established role in tumor suppression. It encodes the protein p53, which most commonly serves as a transcription factor that regulates hundreds of downstream target genes to prevent tumorigenesis (Kasthuber and Lowe, 2017). For decades, it was believed that cell cycle arrest, senescence and apoptosis were the primary modes of tumor suppression and in recent years many other p53 functions have begun to emerge such as control of metabolism, autophagy, cellular redox state, and ROS control (Berkers et al., 2013; Gnanapradeepan et al., 2018). It is clear that the context of p53 activation, such as type of stress encountered or tissue in which this stress occurs, plays a vital role in the type of response p53 subsequently elicits.

A mouse model with a defective acetylation site, known as the 3KR mouse, was characterized as being impaired for cell cycle arrest, senescence and apoptosis, yet still retained its ability to halt tumor formation (Li et al., 2012). This suggested that the canonical functions of p53 are not solely responsible for tumor suppression. Upon further investigation, it was revealed that these mice were protected from cancer because they retained the ability to undergo ferroptosis. Ferroptosis is best described as an iron mediated, caspase independent form of cell death driven through the peroxidation of polyunsaturated fatty acids. It is a process that differs from other forms of cell death on a genetic, biochemical and morphological level (Dixon et al., 2012). GPX4 is a key protein that is inactivated in ferroptosis, as it normally functions to neutralize the harmful lipid reactive oxygen species that build up at the cellular membrane. *SLC7A11* is a gene that encodes part of a cystine/glutamate antiporter, and when repressed leads to ferroptosis



induction (Jiang et al., 2015). Two small molecule inhibitors that are commonly used to induce ferroptosis *in vitro* are RSL3 and erastin, which function by inhibiting GPX4 and SLC7A11, respectively (Stockwell et al., 2017).

Various lipid metabolism genes have been implicated in ferroptosis sensitivity, as lipid peroxidation plays such a crucial role in this process. Acyl-CoA synthetase long-chain family member 4 (ACSL4) has been shown to drive ferroptosis by converting free fatty acids into fatty CoA esters that are required for ferroptosis (Doll et al., 2017; Yuan et al., 2016). ALOX15 and ALOX12 are two p53 target genes that promote ferroptosis by serving as a lipoxygenases, necessary for the peroxidation of the polyunsaturated fatty acids (Chu et al., 2019; Ou et al., 2016). Recently, stearoyl-CoA desaturase 1 (SCD1) was found to protect ovarian cancer cells from ferroptosis by catalyzing the rate-limiting step in monosaturated fatty acid synthesis (Tefay et al., 2019). As ferroptosis is a relatively new field, the precise mechanisms of regulation are still be ironed out.

The exact role of p53 in ferroptosis is likely to be cell type and stimulus specific. Initial studies highlighted the role of p53 in promoting ferroptosis sensitivity (Gao et al., 2015; Jennis et al., 2016; Jiang et al., 2015; Ou et al., 2016). However, other studies have suggested that p53 stabilization can negatively regulate ferroptosis through expression of CDKN1A/p21 (Tarangelo et al., 2018). In colorectal cancer cells, it was found that p53 inhibits ferroptosis by blocking dipeptidyl-peptidase-4 (DPP4) activity (Xie et al., 2017). Thus, further investigation is required in order to dissect the pleiotropic functions of p53 in the control of ferroptosis.

Our lab generated a mouse model with a single nucleotide polymorphism at amino acid 47 in *TP53*, hereafter referred to as the S47 mouse, and discovered it had

impaired tumor suppressive function and a defect in ability to undergo ferroptosis (Jennis et al., 2016). Using S47 as a tool, we have identified phospholipid transfer protein (*PLTP*) as a novel p53 target gene that plays a role in mediating ferroptosis resistance in HepG2 cells. PLTP is a lipid transport protein secreted predominantly from the liver and plays a role in the transfer of various lipid molecules such as phosphatidylcholine, phosphatidylethanolamine and phosphatidylglycerol to name a few (Albers et al., 2012). Our findings characterize the function of PLTP in a p53 dependent context for the first time and suggest a novel role for p53 in regulating ferroptosis through lipid transport.

### **3.3 Results**

#### *3.3.1 PLTP identified as gene that is downregulated by the S47 variant of p53*

We have previously shown that the S47 variant of p53 is resistant to ferroptosis induction, in part through decreased ability to repress *SLC7A11* and transactivate *GLS2* (Jennis 2016). Thus, we sought to use S47 as a tool to identify novel p53 target genes that could play a role in mediating ferroptosis. To address this, human lymphoblastoid cells (LCLs) homozygous for the S47 variant or WT p53 were jointly treated with the ferroptosis inducers Nutlin plus tert-Butyl-hydroperoxide (TBH). TBH is widely used to induce ROS and the combination of Nutlin and TBH has been used as a method of ferroptotic induction (Ou et al., 2016). We focused our initial studies on the Nutlin/TBH combination as we have found the LCLs used in our studies appear to be resistant to erastin. RSL3 was found to be too cytotoxic on this cell type and results in a very low yield of RNA. The RNA obtained from these samples was subjected to RNA sequencing, which revealed *PLTP* as the top gene that was differentially expressed between WT and S47 cells (Table 3.1, Figure 3.1A). To validate these findings, we performed qRT-PCR in

LCLs that were either treated with Nutlin, TBH, or the combination of Nutlin and TBH, and found that *PLTP* was significantly downregulated in S47 LCLs under all tested conditions (Figure 3.1B). This was further confirmed by a similar qRT-PCR in WT and S47 mouse embryonic fibroblasts (MEFs), which showed *Pltp* is also downregulated in the mouse S47 cells (Figure 3.1C). Western blot analyses revealed that the protein levels of PLTP are significantly lower in S47 LCLs (Figure 3.1D). In order to determine if there was a difference in localization of PLTP in mouse tissue, IHC analyses were conducted on liver tissue extracted from WT and S47 mice. It was found that PLTP is a secreted protein that exists mostly in the extracellular space and appears to be present at much lower levels in S47 liver tissue (Figure 3.1E). These collective data demonstrate that PLTP is expressed at much lower levels in S47.

**Table 3.1: Genes identified as being at least 3-fold downregulated in S47 LCLs**

<b>Gene</b>	<b>Function</b>
PLTP	Transfers phospholipids from triglyceride-rich lipoproteins to high density lipoprotein (HDL)
ASPA	Catalyzes conversion of N-Acetyl_L-aspartic acid to aspartate and acetate
RBPM2	Involved in development and dedifferentiation of digestive smooth muscle cells
STRA6	Membrane protein that acts as receptor for retinol/retinol binding protein complexes
EPS8L2	Links growth factor stimulation to actin organization
DUSP14	Dephosphorylates tyrosine and serine/threonine residues
CD6	Encodes protein found on outer membrane of T-lymphocytes/other immune cells; plays role in continuation of T-cell activation

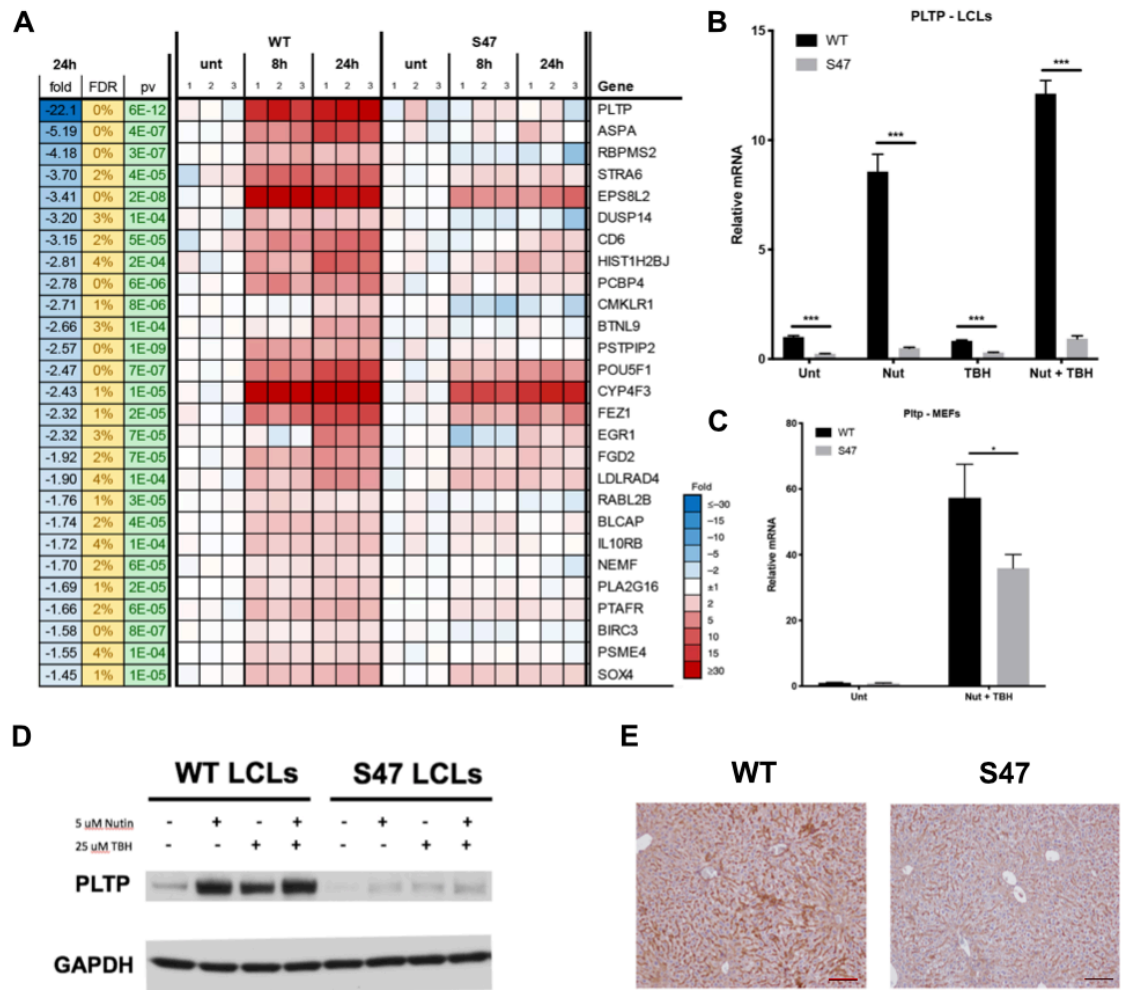


**Figure 3.1: PLTP is differentially regulated by WT p53 and the S47 variant**

(A) RNA-Seq identifying genes with significantly different expression between WT and S47 LCLs treated with 5  $\mu$ M Nutlin and 25  $\mu$ M TBH for 0, 8 and 24 hours. Blue indicates decrease in gene expression relative to untreated WT, red indicates increase. P-value <0.05 (unpaired t-test) and FDR <25%. (B) qRT-PCR analysis of *PLTP* in LCLs treated with 5  $\mu$ M Nutlin, 25  $\mu$ M TBH or combination of both, for 24 hours. All values were normalized to a control gene (18S); n=3, error bars indicate standard error. (\*\*\*) p-value < 0.001, Student's t-test. (C) qRT-PCR analysis of *Pltp*

in MEFs treated with 10  $\mu$ M Nutlin and 25  $\mu$ M TBH for 24 hours. All values were normalized to a control gene (Cyclophilin A); n=3, error bars indicate standard error. (\*) p-value < 0.05, Student's t-test. (D) Western blot analyses comparing PLTP expression in WT and S47 LCLs treated with 5  $\mu$ M Nutlin, 25  $\mu$ M TBH or combination of both, for 24 hours. (E) Immunohistochemical analysis of PLTP in WT and S47 liver tissue. Data are representative of n = 4 fields per genotype. Scale bar represents 100  $\mu$ m.

### 3.3.2 *The role of p53 in regulating PLTP and ferroptosis in HepG2 cells*

The PLTP protein is secreted predominantly from the liver thus we focused our studies on the HepG2 cancer cell line, which is derived from liver and expresses WT p53. To ensure that *PLTP* is activated in a p53 dependent manner, we silenced p53 in HepG2 cells using a short hairpin RNA. Nutlin was used to activate p53, and *PLTP* gene expression was found to be significantly lower in the cells that were silenced for p53 (Figure 3.2A). We next treated our cells with Nutlin over a time course and found that PLTP protein levels were again significantly lower in the sh-p53 cell line (Figure 3.2B). Our data are consistent with previously reported findings, suggesting that *PLTP* is a direct transcriptional target of p53 (Goldstein et al., 2012).

Before directly assessing the role of PLTP in ferroptosis, we wanted to assess the sensitivity of HepG2 cells to ferroptosis, as it has been reported that different cell lines express differential sensitivity to ferroptosis (Doll et al., 2017; Yuan et al., 2016). Both erastin and RSL3 were capable of inducing ferroptosis in HepG2 cells, however RSL3 was found to be a more potent inducer thus was used for the remainder of the studies (Figure 3.2C-D). We compared the effects of silencing p53 on ferroptosis in HepG2 cells and were surprised to detect no significant differences in ferroptosis sensitivity between the silenced p53 cell line and control (Figure 3.2C-D). Recent studies

have emerged suggesting that cell media and metabolism can influence ferroptosis sensitivity in a p53 dependent manner (Leu et al., 2019; Tarangelo et al., 2018), so we repeated this assay under low glucose and low serum media conditions. As expected, these conditions further sensitized cells to ferroptosis using both erastin and RSL3, and surprisingly, p53 silenced cells showed greater susceptibility to ferroptosis (Figure 3.2E-F). Taken together, our data suggest that p53 plays a key role in regulating *PLTP* and that in HepG2 cells, p53 negatively regulates ferroptosis.

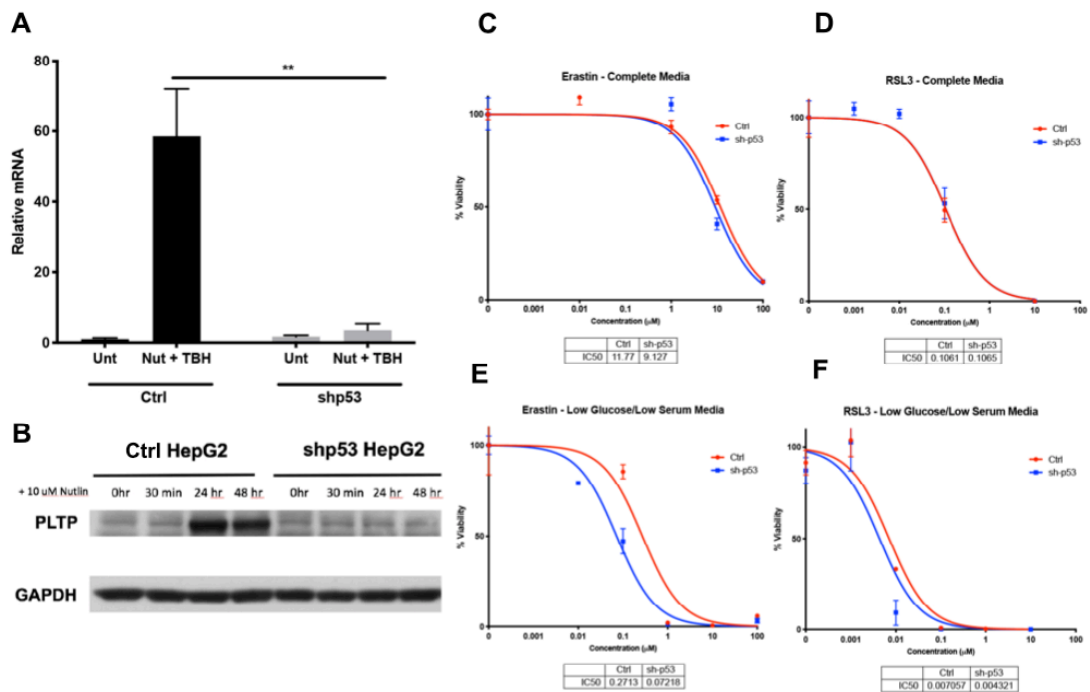


**Figure 3.2: p53 positively regulates PLTP but negatively regulates ferroptosis in HepG2 cells**

(A) qRT-PCR analysis of *PLTP* in HepG2 cells treated with 10  $\mu$ M Nutlin for 24 hours, with and without p53 knockdown. All values were normalized to a control gene (18S); n=3, error bars indicate standard error. (\*\*\*) p-value < 0.001, Student's t-test. (B) Western blot analyses

comparing PLTP expression in HepG2 cells with and without p53 knockdown. Cells were treated with 10  $\mu$ M Nutlin and lysates were harvested at 0 hr, 30 minutes, 24 hrs and 48 hrs. Data representative of 3 independent experiments. (C-D) Viability analysis of HepG2 cells with and without p53 knockdown treated with indicated doses of (c) erastin or (d) RSL3 for 72 hours in complete media. Error bars represent standard error of mean, n=4. (E-F) Viability analysis of HepG2 cells with and without p53 knockdown treated with indicated doses of (e) erastin or (f) RSL3 for 72 hours in low glucose low serum media. Error bars represent standard error of mean, n=4.

### 3.3.3 *PLTP promotes ferroptosis resistance*

Knowing that S47 cells are impaired in ferroptosis prompted us to assess the role PLTP might play in ferroptosis. Two knockdown cell lines were generated using short hairpins for *PLTP* in HepG2 and qRT-PCR confirmed that *PLTP* was effectively silenced (Figure 3.3A). Knockdown of PLTP using two different short hairpins sensitized cells to RSL3 induced cell death (Figure 3.3B and C). We next examined the effects of PLTP silencing on the generation of lipid ROS, as lipid peroxidation is a key hallmark of ferroptosis. Consistent with our viability data, we found that silencing PLTP significantly increased lipid peroxidation that occurs after treatment with RSL3 (Figure 3.3D-E).

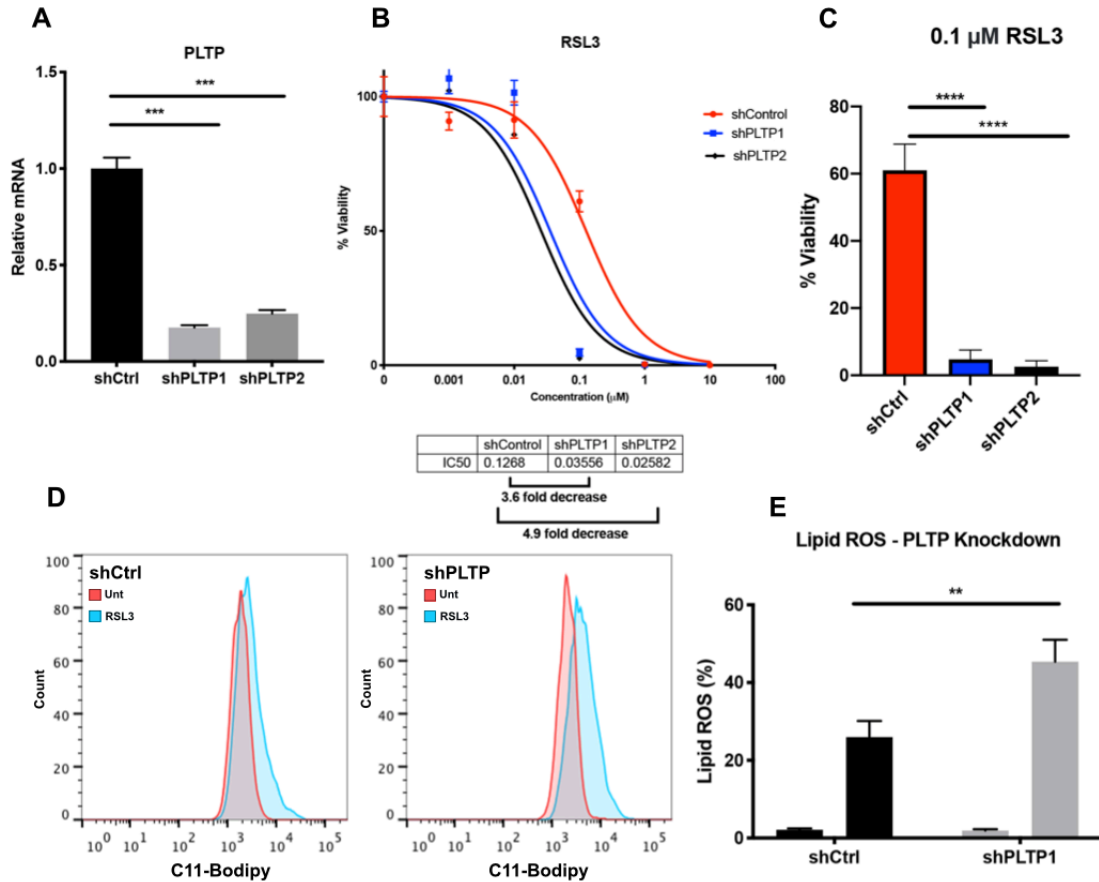


**Figure 3.3: Knockdown of PLTP increases RSL3-induced ferroptosis sensitivity.**

(A) qRT-PCR analysis of *PLTP* expression in indicated knockdown HepG2 cells. All values were normalized to a control gene (18S); n=3, error bars indicate standard error. (\*\*\*) p-value < 0.001, Student's t-test. (B) Viability analysis of short hairpin control or PLTP knockdown cells treated with indicated doses of RSL3 for 72 hours. Data are representative of three independent experiments, four technical replicates, error bars represent standard error of mean. (C) Viability analysis of short hairpin control or PLTP knockdown cells treated 0.1  $\mu$ M RSL3 for 72 hours (single point from b). Error bars represent standard deviation, (\*\*\*\*) p-value < 0.0001, Student's t-test. (D) Lipid peroxidation in knockdown cell lines treated with 0.5  $\mu$ M RSL3 for 3 hours was assessed by flow cytometry using C11-BODIPY. Data are representative of three independent



experiments. (E) Quantification of lipid peroxidation levels. Error bars indicate standard deviation. n=3, (\*\*) p-value < 0.01

To extend these findings, we examined the effect of overexpressing PLTP in HepG2 cells. Once the expression was confirmed via qRT-PCR (Figure 3.4A), we proceeded to assess cell viability after RSL3 treatment. We found that PLTP overexpression leads to ferroptosis resistance in cells treated with Nutlin and RSL3 (Figure 3.4B-C). Overexpression of PLTP significantly decreased RSL3 induced lipid peroxidation (Figure 3.4D-E). The combined data support the premise that PLTP expression drives ferroptosis resistance in HepG2 cells.

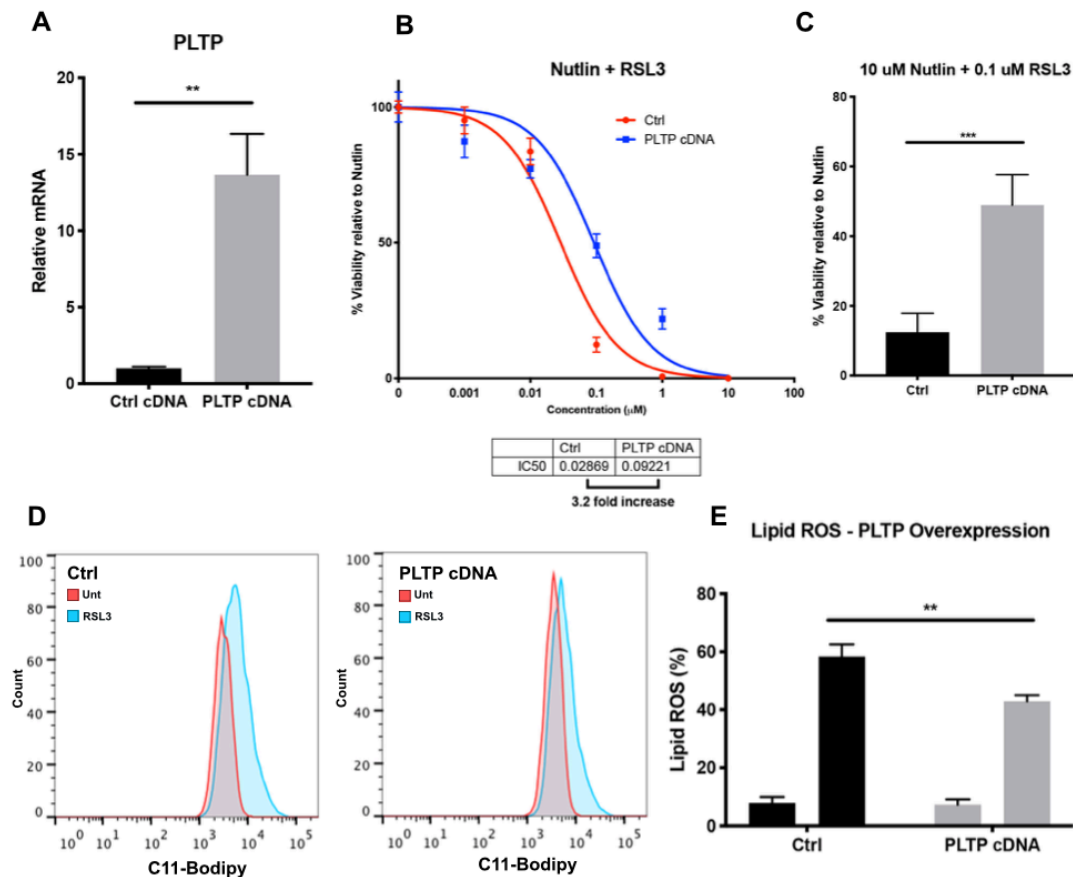


**Figure 3.4: Overexpression of PLTP confers ferroptosis resistance.**

(A) qRT-PCR analysis of *PLTP* expression HepG2 cells containing empty vector and PLTP cDNA. All values were normalized to a control gene (18S); n=3, error bars indicate standard error. (\*\*\*) p-value < 0.001, Student's t-test. (B) Viability analysis of vector control or cells overexpressing PLTP treated with 10  $\mu$ M Nutlin and indicated doses of RSL3 for 72 hours. Viability normalized to treatment with 10  $\mu$ M Nutlin alone. Data are representative of three independent experiments, four technical replicates, error bars represent standard error of mean. (C) Viability analysis of vector control or cells overexpressing PLTP treated with 10  $\mu$ M Nutlin and 0.1  $\mu$ M RSL3 for 72 hours (single point from b). Error bars indicate standard deviation, (\*\*\*) p-value < 0.001. (D) Lipid peroxidation in cells overexpressing PLTP treated with 0.5  $\mu$ M RSL3 for 3 hours was assessed by flow cytometry using C11-BODIPY. Data are representative of three independent experiments. (E) Quantification of lipid peroxidation levels. Error bars indicate standard deviation. n=3, (\*\*) p-value < 0.01

**3.3.4 *PLTP* silencing does not impact other cell death processes**

To verify that the cell death being observed is, in fact, due to ferroptosis, a rescue assay was performed using ferroptosis-specific rescue agents ferrostatin and liproxstatin. PLTP-silenced cells experienced 100% cell death when treated with a high dose of RSL3. However, when PLTP-silenced cells were pretreated with either ferrostatin or liproxstatin for 30 minutes, and then treated with the same dose of RSL3, little to no cell death was observed indicating that ferroptosis is the primary mode of cell death occurring in these PLTP-silenced cells (Figure 3.5A). Prior studies from our lab show that the S47 variant is impaired for cell death by cisplatin (Jennis et al., 2016). No significant differences in cell death were observed in PLTP-silenced cells when treated

with cisplatin (Figure 3.5B-C). We next assessed several other chemotherapeutic agents such as doxorubicin, etoposide, camptothecin and tunicamycin. Our studies revealed no significant differences in cell viability when comparing PLTP-silenced cell lines to the shCtrl cell lines (Figure 3.5D-G), highlighting the fact that PLTP silencing seems to affect ferroptosis but not other cell death pathways.

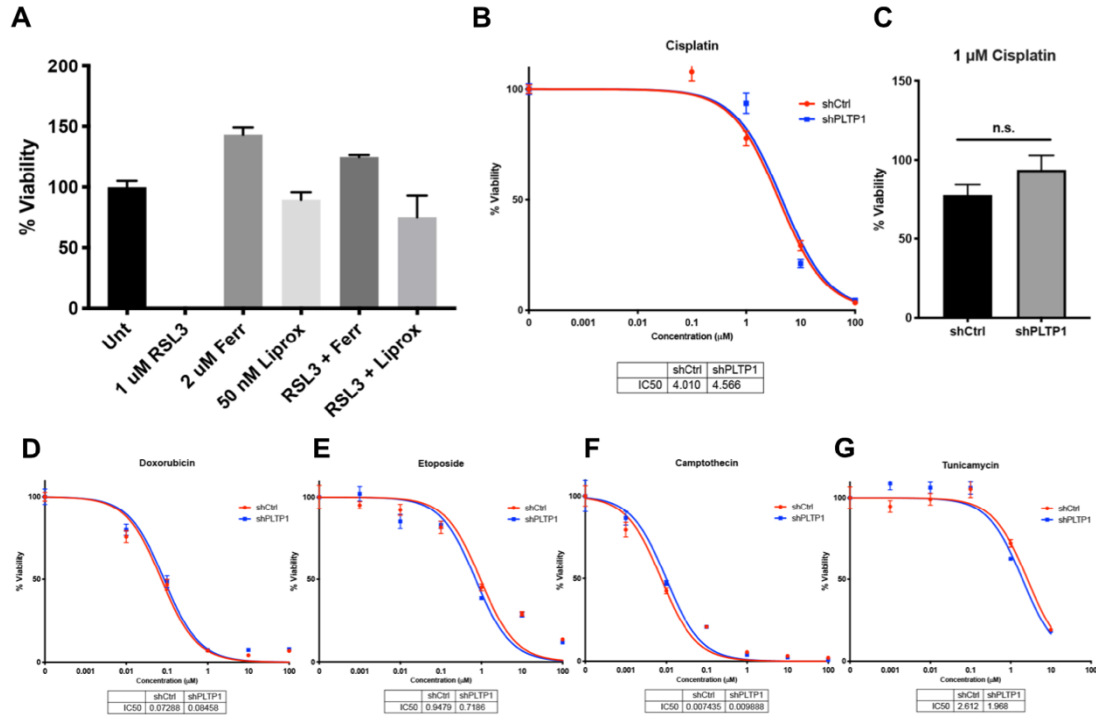


**Figure 3.5: PLTP silencing does not affect sensitivity to other forms of cell death.**

(A) Viability analysis of PLTP knockdown cells subjected to indicated treatments. Cells pretreated with either 2  $\mu$ M ferrostatin or 50 nM liproxstatin for 30 minutes, followed by treatment with 1  $\mu$ M RSL3 for 24 hours. Viability normalized to untreated cells, error bars indicate standard deviation, n = 4. (B) Viability analysis of short hairpin control or PLTP knockdown cells treated with indicated doses of cisplatin for 72 hours. Error bars represent standard error of mean, n = 4. (C) Viability analysis of short hairpin control or PLTP knockdown cells treated 1  $\mu$ M cisplatin for 72 hours (single point from b). Error bars indicate standard deviation, p-value not significant. (D-G) Viability

analysis of short hairpin control or PLTP knockdown cells treated with indicated doses of (d) doxorubicin, (e) etoposide, (f) camptothecin or (g) tunicamycin for 72 hours. Error bars represent standard error of mean, n = 4. No significant differences observed.

### *3.3.5 PLTP protects cells from ferroptotic cell death by promoting lipid storage*

We next sought to determine the mechanism by which PLTP mediates ferroptosis resistance. It is well known that PLTP plays a role in transporting various lipid molecules, including phosphatidylethanolamine which is one of the key lipids that undergo peroxidation at the cellular membrane during ferroptosis (Albers et al., 2012; Kagan et al., 2017). A recent study demonstrated enhanced lipid storage in the form of lipid droplets can inhibit ferroptosis (Bai et al., 2019). This is supported by other studies that show lipid droplet formation can protect cells from forms of oxidative cell death by sequestering polyunsaturated fatty acids away from the cellular membrane (Li et al., 2018). Based on these findings, we hypothesized that PLTP could promote ferroptosis resistance by transporting lipids away from the cellular membrane and into lipid droplets, thereby reducing the lipids available to undergo peroxidation at the membrane.

We verified PLTP influences lipid droplet formation by visualizing cells stained with the lipid droplet marker BODIPY 493/503 and found PLTP-silenced cells showed very few lipid droplets in comparison to the control (Figure 3.6A). To determine whether PLTP drives ferroptosis resistance through enhanced lipid storage, we treated cells overexpressing PLTP with RSL3 and assessed the levels of lipid droplets using flow cytometry. When comparing control cells to cells overexpressing PLTP that are untreated, there is an increase in lipid droplet content as depicted by the rightward shift of the solid green curve to the solid orange curve (Figure 3.6B). Upon treatment with

RSL3, there is a decrease in lipid droplet content in both control cells and cells overexpressing PLTP, as shown by the leftward shift of the curves from the solid colors to the respective transparent colors (Figure 3.6B). These data are consistent with previously reported data showing induction of ferroptosis leads to a decrease in lipid droplet levels (Bai et al., 2019). Whereas RSL3 causes decreased lipid droplet accumulation in cells overexpressing PLTP, the overall lipid droplet levels remain higher compared to the control cells. (Figure 3.6B). Taken together, these data support the premise that PLTP protects cells from ferroptotic cell death by enhancing lipid storage and preventing lipids from undergoing peroxidation at the cellular membrane (Figure 3.6C).

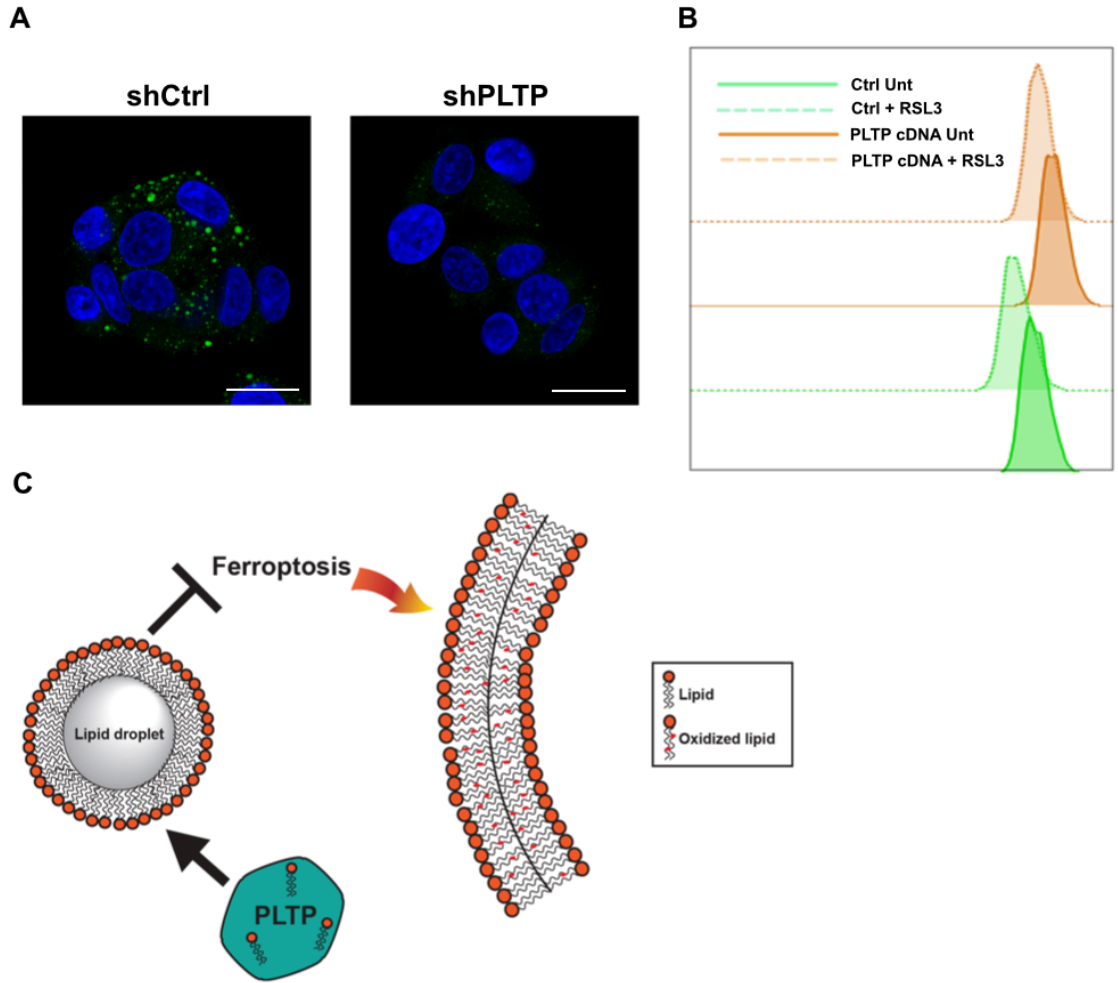


**Figure 3.6: A model for PLTP in ferroptosis resistance by promoting lipid storage.**

(A) Knockdown of PLTP decreases lipid droplet accumulation, visualized using BODIPY 493/503. DAPI staining used to visualize nuclei, scale bar represents 20  $\mu\text{m}$ . (B) Lipid droplet accumulation assessed using BODIPY 493/503 in cells overexpressing PLTP, treated with and without 500 nM RSL3 for 12 hours. Data representative of 2 independent experiments, 4 technical replicates. (C) Proposed mechanism of how PLTP promotes ferroptosis resistance: PLTP enables increased lipid droplet formation, thus protecting polyunsaturated fatty acids from undergoing ferroptosis at the cell membrane.

### 3.4 Discussion

Programmed cell death is a complex network that is mediated by various intrinsic and extrinsic signals. In recent years lipids have emerged as key drivers of various cell death pathways, shown to play roles in apoptosis, necroptosis and ferroptosis (Magtanong et al., 2016). Cell death via ferroptosis occurs by lipid peroxidation at the cellular membrane, yet precise mechanisms of this process are still being ironed out especially with regard to the role of p53 (Gnanapradeepan et al., 2018; Murphy, 2016). In this study, we demonstrate that the p53 target gene *PLTP* promotes ferroptosis resistance in HepG2 cells. Silencing *PLTP* was found to sensitize cells to cell death by RSL3 and increased lipid peroxidation, while overexpressing *PLTP* led to greater resistance to cell death by RSL3 and decreased lipid peroxidation. The cell death differences that were observed were confirmed to be specific to ferroptosis. *PLTP* appears to increase lipid storage in the form of lipid droplets, thereby protecting lipids from peroxidation at the membrane. These data are the first to characterize the function of *PLTP* in a p53 dependent context and reveal a novel potential role for p53 in driving ferroptosis resistance through lipid transport.

There are several experiments that should be done in order to strengthen these findings. An important control for the short hairpin silencing data is to combine treatment with a non-silenceable, rescue cDNA. This study was performed in HepG2 cells, and further work in other liver cancer cell lines containing WT p53 such as SK-Hep-1 are required. It would also be interesting to see if this phenotype is specific to liver cancer cells, thus extending these studies to other lipid rich cancer cell lines such as melanoma or ovarian cancer would be very interesting. We provided evidence that *PLTP* increases lipid storage, yet the exact lipids that are involved remain unknown. Ferroptosis is driven

through oxidation of phosphatidylethanolamines containing arachidonic acid or adrenic acid (Kagan et al., 2017) and it is known that certain lipid types, such as monounsaturated fatty acids, can lead to ferroptosis resistance (Magtanong et al., 2019). A lipidomics study would be very informative to further dissect this mechanism and understand exactly what lipid types are involved in PLTP-mediated transport that results in ferroptosis resistance. PLTP is known to transport Vitamin E (also known as  $\alpha$ -tocopherol), a lipophilic antioxidant that has been shown to protect cells from oxidative damage and ferroptosis (Raederstorff et al., 2015; Yang and Stockwell, 2016). An alternate hypothesis is that PLTP drives ferroptosis resistance by transporting Vitamin E to cells, thus it would be worthwhile to investigate the role of Vitamin E in this process.

Insight into the function of PLTP come from studies of the PLTP knockout mouse. The PLTP knockout mouse displays an interesting and complex phenotype. These mice lose the ability to transfer lipids such as phosphatidylcholine, phosphatidylethanolamine, phosphatidylinositol, and sphingomyelin, as well as partially losing the ability to transfer free cholesterol (Jiang et al., 1999). These data demonstrate the *in vivo* relevance of PLTP and highlights the crucial role PLTP plays in mediating the transfer of lipids implicated in ferroptosis. PLTP knockout mice were also found to have significantly lower levels of HDL cholesterol found in the plasma, due to impaired cholesterol absorption in the intestine (Liu et al., 2007). It was also found that HDL from PLTP deficient mice had improved anti-inflammatory properties and that these mice have decreased atherosclerosis (Yan et al., 2004). PLTP has been shown to regulate the phagocytic activity of macrophages and microglial cells. PLTP deficient mice express much lower levels of cytokine interleukin 6 (IL-6) and lower levels of infiltrating macrophages after stress (Desrumaux and Lagrost, 2018). Studies in humans show



increased PLTP activity in patients with bacterial infection and systemic inflammation, supporting the role of PLTP in immune function (Desrumaux et al., 2016). These combined studies suggest PLTP plays a complex role in mediating several processes ranging from lipid metabolism to immune function, and this could account for why PLTP has altered regulation in the S47 mouse.

The S47 variant is impaired for ferroptosis and tumor suppression. Hence, we predicted that a gene such as *PLTP*, which shows impaired induction in S47 cells, might confer ferroptosis sensitivity. In contrast we found that this gene mediates ferroptosis resistance. Indeed, our data suggest that even p53 confers ferroptosis resistance in HepG2 cells, and not sensitivity as one might have been predicted. These findings reinforce the premise that the role for p53 and its target genes in ferroptosis sensitivity is complex and may be cell type or tissue specific. Our findings add to the growing body of literature on the complex role of p53 in regulating ferroptosis. One point to consider is whether stabilization of p53 is a critical step in mediating ferroptosis resistance. Many of our experiments used Nutlin to activate p53, and prior studies found the most pronounced effects on ferroptosis resistance occur after a 24-hour stabilization of p53 with Nutlin (Tarangelo et al., 2018). It is also necessary to consider the type of stress encountered and location of stress that triggers the p53 response, as it is well known that p53 responds differently under different circumstances (Kasthuber and Lowe, 2017). Our data on the effect of low nutrient media increasing ferroptosis sensitivity in a p53 dependent manner highlights the fact that metabolites play a key role in determining sensitivity to ferroptosis, consistent with prior findings (Tarangelo et al., 2018). The crosstalk between various pathways is also very important to bear in mind. A recent study provided evidence that MDM2 and MDMX, known negative regulators of p53,

promote ferroptosis through PPAR $\alpha$ -mediated lipid remodeling. Thus, it is important to consider the intricate nature of metabolic regulation and context specificity when thinking about both p53 and ferroptosis.

The role of p53 is not limited to tumor suppression, as p53 has been shown to possess anti-atherogenic properties (Mercer and Bennett, 2006; Tabas, 2001). PLTP has been extensively characterized in the context of atherosclerosis and studies have shown that low levels of PLTP are associated with greater risk of atherosclerosis (Schgoer et al., 2008). There is evidence that inhibition of ferroptosis alleviates atherosclerosis (Bai et al., 2020), therefore a possible explanation could be that p53 functions to prevent atherosclerosis by inducing ferroptosis resistance through PLTP. Taken together, our findings provide evidence for a novel role for p53 and a p53 target gene on the regulation of ferroptosis through lipid transport. More studies of the role of p53 and PLTP in ferroptosis sensitivity in the liver and other tissues of the WT and S47 mouse can help clarify these roles.

### **3.5 Materials and Methods**

#### *3.5.1 RNA Sequencing*

WT and S47 LCLs were treated with 5  $\mu$ M Nutlin for 30 minutes followed by the addition of 25  $\mu$ M TBH for 0, 8 and 24 hours. RNA was extracted using RNeasy minikits (Qiagen) following the manufacturer's protocol. The QuantSeq FWD library preparation kit (Lexogen) was used to generate 3' mRNA-seq libraries from DNase I-treated RNA. The Agilent TapeStation and Agilent DNA 5000 ScreenTape were used to determine overall library size and real-time PCR (Kapa Biosystems) was used to quantitate the libraries.

Libraries were pooled and the NextSeq 500 (Illumina) was used to carry out high-out-put single-read 75-base-pair next-generation sequencing. Bowtie2 (Langmead and Salzberg, 2012) was used to align RNA-seq data against the human genome version hg38. Raw read counts for each gene were estimated using RSEM version 1.2.12 software (Li and Dewey, 2011). The significance of differential expression between samples was determined using DESeq2 (Love et al., 2014).

### 3.5.2 qRT-PCR

RNA was extracted from cells using the RNeasy minikits (Qiagen) following the manufacturer's protocol. Equal amounts of the isolated RNA were used to generate cDNA using a high-capacity reverse transcription kit (Applied Biosciences, 4368814). The Brilliant III UltraFast SYBR Green qPCR mix kits (Agilent) were used to conduct qPCR on the Stratagene Mx3005P machine (Agilent). RNA expression levels were normalized to housekeeping gene 18S for human and cyclophilin A for mouse. Primer sequences are as follows: PLTP (human-F) 5'-TGATTGACTCCCCATTGAAGC-3' and (human-R) 5'-CGTCCATAGTCATGCTGGACA-3'. Pltp (mouse-F) 5'-TTCCTCCTCAACCAGCAGATCT-3' and (mouse-R) 5'-CAGGAGGGAGTTGAGCAACAC-3'.

### 3.5.3 Silencing and overexpression studies

PLTP knockdown cell lines were generated by lentiviral infection, using the vector pLKO.1-puro-carrying shRNA sequence against human PLTP (shRNA1 [CTGATGCTTCAAATCACCAAT; TRCN0000150129], shRNA2

[CGAATCTATTCCAACCATTCT; TRCN0000148250]) and human *TP53* (TCAGACCTATGGAAACTACTT, TRCN0000003754). Short hairpin constructs and packaging vectors were cotransfected in 293-FT cells to generate lentivirus. HepG2 cells were infected with lentivirus with 8 µg/mL polybrene, spun for 30 minutes at 2250 rpm, allowed to rest for 3.5 hours followed by a media change. Puromycin was added the following day at 2 µg/mL and gene knockdown was validated by qRT-PCR. Cells overexpressing PLTP were generated by transfecting the vector pcDNA3.1+/C-(K)DYK with and without PLTP ORF (NM\_006227.3) obtained from GenScript. Transfections were performed with Lipofectamine 3000 (ThermoFisher) following the manufacturer's protocol.

#### 3.5.4 Flow cytometry

Analysis of lipid peroxidation was performed using C11-BODIPY 581/591 (ThermoFisher D3861) and analysis of lipid droplet accumulation was performed using BODIPY 493/503 (ThermoFisher D3922). Cells were plated at a density of  $3 \times 10^5$  cells per well in 6-well plates. The following day, cells were treated with 0.5 µM of RSL3 for 3 hours. Cells were collected, washed with PBS and stained with 5 µM of C11-Bodipy for 30 minutes at 37°C for lipid peroxidation analysis or 2 µM of Bodipy 493/503 for 15 minutes at 37°C for lipid droplet analysis. Cells were then washed with PBS three times and analyzed using FACSCelesta (Becton Dickinson) flow cytometer. Dead cells were removed from analysis using FSC/SSC profiles, and cell doublets were eliminated by comparing forward scatter signal height vs forward scatter signal area. At least 10,000 events in the analysis gate were obtained.

### *3.5.5 Immunofluorescence staining*

Cells were washed once with PBS, fixed in 4% PFA for 10 minutes, followed by 3 PBS washes. Samples were then treated with 2  $\mu$ M of Bodipy 493/503 (ThermoFisher D3922) for 15 minutes at 37°C in the dark. The cells were mounted with media containing DAPI and images were captured using the Leica TSC SP5 microscope.

### *3.5.6 Immunohistochemistry*

Liver tissues were fixed in formalin overnight at 4°C. The following day, tissues were washed in 1X PBS and placed in 70% ethanol. The tissue embedding and sectioning were performed by the Wistar Institute Histotechnology Facility. Paraffin embedded sections were de-paraffinized in xylene (Fisher, X5-SK4), re-hydrated in ethanol (100%-95%-85%-75%) and then placed in distilled water. Sample slides were steamed in 10 mM Citrate Buffer, pH 6, for antigen retrieval. Three percent hydrogen peroxide was used to quench endogenous peroxidase activity and slides were blocked for 1 hour (Vector Laboratories, S-2012). The slides were incubated with the primary antibody PLTP (1:100, Santa Cruz sc-271596) overnight at 4°C. The next day, slides were washed with PBS, incubated with HRP-conjugated secondary antibody for 30 minutes and treated with DAB chromogen (D5637). Hematoxylin was used to perform a light counterstaining. The Nikon 80i upright microscope was used to image slides, at least four fields per section were imaged.

### *3.5.7 Viability assays*

Cells were seeded at 2000 cells per well on a 96-well plate and were grown overnight at 37°C. The following day cells were treated with the following drugs at indicated

concentrations for 72 hours for IC50 assays: erastin (Cayman Chemicals), RSL3 (Apex Bio), tert-Butyl hydroperoxide/TBH(Sigma), Nutlin (Calbiochem), cisplatin (Acros Organics), Etoposide (Sigma), Camptothecin (Cayman Chemicals), Doxorubicin (Cell Signaling). For rescue assays, cells were pretreated with ferrostatin (Cayman Chemicals) or liproxstatin (Sigma) for 30 minutes prior to treatment with RSL3 for 24 hours. At assay endpoint, cells were treated with Alamar blue (Life Technologies Dal1025) for 3 hours at 37°C and absorbance was read out using a SynergyHT plate reader (BioTek). GraphPad Prism software was used to perform the data analysis.

### *3.5.8 Mammalian Cell Culture*

Human WT LCLs (Catalog ID GM18870) and S47 LCLs (Catalog ID GM18871) were obtained from the Coriell Institute (Camden, New Jersey) and grown in RPMI (Corning Cellgro) supplemented with 15% heat inactivated fetal bovine serum (HyClone, GE Healthcare Life Sciences) and 1% penicillin/streptomycin (Corning Cellgro). WT and S47 MEFs were generated as previously described (Jennis et al., 2016) and maintained in complete growth medium. HepG2 cells were obtained from ATCC (ATCC HB-8065) and maintained in complete growth medium. Complete growth medium is composed of DMEM (Corning Cellgro, 4.5 g/L glucose) supplemented with 10% fetal bovine serum (HyClone, GE Healthcare Life Sciences) and 1% penicillin/streptomycin (Corning Cellgro). Cells were grown in a 5% CO<sub>2</sub> humidified incubator at 37°C. For low glucose low serum experiments, cells were grown in DMEM containing 1 g/L (Gibco 11885084) and 1% fetal bovine serum.

### 3.5.9 Western blot

Protein lysates were obtained from indicated cell lines and 50-100 µg of protein was run on SDS-PAGE gels using 10% NuPAGE Bis-Tris precast gels (Life Technologies). Proteins were transferred onto polyvinylidene difluoride membranes (IPVH00010, pore size: 0.45 mm; Millipore Sigma) and blocked for 1 hour in 5% milk. Primary antibodies include PLTP 1:1000 (Abcam ab18990) and GAPDH 1:10,000 (14C10, Cell Signaling, 2118). HRP-conjugated rabbit secondary antibody (Jackson Immunochemicals) was used at a 1:10,000 dilution. Blots were treated for 5 minutes with ECL (Amersham, RPN2232) and autoradiography was used to determine protein levels.

### 3.5.10 Statistical Analysis

All experiments were performed in triplicate unless otherwise stated and the two-tailed unpaired Student t-test was performed to determine significance. All *in vitro* data are reported as the mean ± SD unless stated otherwise. Statistical analyses were performed using GraphPad Prism, p-values are as follows: (\*) p-value < 0.05, (\*\*) p-value < 0.01, (\*\*\*) p-value < 0.001, (\*\*\*\*) p-value < 0.0001.

## Chapter 4: Future Direction and Concluding Remarks

### 4.1 Summary of findings

For decades it was believed that p53 functions as a tumor suppressor predominantly by controlling apoptosis, senescence and cell cycle arrest. However, in recent years more data has begun to emerge highlighting the key role p53 plays in less studied processes such as metabolism and ferroptosis. This is a rapidly expanding field and much more work remains to be done to fully understand how exactly p53 behaves in various contexts. Coding region variants of p53 can be used as tools to further dissect such mechanisms and enable us to develop a broader understanding of how p53 functions. This thesis provides deeper insight on how the S47 SNP of *TP53* regulates metabolism and ferroptosis.

In our first study, we sought to characterize the metabolic phenotype that we had observed in the S47 mouse. I was able to demonstrate the following:

1. S47 cells and tissues exhibit increased mTOR activity compared to the WT counterpart, as determined by assessing levels of mTOR markers using Western blot and immunohistochemistry.



2. S47 cells show higher rates of cellular metabolism, as demonstrated through Seahorse assays assessing cellular respiration and glycolysis, as well as analysis of metabolites using the YSI analyzer.
  
3. The increased mTOR activity in S47 cells can be attributed to greater interaction between mTOR and Rheb, resulting from a decreased interaction between GAPDH and Rheb. This was validated by performing both proximity ligation assays and co-immunoprecipitation assays.
  
4. The altered mTOR-Rheb binding observed in S47 ultimately stems from the altered redox state present in S47 cells. The conformation of GAPDH is altered in S47 cells due to elevated glutathione levels, thus impairing the GAPDH-Rheb interaction. We were able to show that manipulating levels of glutathione could alter the GAPDH-Rheb interaction.
  
5. S47 mice possess greater metabolic efficiency compared to WT mice. In both comprehensive lab animal monitoring studies and treadmill studies, S47 mice demonstrated greater metabolic resilience.

Taken together, this study shows how a single amino acid change in p53 can lead to a profound change in various metabolic processes. Our work elegantly connects the mTOR pathway, p53 and the role of redox state together, and provides a unique lens to think about the interplay between these various pathways.

We next sought to use the S47 variant as a tool to unearth novel p53 target genes that could play a role in mediating ferroptosis. In our second study, I identified *PLTP* as a p53 target gene that appears to mediate ferroptosis resistance and demonstrated the following:

1. PLTP is expressed at much lower levels in S47 compared to WT. I validated this through multiple methods assessing expression on the mRNA, protein and tissue level.
2. p53 regulates the expression of PLTP in HepG2 cells. By generating a p53 null cell line, I was able to validate that PLTP is expressed in a p53 dependent manner.
3. PLTP promotes ferroptosis resistance. After silencing PLTP, I found increased sensitivity to RSL3-induced cell death and increased levels of lipid peroxidation. Consistent with this finding, overexpressing PLTP led to decreased sensitivity to RSL-induced cell death and decreased levels of lipid peroxidation.
4. The RSL3-induced cell death that is observed is ferroptosis specific. This was validated by using ferroptosis specific rescue agents, as well as observing no significant differences in viability after treatment with many other chemotherapeutic agents.
5. PLTP protects cells from ferroptosis by enhancing lipid storage. We found that PLTP contributed to increased levels of lipid droplets and also had overall

increased levels of lipid droplets after treatment with RSL3. This suggests that PLTP is sequestering lipids away from the cell membrane, leaving less lipids available to undergo peroxidation.

This study identifies *PLTP* as a novel p53 target gene that plays a role in regulating ferroptosis and adds to the growing body of literature on the perplexing role of p53 in ferroptosis. The exact role of p53 in mediating ferroptosis remains inconclusive, as it promotes ferroptosis in certain situations and prevents ferroptosis in other situations. However, what is clear from both studies presented in this dissertation is that the function of p53 appears to be very context specific. Several factors such as type of stress, duration of stress, location of the stress, and other parameters all contribute to the response p53 elicits.

#### **4.2 Outstanding questions regarding p53, S47, mTOR, ferroptosis and tumor suppression**

There are many remaining questions with regard to the S47 variant. One major point of future investigation regards the impact of this genetic variant on glucose metabolism. A difference that was observed but not further pursued is that the GLUT family of glucose transporters are expressed at much lower levels in S47 compared to WT. It is known that p53 downregulates the expression of GLUT1 and GLUT4 (Schwartzberg-Bar-Yoseph et al., 2004), which would result in less available glucose in a cancer cell that could be used for other anabolic processes. Our data suggest S47 cells consume more glucose, yet we have observed that various members of the GLUT

family, including GLUT 1, GLUT3, GLUT4 and GLUT5, are expressed at much lower levels in S47 tissues compared to WT. This raises the question, how exactly are S47 cells importing this excess glucose? It suggests that the S47 cells are likely utilizing other pathways to modulate glucose uptake and usage. Moreover, one might have hypothesized that increased glucose consumption would result in larger cells or increased rates of proliferation in S47. However, we have not observed any changes in proliferation rate or cell size in S47 MEFs or lymphoblastoid cells, compared to WT, *in vitro*. That being said, we have noted increased Ki-67 staining in tumors containing the S47 variant, compared to WT (Barnoud et al., 2018). Additionally, Ki-67 staining in small intestine and skeletal tissue appears to be increased in S47 mouse tissues (K. Gnanapradeepan, unpublished results). It is also worthwhile to note that the ferroptotic defect in S47 contributes to iron accumulation in macrophages and the spleen, however no major differences are observed in tissues such as the liver. These data reinforce our findings that the phenotype of the S47 variant appears to be restricted to certain tissues.

Another unresolved question is the basis for the tissue-restricted increase in mTOR activity that we observed in S47 tissues, in spite of the fact that we found evidence for increased levels of reduced glutathione in multiple tissues of the S47 mouse. For example, we were unable to detect significant changes in levels of mTOR markers when comparing S47 liver to WT liver, however S47 liver does exhibit higher levels of glutathione (Leu et al., 2019). These data suggest that there are other pathways that are likely contributing to the increased mTOR phenotype aside from the mTOR-Rheb-GAPDH interaction that we described, and more work remains to be done in this area.

We have identified the regulation of glutathione synthesis, and the consequent regulation of cellular redox state, on the regulation of mTOR. Two obvious avenues stem from this area. The first involves the potential for redox regulation of other enzymes in metabolism. Indeed, our collaborators have identified at least two other key metabolic enzymes, PKM2 and G6PDH, as redox sensitive proteins that also show altered regulation in S47 cells (Leu et al., 2020). It is likely that there are several other redox sensitive proteins impacted in S47 cells, thereby affecting several other processes beyond what is normally regulated by p53.

A second area for future analysis is the potential contribution of enhanced mTOR activity to the increased cancer risk, and resistance to ferroptosis in S47 mice and humans. Whereas the contribution of increased mTOR activity to cancer risk in S47 humans remains to be determined, there are data supporting increased mTOR activity in ferroptosis resistance. For example, Yi et al. found that oncogenic activation of the PI3K-AKT-mTORC1 signaling axis causes ferroptosis resistance (Yi et al., 2020). The authors found that cancer cells containing mutations in the PI3K-AKT-mTORC1 pathway were far more resistant to cell death by RSL3. Interestingly, these cells were sensitized to cell death by RSL3 when treated concurrently with mTOR inhibitors such as Temsirolimus and Torin1. The authors went on to show that this ultimately stems from mTORC1 activating the master regulator of lipid metabolism, SREBP1, which then goes on to upregulate the expression of *SCD1*, a gene implicated in mediating ferroptosis resistance. Pharmacological and genetic inhibition of both SREBP1 and *SCD1* resulted in increasing ferroptosis sensitivity in cancer cells harboring the PI3K-AKT-mTOR mutation. The authors demonstrated how the synergistic effects of combining ferroptotic induction with mTOR inhibition can significantly reduce tumor formation *in vivo* (Yi et al.,

2020). This study highlights how inducing ferroptosis can serve as a promising therapeutic approach for cancers that possess specific genetic backgrounds.

This study connects lipid metabolism to the mTOR/ferroptosis phenotype and highlights how these pathways appear to be intricately connected. The data presented corroborate a previous study that also demonstrated elevated mTOR activity suppresses ferroptosis in cardiomyocytes (Baba et al., 2018). Knowing that S47 exhibits elevated mTORC1 activity, impaired ferroptosis and altered expression of lipid metabolism genes, it would be worthwhile to explore if and how these various pathways are interconnected. For example, it would be interesting to determine if the elevated mTOR activity observed in S47 is directly responsible for the ferroptosis defect. To assess this, one could first treat S47 cells with mTOR inhibitors such as Temsirolimus or Torin1, and then determine if ferroptosis sensitivity is affected in S47 cells. If this looks promising, the next logical step would be to assess the impact of this combined therapy *in vivo*. A key experiment would be to treat S47 mice with a ferroptosis inducer such as imidazole ketone erastin (IKE), and with an mTOR inhibitor such as Temsirolimus or Torin1 and see if this combined therapy significantly reduces tumor formation.

There is also therapeutic potential for combined therapy with mTORC1 inhibitors and inhibitors of glutathione. A study published by Li et al. demonstrated that combining inhibitors of mTORC1 and glutamate cysteine ligase (GCLC), the rate limiting enzyme in glutathione synthesis, can enhance cell death in cells with high mTORC1 activity. The authors created mTORC1 driven tumor cells by generating mouse embryonic fibroblasts null for Tsc2, a negative regulator of the mTOR pathway. When mTORC1 is hyperactive, the authors found increased levels of antioxidants such as NADPH and glutathione. Interestingly, the authors discovered treating cells with rapamycin decreases overall

glutathione content in addition to decreasing mTOR activity. *In vivo*, it was found that using nontoxic doses of BSO, an inhibitor of GSH synthesis, with rapamycin promotes significant tumor regression in Tsc2-deficient xenograft models (Li et al., 2016). As described in Chapter 2, the S47 variant has higher mTOR activity and higher glutathione levels, thus it would be worthwhile to treat S47 mice with an inhibitor of glutathione such as BSO or DEM in conjunction with rapamycin.

In conclusion, there are several opportunities for further exploration harnessing the mTOR, ferroptosis, metabolism and redox phenotype observed in the S47 variant. The following experiments are ways to exploit the unique differences observed in the S47 variant, and determine if manipulating these factors can reduce cancer risk *in vivo*:

1. Treat S47 mice with reagents that deplete glutathione levels such as DEM and BSO.
2. Treat S47 mice with mTOR inhibitors such as rapamycin, Temsirolimus and Torin1.
3. Treat S47 mice with a combination of the aforementioned mTOR inhibitors and glutathione inhibitors, such as BSO.
4. Treat S47 mice with a combination of the aforementioned mTOR inhibitors and ferroptosis inducers, such as imidazole ketone erastin.

The ultimate goal of studying the S47 variant is to develop better therapeutic options for patients who carry this allele. To that end, our lab has identified cisplatin and BET inhibitors as two classes of drugs that have superior efficacy on S47 tumors compared to

WT tumors (Barnoud et al., 2018). S47 tumor cells have also shown preferential sensitivity to the glycolytic poison 2-deoxy-glucose (Barnoud et al., 2019). Much of the data presented and discussed are taken from cells and mouse experiments, thus it is of utmost importance to gather more genetic data from human studies with patients carrying this S47 variant. Doing so will enable a better understanding of the phenotype and provide opportunity for improved personalized medicine approaches.



## BIBLIOGRAPHY

- Albers, J. J., Vuletic, S., and Cheung, M. C. (2012). Role of plasma phospholipid transfer protein in lipid and lipoprotein metabolism. *Biochim Biophys Acta* 1821, 345-357.
- Assaily, W., Rubinger, D. A., Wheaton, K., Lin, Y., Ma, W., Xuan, W., Brown-Endres, L., Tsuchihara, K., Mak, T. W., and Benchimol, S. (2011). ROS-mediated p53 induction of Lpin1 regulates fatty acid oxidation in response to nutritional stress. *Mol Cell* 44, 491-501.
- Baar, E. L., Carbajal, K. A., Ong, I. M., and Lamming, D. W. (2016). Sex- and tissue-specific changes in mTOR signaling with age in C57BL/6J mice. *Aging Cell* 15, 155-166.
- Baba, Y., Higa, J. K., Shimada, B. K., Horiuchi, K. M., Suhara, T., Kobayashi, M., Woo, J. D., Aoyagi, H., Marh, K. S., Kitaoka, H., and Matsui, T. (2018). Protective effects of the mechanistic target of rapamycin against excess iron and ferroptosis in cardiomyocytes. *Am J Physiol Heart Circ Physiol* 314, H659-H668.
- Bai, T., Li, M., Liu, Y., Qiao, Z., and Wang, Z. (2020). Inhibition of ferroptosis alleviates atherosclerosis through attenuating lipid peroxidation and endothelial dysfunction in mouse aortic endothelial cell. *Free Radic Biol Med* 160, 92-102.
- Bai, Y., Meng, L., Han, L., Jia, Y., Zhao, Y., Gao, H., Kang, R., Wang, X., Tang, D., and Dai, E. (2019). Lipid storage and lipophagy regulates ferroptosis. *Biochem Biophys Res Commun* 508, 997-1003.
- Barnoud, T., Budina-Kolomets, A., Basu, S., Leu, J. I., Good, M., Kung, C. P., Liu, J., Liu, Q., Villanueva, J., Zhang, R., *et al.* (2018). Tailoring Chemotherapy for the African-Centric S47 Variant of TP53. *Cancer Res* 78, 5694-5705.
- Barnoud, T., Parris, J. L. D., and Murphy, M. E. (2019). Tumor cells containing the African-Centric S47 variant of TP53 show increased Warburg metabolism. *Oncotarget* 10, 1217-1223.
- Basu, S., Gnanapradeepan, K., Barnoud, T., Kung, C. P., Tavecchio, M., Scott, J., Watters, A., Chen, Q., Kossenkov, A. V., and Murphy, M. E. (2018). Mutant p53 controls tumor metabolism and metastasis by regulating PGC-1alpha. *Genes Dev* 32, 230-243.
- Basu, S., and Murphy, M. E. (2016). Genetic Modifiers of the p53 Pathway. *Cold Spring Harb Perspect Med* 6, a026302.
- Ben-Sahra, I., and Manning, B. D. (2017). mTORC1 signaling and the metabolic control of cell growth. *Curr Opin Cell Biol* 45, 72-82.
- Bensaad, K., Tsuruta, A., Selak, M. A., Vidal, M. N., Nakano, K., Bartrons, R., Gottlieb, E., and Vousden, K. H. (2006). TIGAR, a p53-inducible regulator of glycolysis and apoptosis. *Cell* 126, 107-120.

- Berkers, C. R., Maddocks, O. D., Cheung, E. C., Mor, I., and Vousden, K. H. (2013). Metabolic regulation by p53 family members. *Cell Metab* 18, 617-633.
- Brady, C. A., Jiang, D., Mello, S. S., Johnson, T. M., Jarvis, L. A., Kozak, M. M., Kenzelmann Broz, D., Basak, S., Park, E. J., McLaughlin, M. E., *et al.* (2011). Distinct p53 transcriptional programs dictate acute DNA-damage responses and tumor suppression. *Cell* 145, 571-583.
- Brandes, N., Schmitt, S., and Jakob, U. (2009). Thiol-based redox switches in eukaryotic proteins. *Antioxid Redox Signal* 11, 997-1014.
- Brugarolas, J., Chandrasekaran, C., Gordon, J. I., Beach, D., Jacks, T., and Hannon, G. J. (1995). Radiation-induced cell cycle arrest compromised by p21 deficiency. *Nature* 377, 552-557.
- Budanov, A. V., and Karin, M. (2008). p53 target genes sestrin1 and sestrin2 connect genotoxic stress and mTOR signaling. *Cell* 134, 451-460.
- Bulavin, D. V., Saito, S., Hollander, M. C., Sakaguchi, K., Anderson, C. W., Appella, E., and Fornace, A. J., Jr. (1999). Phosphorylation of human p53 by p38 kinase coordinates N-terminal phosphorylation and apoptosis in response to UV radiation. *EMBO J* 18, 6845-6854.
- Canadillas, J. M., Tidow, H., Freund, S. M., Rutherford, T. J., Ang, H. C., and Fersht, A. R. (2006). Solution structure of p53 core domain: structural basis for its instability. *Proc Natl Acad Sci U S A* 103, 2109-2114.
- Chernorizov, K. A., Elkina, J. L., Semenyuk, P. I., Svedas, V. K., and Muronetz, V. I. (2010). Novel inhibitors of glyceraldehyde-3-phosphate dehydrogenase: covalent modification of NAD-binding site by aromatic thiols. *Biochemistry (Mosc)* 75, 1444-1449.
- Chipuk, J. E., Kuwana, T., Bouchier-Hayes, L., Droin, N. M., Newmeyer, D. D., Schuler, M., and Green, D. R. (2004). Direct activation of Bax by p53 mediates mitochondrial membrane permeabilization and apoptosis. *Science* 303, 1010-1014.
- Cho, Y., Gorina, S., Jeffrey, P. D., and Pavletich, N. P. (1994). Crystal structure of a p53 tumor suppressor-DNA complex: understanding tumorigenic mutations. *Science* 265, 346-355.
- Chu, B., Kon, N., Chen, D., Li, T., Liu, T., Jiang, L., Song, S., Tavana, O., and Gu, W. (2019). ALOX12 is required for p53-mediated tumour suppression through a distinct ferroptosis pathway. *Nat Cell Biol* 21, 579-591.
- Coleman, M. E., DeMayo, F., Yin, K. C., Lee, H. M., Geske, R., Montgomery, C., and Schwartz, R. J. (1995). Myogenic vector expression of insulin-like growth factor I stimulates muscle cell differentiation and myofiber hypertrophy in transgenic mice. *J Biol Chem* 270, 12109-12116.

- Corradetti, M. N., and Guan, K. L. (2006). Upstream of the mammalian target of rapamycin: do all roads pass through mTOR? *Oncogene* 25, 6347-6360.
- DeLeo, A. B., Jay, G., Appella, E., Dubois, G. C., Law, L. W., and Old, L. J. (1979). Detection of a transformation-related antigen in chemically induced sarcomas and other transformed cells of the mouse. *Proc Natl Acad Sci U S A* 76, 2420-2424.
- Deng, C., Zhang, P., Harper, J. W., Elledge, S. J., and Leder, P. (1995). Mice lacking p21CIP1/WAF1 undergo normal development, but are defective in G1 checkpoint control. *Cell* 82, 675-684.
- Desrumaux, C., and Lagrost, L. (2018). Plasma phospholipid transfer protein (PLTP) as an emerging determinant of the adaptive immune response. *Cell Mol Immunol* 15, 1077-1079.
- Desrumaux, C., Lemaire-Ewing, S., Ogier, N., Yessoufou, A., Hammann, A., Sequeira-Le Grand, A., Deckert, V., Pais de Barros, J. P., Le Guern, N., Guy, J., *et al.* (2016). Plasma phospholipid transfer protein (PLTP) modulates adaptive immune functions through alternation of T helper cell polarization. *Cell Mol Immunol* 13, 795-804.
- Di Lello, P., Jenkins, L. M. M., Jones, T. N., Nguyen, B. D., Hara, T., Yamaguchi, H., Dikeakos, J. D., Appella, E., Legault, P., and Omichinski, J. G. (2006). Structure of the Tfb1/p53 complex: Insights into the interaction between the p62/Tfb1 subunit of TFIID and the activation domain of p53. *Mol Cell* 22, 731-740.
- Dickinson, J. M., and Rasmussen, B. B. (2011). Essential amino acid sensing, signaling, and transport in the regulation of human muscle protein metabolism. *Curr Opin Clin Nutr Metab Care* 14, 83-88.
- Dixon, S. J., Lemberg, K. M., Lamprecht, M. R., Skouta, R., Zaitsev, E. M., Gleason, C. E., Patel, D. N., Bauer, A. J., Cantley, A. M., Yang, W. S., *et al.* (2012). Ferroptosis: an iron-dependent form of nonapoptotic cell death. *Cell* 149, 1060-1072.
- Doll, S., Proneth, B., Tyurina, Y. Y., Panzilius, E., Kobayashi, S., Ingold, I., Irmiler, M., Beckers, J., Aichler, M., Walch, A., *et al.* (2017). ACSL4 dictates ferroptosis sensitivity by shaping cellular lipid composition. *Nat Chem Biol* 13, 91-98.
- Donehower, L. A., Harvey, M., Slagle, B. L., McArthur, M. J., Montgomery, C. A., Jr., Butel, J. S., and Bradley, A. (1992). Mice deficient for p53 are developmentally normal but susceptible to spontaneous tumours. *Nature* 356, 215-221.
- Drummond, M. J., Fry, C. S., Glynn, E. L., Dreyer, H. C., Dhanani, S., Timmerman, K. L., Volpi, E., and Rasmussen, B. B. (2009). Rapamycin administration in humans blocks the contraction-induced increase in skeletal muscle protein synthesis. *J Physiol* 587, 1535-1546.
- Eliyahu, D., Michalovitz, D., Eliyahu, S., Pinhasi-Kimhi, O., and Oren, M. (1989). Wild-type p53 can inhibit oncogene-mediated focus formation. *Proc Natl Acad Sci U S A* 86, 8763-8767.

- Ettinger, S. L., Sobel, R., Whitmore, T. G., Akbari, M., Bradley, D. R., Gleave, M. E., and Nelson, C. C. (2004). Dysregulation of sterol response element-binding proteins and downstream effectors in prostate cancer during progression to androgen independence. *Cancer Res* 64, 2212-2221.
- Fang, Y., Westbrook, R., Hill, C., Boparai, R. K., Arum, O., Spong, A., Wang, F., Javors, M. A., Chen, J., Sun, L. Y., and Bartke, A. (2013). Duration of rapamycin treatment has differential effects on metabolism in mice. *Cell Metab* 17, 456-462.
- Felley-Bosco, E., Weston, A., Cawley, H. M., Bennett, W. P., and Harris, C. C. (1993). Functional studies of a germ-line polymorphism at codon 47 within the p53 gene. *Am J Hum Genet* 53, 752-759.
- Feng, Z., Hu, W., de Stanchina, E., Teresky, A. K., Jin, S., Lowe, S., and Levine, A. J. (2007). The regulation of AMPK beta1, TSC2, and PTEN expression by p53: stress, cell and tissue specificity, and the role of these gene products in modulating the IGF-1-AKT-mTOR pathways. *Cancer Res* 67, 3043-3053.
- Feng, Z., Zhang, H., Levine, A. J., and Jin, S. (2005). The coordinate regulation of the p53 and mTOR pathways in cells. *Proc Natl Acad Sci U S A* 102, 8204-8209.
- Finck, B. N., Gropler, M. C., Chen, Z., Leone, T. C., Croce, M. A., Harris, T. E., Lawrence, J. C., Jr., and Kelly, D. P. (2006). Lipin 1 is an inducible amplifier of the hepatic PGC-1alpha/PPARalpha regulatory pathway. *Cell Metab* 4, 199-210.
- Finlay, C. A., Hinds, P. W., and Levine, A. J. (1989). The p53 proto-oncogene can act as a suppressor of transformation. *Cell* 57, 1083-1093.
- Finlay, C. A., Hinds, P. W., Tan, T. H., Eliyahu, D., Oren, M., and Levine, A. J. (1988). Activating mutations for transformation by p53 produce a gene product that forms an hsc70-p53 complex with an altered half-life. *Mol Cell Biol* 8, 531-539.
- Fu, Y., Mukhamedova, N., Ip, S., D'Souza, W., Henley, K. J., DiTommaso, T., Kesani, R., Ditiatkovski, M., Jones, L., Lane, R. M., *et al.* (2013). ABCA12 regulates ABCA1-dependent cholesterol efflux from macrophages and the development of atherosclerosis. *Cell Metab* 18, 225-238.
- Gao, M., Monian, P., Quadri, N., Ramasamy, R., and Jiang, X. (2015). Glutaminolysis and Transferrin Regulate Ferroptosis. *Mol Cell* 59, 298-308.
- Gnanapradeepan, K., Basu, S., Barnoud, T., Budina-Kolomets, A., Kung, C. P., and Murphy, M. E. (2018). The p53 Tumor Suppressor in the Control of Metabolism and Ferroptosis. *Front Endocrinol (Lausanne)* 9, 124.
- Goldstein, I., Ezra, O., Rivlin, N., Molchadsky, A., Madar, S., Goldfinger, N., and Rotter, V. (2012). p53, a novel regulator of lipid metabolism pathways. *J Hepatol* 56, 656-662.
- Goldstein, I., and Rotter, V. (2012). Regulation of lipid metabolism by p53 - fighting two villains with one sword. *Trends Endocrinol Metab* 23, 567-575.

- Goodman, C. A. (2019). Role of mTORC1 in mechanically induced increases in translation and skeletal muscle mass. *J Appl Physiol* (1985) *127*, 581-590.
- Green, N. S., Reisler, E., and Houk, K. N. (2001). Quantitative evaluation of the lengths of homobifunctional protein cross-linking reagents used as molecular rulers. *Protein Sci* *10*, 1293-1304.
- Guo, D., Prins, R. M., Dang, J., Kuga, D., Iwanami, A., Soto, H., Lin, K. Y., Huang, T. T., Akhavan, D., Hock, M. B., *et al.* (2009). EGFR signaling through an Akt-SREBP-1-dependent, rapamycin-resistant pathway sensitizes glioblastomas to antilipogenic therapy. *Sci Signal* *2*, ra82.
- Hafner, A., Bulyk, M. L., Jambhekar, A., and Lahav, G. (2019). The multiple mechanisms that regulate p53 activity and cell fate. *Nat Rev Mol Cell Biol* *20*, 199-210.
- Halevy, O., Rodel, J., Peled, A., and Oren, M. (1991). Frequent p53 mutations in chemically induced murine fibrosarcoma. *Oncogene* *6*, 1593-1600.
- Hasty, P., Sharp, Z. D., Curiel, T. J., and Campisi, J. (2013). mTORC1 and p53: clash of the gods? *Cell Cycle* *12*, 20-25.
- Hay, N., and Sonenberg, N. (2004). Upstream and downstream of mTOR. *Genes Dev* *18*, 1926-1945.
- Hofmann, T. G., Moller, A., Sirma, H., Zentgraf, H., Taya, Y., Droge, W., Will, H., and Schmitz, M. L. (2002). Regulation of p53 activity by its interaction with homeodomain-interacting protein kinase-2. *Nat Cell Biol* *4*, 1-10.
- Hollstein, M., Sidransky, D., Vogelstein, B., and Harris, C. C. (1991). p53 mutations in human cancers. *Science* *253*, 49-53.
- Hong, H., Takahashi, K., Ichisaka, T., Aoi, T., Kanagawa, O., Nakagawa, M., Okita, K., and Yamanaka, S. (2009). Suppression of induced pluripotent stem cell generation by the p53-p21 pathway. *Nature* *460*, 1132-1135.
- Hu, W., Zhang, C., Wu, R., Sun, Y., Levine, A., and Feng, Z. (2010). Glutaminase 2, a novel p53 target gene regulating energy metabolism and antioxidant function. *Proc Natl Acad Sci U S A* *107*, 7455-7460.
- Jennis, M., Kung, C. P., Basu, S., Budina-Kolomets, A., Leu, J. I., Khaku, S., Scott, J. P., Cai, K. Q., Campbell, M. R., Porter, D. K., *et al.* (2016). An African-specific polymorphism in the TP53 gene impairs p53 tumor suppressor function in a mouse model. *Genes Dev* *30*, 918-930.
- Jiang, L., Kon, N., Li, T., Wang, S. J., Su, T., Hibshoosh, H., Baer, R., and Gu, W. (2015). Ferroptosis as a p53-mediated activity during tumour suppression. *Nature* *520*, 57-62.

- Jiang, P., Du, W., Wang, X., Mancuso, A., Gao, X., Wu, M., and Yang, X. (2011). p53 regulates biosynthesis through direct inactivation of glucose-6-phosphate dehydrogenase. *Nat Cell Biol* 13, 310-316.
- Jiang, X. C., Bruce, C., Mar, J., Lin, M., Ji, Y., Francone, O. L., and Tall, A. R. (1999). Targeted mutation of plasma phospholipid transfer protein gene markedly reduces high-density lipoprotein levels. *J Clin Invest* 103, 907-914.
- Joerger, A. C., and Fersht, A. R. (2016). The p53 Pathway: Origins, Inactivation in Cancer, and Emerging Therapeutic Approaches. *Annu Rev Biochem* 85, 375-404.
- Jones, R. G., Plas, D. R., Kubek, S., Buzzai, M., Mu, J., Xu, Y., Birnbaum, M. J., and Thompson, C. B. (2005). AMP-activated protein kinase induces a p53-dependent metabolic checkpoint. *Mol Cell* 18, 283-293.
- Jung, C. H., Ro, S. H., Cao, J., Otto, N. M., and Kim, D. H. (2010). mTOR regulation of autophagy. *FEBS Lett* 584, 1287-1295.
- Kagan, V. E., Mao, G., Qu, F., Angeli, J. P., Doll, S., Croix, C. S., Dar, H. H., Liu, B., Tyurin, V. A., Ritov, V. B., *et al.* (2017). Oxidized arachidonic and adrenic PEs navigate cells to ferroptosis. *Nat Chem Biol* 13, 81-90.
- Kaiser, A. M., and Attardi, L. D. (2018). Deconstructing networks of p53-mediated tumor suppression in vivo. *Cell Death Differ* 25, 93-103.
- Kang, H. J., Feng, Z., Sun, Y., Atwal, G., Murphy, M. E., Rebbeck, T. R., Rosenwaks, Z., Levine, A. J., and Hu, W. (2009). Single-nucleotide polymorphisms in the p53 pathway regulate fertility in humans. *Proc Natl Acad Sci U S A* 106, 9761-9766.
- Kastan, M. B., Onyekwere, O., Sidransky, D., Vogelstein, B., and Craig, R. W. (1991). Participation of p53 protein in the cellular response to DNA damage. *Cancer Res* 51, 6304-6311.
- Kasthuber, E. R., and Lowe, S. W. (2017). Putting p53 in Context. *Cell* 170, 1062-1078.
- Kim, H. R., Roe, J. S., Lee, J. E., Cho, E. J., and Youn, H. D. (2013). p53 regulates glucose metabolism by miR-34a. *Biochem Biophys Res Commun* 437, 225-231.
- Kim, N. H., Kim, H. S., Li, X. Y., Lee, I., Choi, H. S., Kang, S. E., Cha, S. Y., Ryu, J. K., Yoon, D., Fearon, E. R., *et al.* (2011). A p53/miRNA-34 axis regulates Snail1-dependent cancer cell epithelial-mesenchymal transition. *J Cell Biol* 195, 417-433.
- Kruiswijk, F., Labuschagne, C. F., and Vousden, K. H. (2015). p53 in survival, death and metabolic health: a lifeguard with a licence to kill. *Nat Rev Mol Cell Biol* 16, 393-405.
- Kung, C. P., Leu, J. I., Basu, S., Khaku, S., Anokye-Danso, F., Liu, Q., George, D. L., Ahima, R. S., and Murphy, M. E. (2016). The P72R Polymorphism of p53 Predisposes to Obesity and Metabolic Dysfunction. *Cell Rep* 14, 2413-2425.

- Lane, D. P., and Crawford, L. V. (1979). T antigen is bound to a host protein in SV40-transformed cells. *Nature* 278, 261-263.
- Lang, G. A., Iwakuma, T., Suh, Y. A., Liu, G., Rao, V. A., Parant, J. M., Valentin-Vega, Y. A., Terzian, T., Caldwell, L. C., Strong, L. C., *et al.* (2004). Gain of function of a p53 hot spot mutation in a mouse model of Li-Fraumeni syndrome. *Cell* 119, 861-872.
- Langmead, B., and Salzberg, S. L. (2012). Fast gapped-read alignment with Bowtie 2. *Nat Methods* 9, 357-359.
- Laplante, M., and Sabatini, D. M. (2012). mTOR signaling in growth control and disease. *Cell* 149, 274-293.
- Lee, C. W., Ferreon, J. C., Ferreon, A. C., Arai, M., and Wright, P. E. (2010). Graded enhancement of p53 binding to CREB-binding protein (CBP) by multisite phosphorylation. *Proc Natl Acad Sci U S A* 107, 19290-19295.
- Lee, M. N., Ha, S. H., Kim, J., Koh, A., Lee, C. S., Kim, J. H., Jeon, H., Kim, D. H., Suh, P. G., and Ryu, S. H. (2009). Glycolytic flux signals to mTOR through glyceraldehyde-3-phosphate dehydrogenase-mediated regulation of Rheb. *Mol Cell Biol* 29, 3991-4001.
- Leroy, B., Anderson, M., and Soussi, T. (2014). TP53 mutations in human cancer: database reassessment and prospects for the next decade. *Hum Mutat* 35, 672-688.
- Leu, J. I., Murphy, M. E., and George, D. L. (2019). Mechanistic basis for impaired ferroptosis in cells expressing the African-centric S47 variant of p53. *Proc Natl Acad Sci U S A* 116, 8390-8396.
- Leu, J. I., Murphy, M. E., and George, D. L. (2020). Functional interplay among thiol-based redox signaling, metabolism, and ferroptosis unveiled by a genetic variant of TP53. *Proc Natl Acad Sci U S A* 117, 26804-26811.
- Levine, A. J., and Oren, M. (2009). The first 30 years of p53: growing ever more complex. *Nat Rev Cancer* 9, 749-758.
- Li, B., and Dewey, C. N. (2011). RSEM: accurate transcript quantification from RNA-Seq data with or without a reference genome. *BMC Bioinformatics* 12, 323.
- Li, J., Shin, S., Sun, Y., Yoon, S. O., Li, C., Zhang, E., Yu, J., Zhang, J., and Blenis, J. (2016). mTORC1-Driven Tumor Cells Are Highly Sensitive to Therapeutic Targeting by Antagonists of Oxidative Stress. *Cancer Res* 76, 4816-4827.
- Li, N., Sancak, Y., Frasier, J., and Atilla-Gokcumen, G. E. (2018). A Protective Role for Triacylglycerols during Apoptosis. *Biochemistry* 57, 72-80.
- Li, T., Kon, N., Jiang, L., Tan, M., Ludwig, T., Zhao, Y., Baer, R., and Gu, W. (2012). Tumor suppression in the absence of p53-mediated cell-cycle arrest, apoptosis, and senescence. *Cell* 149, 1269-1283.

- Li, X., Dumont, P., Della Pietra, A., Shetler, C., and Murphy, M. E. (2005). The codon 47 polymorphism in p53 is functionally significant. *J Biol Chem* 280, 24245-24251.
- Linzer, D. I., and Levine, A. J. (1979). Characterization of a 54K dalton cellular SV40 tumor antigen present in SV40-transformed cells and uninfected embryonal carcinoma cells. *Cell* 17, 43-52.
- Liu, G. Y., and Sabatini, D. M. (2020a). mTOR at the nexus of nutrition, growth, ageing and disease. *Nat Rev Mol Cell Biol*.
- Liu, G. Y., and Sabatini, D. M. (2020b). mTOR at the nexus of nutrition, growth, ageing and disease. *Nat Rev Mol Cell Biol* 21, 183-203.
- Liu, R., Iqbal, J., Yeang, C., Wang, D. Q., Hussain, M. M., and Jiang, X. C. (2007). Phospholipid transfer protein-deficient mice absorb less cholesterol. *Arterioscler Thromb Vasc Biol* 27, 2014-2021.
- Londono Gentile, T., Lu, C., Lodato, P. M., Tse, S., Olejniczak, S. H., Witze, E. S., Thompson, C. B., and Wellen, K. E. (2013). DNMT1 is regulated by ATP-citrate lyase and maintains methylation patterns during adipocyte differentiation. *Mol Cell Biol* 33, 3864-3878.
- Long, X., Lin, Y., Ortiz-Vega, S., Yonezawa, K., and Avruch, J. (2005). Rheb binds and regulates the mTOR kinase. *Curr Biol* 15, 702-713.
- Love, M. I., Huber, W., and Anders, S. (2014). Moderated estimation of fold change and dispersion for RNA-seq data with DESeq2. *Genome Biol* 15, 550.
- Magtanong, L., Ko, P. J., and Dixon, S. J. (2016). Emerging roles for lipids in non-apoptotic cell death. *Cell Death Differ* 23, 1099-1109.
- Magtanong, L., Ko, P. J., To, M., Cao, J. Y., Forcina, G. C., Tarangelo, A., Ward, C. C., Cho, K., Patti, G. J., Nomura, D. K., *et al.* (2019). Exogenous Monounsaturated Fatty Acids Promote a Ferroptosis-Resistant Cell State. *Cell Chem Biol* 26, 420-432 e429.
- Malkin, D., Li, F. P., Strong, L. C., Fraumeni, J. F., Jr., Nelson, C. E., Kim, D. H., Kassel, J., Gryka, M. A., Bischoff, F. Z., Tainsky, M. A., and *et al.* (1990). Germ line p53 mutations in a familial syndrome of breast cancer, sarcomas, and other neoplasms. *Science* 250, 1233-1238.
- Marion, R. M., Strati, K., Li, H., Murga, M., Blanco, R., Ortega, S., Fernandez-Capetillo, O., Serrano, M., and Blasco, M. A. (2009). A p53-mediated DNA damage response limits reprogramming to ensure iPS cell genomic integrity. *Nature* 460, 1149-1153.
- Masson, D., Jiang, X. C., Lagrost, L., and Tall, A. R. (2009). The role of plasma lipid transfer proteins in lipoprotein metabolism and atherogenesis. *J Lipid Res* 50 Suppl, S201-206.



- Matoba, S., Kang, J. G., Patino, W. D., Wragg, A., Boehm, M., Gavrilova, O., Hurley, P. J., Bunz, F., and Hwang, P. M. (2006). p53 regulates mitochondrial respiration. *Science* 312, 1650-1653.
- Mercer, J., and Bennett, M. (2006). The role of p53 in atherosclerosis. *Cell Cycle* 5, 1907-1909.
- Miller Jenkins, L. M., Feng, H., Durell, S. R., Tagad, H. D., Mazur, S. J., Tropea, J. E., Bai, Y., and Appella, E. (2015). Characterization of the p300 Taz2-p53 TAD2 complex and comparison with the p300 Taz2-p53 TAD1 complex. *Biochemistry* 54, 2001-2010.
- Morita, M., Gravel, S. P., Chenard, V., Sikstrom, K., Zheng, L., Alain, T., Gandin, V., Avizonis, D., Arguello, M., Zakaria, C., *et al.* (2013). mTORC1 controls mitochondrial activity and biogenesis through 4E-BP-dependent translational regulation. *Cell Metab* 18, 698-711.
- Murphy, M. E. (2016). Ironing out how p53 regulates ferroptosis. *Proc Natl Acad Sci U S A* 113, 12350-12352.
- Murphy, M. E., Liu, S., Yao, S., Huo, D., Liu, Q., Dolfi, S. C., Hirshfield, K. M., Hong, C. C., Hu, Q., Olshan, A. F., *et al.* (2017). A functionally significant SNP in TP53 and breast cancer risk in African-American women. *NPJ Breast Cancer* 3, 5.
- Musaro, A., McCullagh, K., Paul, A., Houghton, L., Dobrowolny, G., Molinaro, M., Barton, E. R., Sweeney, H. L., and Rosenthal, N. (2001). Localized Igf-1 transgene expression sustains hypertrophy and regeneration in senescent skeletal muscle. *Nat Genet* 27, 195-200.
- Olive, K. P., Tuveson, D. A., Ruhe, Z. C., Yin, B., Willis, N. A., Bronson, R. T., Crowley, D., and Jacks, T. (2004). Mutant p53 gain of function in two mouse models of Li-Fraumeni syndrome. *Cell* 119, 847-860.
- Ou, Y., Wang, S. J., Li, D., Chu, B., and Gu, W. (2016). Activation of SAT1 engages polyamine metabolism with p53-mediated ferroptotic responses. *Proc Natl Acad Sci U S A* 113, E6806-E6812.
- Parrales, A., and Iwakuma, T. (2016). p53 as a Regulator of Lipid Metabolism in Cancer. *Int J Mol Sci* 17.
- Raederstorff, D., Wyss, A., Calder, P. C., Weber, P., and Eggersdorfer, M. (2015). Vitamin E function and requirements in relation to PUFA. *Br J Nutr* 114, 1113-1122.
- Raj, N., and Attardi, L. D. (2017). The Transactivation Domains of the p53 Protein. *Cold Spring Harb Perspect Med* 7.
- Rotter, V. (1983). p53, a transformation-related cellular-encoded protein, can be used as a biochemical marker for the detection of primary mouse tumor cells. *Proc Natl Acad Sci U S A* 80, 2613-2617.

Sanchez-Macedo, N., Feng, J., Faubert, B., Chang, N., Elia, A., Rushing, E. J., Tsuchihara, K., Bungard, D., Berger, S. L., Jones, R. G., *et al.* (2013). Depletion of the novel p53-target gene carnitine palmitoyltransferase 1C delays tumor growth in the neurofibromatosis type I tumor model. *Cell Death Differ* 20, 659-668.

Schgoer, W., Mueller, T., Jauhiainen, M., Wehinger, A., Gander, R., Tancevski, I., Salzmann, K., Eller, P., Ritsch, A., Haltmayer, M., *et al.* (2008). Low phospholipid transfer protein (PLTP) is a risk factor for peripheral atherosclerosis. *Atherosclerosis* 196, 219-226.

Schieke, S. M., Phillips, D., McCoy, J. P., Jr., Aponte, A. M., Shen, R. F., Balaban, R. S., and Finkel, T. (2006). The mammalian target of rapamycin (mTOR) pathway regulates mitochondrial oxygen consumption and oxidative capacity. *J Biol Chem* 281, 27643-27652.

Schwartzenberg-Bar-Yoseph, F., Armoni, M., and Karnieli, E. (2004). The tumor suppressor p53 down-regulates glucose transporters GLUT1 and GLUT4 gene expression. *Cancer Res* 64, 2627-2633.

Shaw, R. J., Bardeesy, N., Manning, B. D., Lopez, L., Kosmatka, M., DePinho, R. A., and Cantley, L. C. (2004). The LKB1 tumor suppressor negatively regulates mTOR signaling. *Cancer Cell* 6, 91-99.

Singh, K. S., Leu, J. I., Barnoud, T., Vonteddu, P., Gnanapradeepan, K., Lin, C., Liu, Q., Barton, J. C., Kossenkov, A. V., George, D. L., *et al.* (2020). African-centric TP53 variant increases iron accumulation and bacterial pathogenesis but improves response to malaria toxin. *Nat Commun* 11, 473.

Smeenk, L., van Heeringen, S. J., Koeppel, M., Gilbert, B., Janssen-Megens, E., Stunnenberg, H. G., and Lohrum, M. (2011). Role of p53 serine 46 in p53 target gene regulation. *PLoS One* 6, e17574.

Smith, K. R., Hanson, H. A., Mineau, G. P., and Buys, S. S. (2012). Effects of BRCA1 and BRCA2 mutations on female fertility. *Proc Biol Sci* 279, 1389-1395.

Song, Z., Moore, D. R., Hodson, N., Ward, C., Dent, J. R., O'Leary, M. F., Shaw, A. M., Hamilton, D. L., Sarkar, S., Gangloff, Y. G., *et al.* (2017). Resistance exercise initiates mechanistic target of rapamycin (mTOR) translocation and protein complex co-localisation in human skeletal muscle. *Sci Rep* 7, 5028.

Soussi, T., and Lozano, G. (2005). p53 mutation heterogeneity in cancer. *Biochem Biophys Res Commun* 331, 834-842.

Srivastava, S., Zou, Z. Q., Pirolo, K., Blattner, W., and Chang, E. H. (1990). Germ-line transmission of a mutated p53 gene in a cancer-prone family with Li-Fraumeni syndrome. *Nature* 348, 747-749.

Stockwell, B. R., Friedmann Angeli, J. P., Bayir, H., Bush, A. I., Conrad, M., Dixon, S. J., Fulda, S., Gascon, S., Hatzios, S. K., Kagan, V. E., *et al.* (2017). Ferroptosis: A

Regulated Cell Death Nexus Linking Metabolism, Redox Biology, and Disease. *Cell* 171, 273-285.

Tabas, I. (2001). p53 and atherosclerosis. *Circ Res* 88, 747-749.

Tarangelo, A., Magtanong, L., Biegging-Rolett, K. T., Li, Y., Ye, J., Attardi, L. D., and Dixon, S. J. (2018). p53 Suppresses Metabolic Stress-Induced Ferroptosis in Cancer Cells. *Cell Rep* 22, 569-575.

Tesfay, L., Paul, B. T., Konstorum, A., Deng, Z., Cox, A. O., Lee, J., Furdui, C. M., Hegde, P., Torti, F. M., and Torti, S. V. (2019). Stearoyl-CoA Desaturase 1 Protects Ovarian Cancer Cells from Ferroptotic Cell Death. *Cancer Res* 79, 5355-5366.

Teufel, D. P., Bycroft, M., and Fersht, A. R. (2009). Regulation by phosphorylation of the relative affinities of the N-terminal transactivation domains of p53 for p300 domains and Mdm2. *Oncogene* 28, 2112-2118.

Tomita, Y., Marchenko, N., Erster, S., Nemajerova, A., Dehner, A., Klein, C., Pan, H., Kessler, H., Pancoska, P., and Moll, U. M. (2006). WT p53, but not tumor-derived mutants, bind to Bcl2 via the DNA binding domain and induce mitochondrial permeabilization. *J Biol Chem* 281, 8600-8606.

Vandenburgh, H. H., Karlisch, P., Shansky, J., and Feldstein, R. (1991). Insulin and IGF-I induce pronounced hypertrophy of skeletal myofibers in tissue culture. *Am J Physiol* 260, C475-484.

Venkatesh, D., O'Brien, N. A., Zandkarimi, F., Tong, D. R., Stokes, M. E., Dunn, D. E., Kengmana, E. S., Aron, A. T., Klein, A. M., Csuka, J. M., *et al.* (2020). MDM2 and MDMX promote ferroptosis by PPAR $\alpha$ -mediated lipid remodeling. *Genes Dev* 34, 526-543.

Vicens, A., and Posada, D. (2018). Selective Pressures on Human Cancer Genes along the Evolution of Mammals. *Genes (Basel)* 9.

Vogelstein, B., Fearon, E. R., Kern, S. E., Hamilton, S. R., Preisinger, A. C., Nakamura, Y., and White, R. (1989). Allelotype of colorectal carcinomas. *Science* 244, 207-211.

Vousden, K. H., and Lane, D. P. (2007). p53 in health and disease. *Nat Rev Mol Cell Biol* 8, 275-283.

Vousden, K. H., and Prives, C. (2009). Blinded by the Light: The Growing Complexity of p53. *Cell* 137, 413-431.

Walton, Z. E., Patel, C. H., Brooks, R. C., Yu, Y., Ibrahim-Hashim, A., Riddle, M., Porcu, A., Jiang, T., Ecker, B. L., Tameire, F., *et al.* (2018). Acid Suspends the Circadian Clock in Hypoxia through Inhibition of mTOR. *Cell* 174, 72-87 e32.

- Wang, P. Y., Ma, W., Park, J. Y., Celi, F. S., Arena, R., Choi, J. W., Ali, Q. A., Tripodi, D. J., Zhuang, J., Lago, C. U., *et al.* (2013). Increased oxidative metabolism in the Li-Fraumeni syndrome. *N Engl J Med* 368, 1027-1032.
- Wang, S. J., Li, D., Ou, Y., Jiang, L., Chen, Y., Zhao, Y., and Gu, W. (2016). Acetylation Is Crucial for p53-Mediated Ferroptosis and Tumor Suppression. *Cell Rep* 17, 366-373.
- Wang, S. P., Wang, W. L., Chang, Y. L., Wu, C. T., Chao, Y. C., Kao, S. H., Yuan, A., Lin, C. W., Yang, S. C., Chan, W. K., *et al.* (2009). p53 controls cancer cell invasion by inducing the MDM2-mediated degradation of Slug. *Nat Cell Biol* 11, 694-704.
- Warden, S. M., Richardson, C., O'Donnell, J., Jr., Stapleton, D., Kemp, B. E., and Witters, L. A. (2001). Post-translational modifications of the beta-1 subunit of AMP-activated protein kinase affect enzyme activity and cellular localization. *Biochem J* 354, 275-283.
- White, E. J., Martin, V., Liu, J. L., Klein, S. R., Piya, S., Gomez-Manzano, C., Fueyo, J., and Jiang, H. (2011). Autophagy regulation in cancer development and therapy. *Am J Cancer Res* 1, 362-372.
- Williams, A. B., and Schumacher, B. (2016). p53 in the DNA-Damage-Repair Process. *Cold Spring Harb Perspect Med* 6.
- Wolf, D., and Rotter, V. (1985). Major deletions in the gene encoding the p53 tumor antigen cause lack of p53 expression in HL-60 cells. *Proc Natl Acad Sci U S A* 82, 790-794.
- Xie, Y., Zhu, S., Song, X., Sun, X., Fan, Y., Liu, J., Zhong, M., Yuan, H., Zhang, L., Billiar, T. R., *et al.* (2017). The Tumor Suppressor p53 Limits Ferroptosis by Blocking DPP4 Activity. *Cell Rep* 20, 1692-1704.
- Xue, W., Zender, L., Miething, C., Dickins, R. A., Hernando, E., Krizhanovskiy, V., Cordon-Cardo, C., and Lowe, S. W. (2007). Senescence and tumour clearance is triggered by p53 restoration in murine liver carcinomas. *Nature* 445, 656-660.
- Yahagi, N., Shimano, H., Matsuzaka, T., Najima, Y., Sekiya, M., Nakagawa, Y., Ide, T., Tomita, S., Okazaki, H., Tamura, Y., *et al.* (2003). p53 Activation in adipocytes of obese mice. *J Biol Chem* 278, 25395-25400.
- Yan, D., Navab, M., Bruce, C., Fogelman, A. M., and Jiang, X. C. (2004). PLTP deficiency improves the anti-inflammatory properties of HDL and reduces the ability of LDL to induce monocyte chemotactic activity. *J Lipid Res* 45, 1852-1858.
- Yang, W. S., Kim, K. J., Gaschler, M. M., Patel, M., Shchepinov, M. S., and Stockwell, B. R. (2016). Peroxidation of polyunsaturated fatty acids by lipoxygenases drives ferroptosis. *Proc Natl Acad Sci U S A* 113, E4966-4975.

- Yang, W. S., SriRamaratnam, R., Welsch, M. E., Shimada, K., Skouta, R., Viswanathan, V. S., Cheah, J. H., Clemons, P. A., Shamji, A. F., Clish, C. B., *et al.* (2014). Regulation of ferroptotic cancer cell death by GPX4. *Cell* 156, 317-331.
- Yang, W. S., and Stockwell, B. R. (2016). Ferroptosis: Death by Lipid Peroxidation. *Trends Cell Biol* 26, 165-176.
- Yang, Y. P., Liang, Z. Q., Gu, Z. L., and Qin, Z. H. (2005). Molecular mechanism and regulation of autophagy. *Acta Pharmacol Sin* 26, 1421-1434.
- Ye, D., Meurs, I., Ohigashi, M., Calpe-Berdiel, L., Habets, K. L., Zhao, Y., Kubo, Y., Yamaguchi, A., Van Berkel, T. J., Nishi, T., and Van Eck, M. (2010). Macrophage ABCA5 deficiency influences cellular cholesterol efflux and increases susceptibility to atherosclerosis in female LDLr knockout mice. *Biochem Biophys Res Commun* 395, 387-394.
- Ye, L., Varamini, B., Lamming, D. W., Sabatini, D. M., and Baur, J. A. (2012). Rapamycin has a biphasic effect on insulin sensitivity in C2C12 myotubes due to sequential disruption of mTORC1 and mTORC2. *Front Genet* 3, 177.
- Ye, L., Widlund, A. L., Sims, C. A., Lamming, D. W., Guan, Y., Davis, J. G., Sabatini, D. M., Harrison, D. E., Vang, O., and Baur, J. A. (2013). Rapamycin doses sufficient to extend lifespan do not compromise muscle mitochondrial content or endurance. *Aging (Albany NY)* 5, 539-550.
- Yi, J., Zhu, J., Wu, J., Thompson, C. B., and Jiang, X. (2020). Oncogenic activation of PI3K-AKT-mTOR signaling suppresses ferroptosis via SREBP-mediated lipogenesis. *Proc Natl Acad Sci U S A*.
- Yoon, M. S. (2017). mTOR as a Key Regulator in Maintaining Skeletal Muscle Mass. *Front Physiol* 8, 788.
- Yuan, H., Li, X., Zhang, X., Kang, R., and Tang, D. (2016). Identification of ACSL4 as a biomarker and contributor of ferroptosis. *Biochem Biophys Res Commun* 478, 1338-1343.
- Zhang, C., Liu, J., Liang, Y., Wu, R., Zhao, Y., Hong, X., Lin, M., Yu, H., Liu, L., Levine, A. J., *et al.* (2013). Tumour-associated mutant p53 drives the Warburg effect. *Nat Commun* 4, 2935.
- Zhang, C., Liu, J., Wu, R., Liang, Y., Lin, M., Liu, J., Chan, C. S., Hu, W., and Feng, Z. (2014). Tumor suppressor p53 negatively regulates glycolysis stimulated by hypoxia through its target RRAD. *Oncotarget* 5, 5535-5546.
- Zhao, Y., Wu, L., Yue, X., Zhang, C., Wang, J., Li, J., Sun, X., Zhu, Y., Feng, Z., and Hu, W. (2018). A polymorphism in the tumor suppressor p53 affects aging and longevity in mouse models. *Elife* 7.